AN ABSTRACT OF THE DISSERTATION OF

Justin Pommerenck for the degree of Doctor of Philosophy in Chemical Engineering presented on November 24, 2015.

Title: Nonthermal Plasma Microreaction Engineering for Gas and Liquid Processing.

Abstract approved:

_____

Alexandre F.T. Yokochi

Atmospheric pressure plasma is non-thermal at millimeter to micrometer separations. It represents an alternative low exergy initiator of many chemical reactions. In many instances heat, light or sound are not efficient providers of the necessary energy to overcome chemical activation barriers. The focus of this research is applying dc nonthermal plasma for gas and liquid chemical processing. The sub-millimeter dimensions offered by microtechnology are utilized to activate the majority of the gas or liquid stream. This enhances conversion, product yield and process efficiency.

The first reported sustained dc emission from arrays of micro-emitter electrodes is contained within this thesis. This is the first formation of constant dc microcorona fields at atmospheric pressure in air and hydrocarbon gases.

Methane is chemically converted in several microchannel devices to higher value products. A discovery that may lead to improved recoverability of stranded natural gas in our current energy cycle. Methane conversion to either C_2 or C_3 hydrocarbons of up to 80% with high selectivity are demonstrated. A finite element chemical engineering mathematical model for the hydrocarbon coupling reaction is developed.

Plasma microreactors can also dry reform methane to synthesis gas. The feasibility of microplasma carbon dioxide dry reforming in a microreactor with a dc sustaining voltage under 1kV has been demonstrated. More than 60% conversion is achieved in the unoptimized reactor with nearly complete selectivity to synthesis gas.

A plasma microchannel device can completely degrade representative trace toxic organic contaminants in a single pass. Rhodamine B is a colorimetric dye used as an example organic compound. A $G_{50\%}$ factor, which represents the energy required to remove half of the starting contaminant, is tabulated for both a batch reactor and microchannel device. The plasma electrochemical activation of advanced oxidation chemistry converts from E-6 to E-11 moles per joule of input energy.

Nonthermal Plasma Microreaction Engineering for Gas and Liquid Processing

by
Justin Pommerenck

A DISSERTATION

submitted to

Oregon State University

in partial fulfillment of
the requirements for the
degree of

Doctor of Philosophy

Presented November 24, 2015
Commencement June 2016

Doctor of Philosophy dissertation of Justin Pommerenck presented on November 24, 2015

APPROVED:

Major Professor, representing Chemical Engineering

Head of the School of Chemical, Biological, and Environmental Engineering

Dean of the Graduate School

I understand that my dissertation will become part of the permanent collection of Oregon State University libraries. My signature below authorizes release of my dissertation to any reader upon request.

Justin Pommerenck, Author

ACKNOWLEDGEMENTS

I praise, honor and exalt the Living God who holds my life breath in His hands and enabled me to undertake this research. I am grateful to each of my family members. My father and mother and siblings made this research memorable. Jordan and Joel, both of you were the best part of graduate school. It is very special to be able to share this moment with you. I am particularly thankful to Mom and Dad who encouraged me to hold my walk with God of first importance during my doctoral studies.

My graduate advisor is an incredible person. His character is remarkable and his commitment to excellence is tremendous. It has been a privilege to learn from him during my tenure in his laboratory. His laboratory is a welcoming, diverse and wholesome place such as I thought could not exist in a public university. I would encourage other young men and women from rural Oregon who shy away from STEM to think about the positive environment that Oregon State University fosters.

I would like to thank Oregon State University for their steadfast support of a healthy learning environment. It has been a joy to meet and share core values and ideas across the board with school leaders. I would like to especially acknowledge and praise the kindness of the late Beth Ray. Oregon State University is great because of great people like her.

I would like to thank NSF for graduate funding and ARCS for their unconditional scholastic support of scientists. The achievement award helped immensely in my pursuit of a higher education.

Psalm 42:1 As the deer panteth after the water brooks, so panteth my soul after thee, O God.

TABLE OF CONTENTS

Page

LIST OF FIGURES

Figure Page

Chapter 1- Introduction

1.1 – Thesis Goals

The objective of this study is to demonstrate the activation of chemical reactions using nano or micro-sharp electrodes for the formation of non-thermal plasma in high pressure air and a condensed phase. Understanding non-thermal plasma chemical activation of these reactions opens new chemical synthesis pathways that previously required thermal excitation or catalysts to supply the activation energy for a reaction. The advantage of driving chemical reactions electrically rather than through light, thermal or catalytic stimulus will contribute to higher conversion, selectivity and process efficiency.

The first goal is to catalog the energy savings that arise from reducing the size of the plasma to the microscale. This tends to soften the plasma electron energy distribution toward lower electron energy. Part of this goal is also to quantify the conditions which are necessary in order to create microscale fields of dc plasma emitter electrodes. These fields of emitters allow a dense uniform emission of electrically parallel microcoronas to be activated in a single continuous flow device for use in chemical processing. This is the first report of an active field of dc coronas in a microchannel device in electrical parallel at atmospheric pressure in air or other gases. The current-voltage characteristic of several nano and micro-emitters is identified. Native electrochemically fabricated metal microstructures and nanostructures, grown via thermal chemical vapor deposition on an electrodeposited metal catalyst, have been tested for reliability in flow-through microreactor conditions. Material constraints are identified and subsequently addressed. The stages of corona, spark, glow discharge, and pulsed discharges are identified and applied to the gases of interest for the generation of stable non-thermal plasma at 100μm, 150μm, 250μm and 400μm electrode separation distances. The characteristics associated with electrical transport within atmospheric pressure gas are catalogued with respect to applied potential. The current is measured continuously and the microplasma discharge is spectroscopically monitored through transparent reactor components.

The second goal of the atmospheric pressure plasmas employed in a microreactor is to hydrocarbon couple methane feeds to valuable higher molecular weight feedstocks. This is performed using microgaps which enables high conversion to be achieved over one or many paralleled emitters at the necessary ultrafast residence times. This first step is a platform from which to efficiently examine the possibility of generating non-thermal plasma environments in plasma microchannel devices for sustainable chemistries. Dry reforming of methane with carbon dioxide is also studied to examine the practicality of extending this microreactor plasma conversion to other reaction sets.

The third goal is to characterize the hydrocarbon coupling microreactor in detail and model the probable reactions as a finite element model that is fit using kinetic data. This model is then used to predict a second set of data from the same reactor under different conditions. The second set of data can be produced by parameterizing any other process variable. The robustness of the model indicates the correctness of the assumptions made regarding the plasmas reactive size and energy distribution.

The fourth goal is the degradation of trace organic toxins in ppm concentrations. A goal which is represented by the decoloration of Rhodamine B. The application of an identical pulse network to both a stirred cuvette reactor and a flow-through plasma microchannel reactor will be used to demonstrate that microcorona discharges can completely decolor Rhodamine B in the length of a single microchannel. The ability to drive efficient dc microplasmas in the liquid phase is developed as a platform to remove trace organic contaminants from groundwater. This advanced oxidation process is proved to be effective at reducing representative contaminants from ppm to ppb levels.

These goals are unique to this dissertation. The ability to use micro-emitter arrays to process and perform synthetic chemistry in a dc corona microreactor has not been accomplished prior. Two groups world-wide have studied non-thermal plasma using nanostructures to achieve improved results in power consumption. These studies use dielectric barrier discharge at the half millimeter scale in a gas phase and dc high power

discharges generated at nanotube probes for chemical sensing in aqueous medium. No study has attempted to miniaturize low energy stable, pulsed dc or constant dc corona discharge to the scales required to treat microreactor flows in the liquid or gas phase with nano or micro-emitter electrodes. The microscale allows non-thermal plasma to activate at much lower potentials; thereby achieving better reactivity per input energy per fluid volume and while activating the fluid uniformly at the emission site.

The corona discharge produces an intense electric field at the interface of the plasma-liquid boundary. Solvated electrons from the intense field theorized to generate hydroxyl radicals directly at the interface of the corona and the condensed phase.[1] Short application of the waveform results in energy savings because the lifetime of the most active degradation species are limited in duration to several microseconds. Time must be allowed to make full use of as many active species as possible before applying another pulse to maximize advanced oxidation process efficiencies. The dc voltage was applied continuously and pulsed while performing these studies on plasma microreactors. The pulse speed varies from several hundred microseconds to nanoseconds in duration. Either a high power dual spark gap with charging circuit or IGBT solid state switch is employed to generate the applied waveforms. A signal transformer is coupled to an oscilloscope in order to sample waveforms at 2Gs/s and nanosecond resolution. The dc discharges are measured in several gases and above a liquid as described in each of the goals sections.

1.2 – Primary Objective

The ability to drive reactions in a plasma microreactor for energy production and clean water is the primary objective that will be supported upon completing each of the goals mentioned in this dissertation. It must be understood whether plasma microreactors have the potential to perform C_1 to C_2 conversion chemistry at high efficiencies or if plasma microreactors can produce syngas from carbon dioxide, methane mixtures. Microcorona flow-through microchannel devices have never been studied for advanced

oxidation of trace toxic organic contaminants. The ability of the corona discharge to completely decolor a dye in a single pass through a microchannel device is reported. Reactions that are included in this study are hydrocarbon upgrading, methane dry reforming and liquid dye decoloration. These reactions are analyzed using Fourier transform infrared attenuated reflectance (FTIR-ATR), optical spectroscopy, high performance liquid chromatography, gas chromatography thermal and helium ionization detectors (GC-TCD/HID) and mass spectroscopy (MS).

The gas phase data indicates conversion of methane in dc microplasma filaments to higher molecular weight hydrocarbons that are successively dehydrogenated. Attempts to chemically catalog the conversion, selectivity, and efficiency of the plasma process are performed through the use of gas chromatography.

The experimental liquid phase oxidation of organics in aqueous phase is conducted with dyes as the chemimetric that represents many possible toxic organic contaminants and demonstrates the efficiency of the plasma microreactor process. Dyes have frequently been treated in literature using other advanced oxidation processes in order to provide a useful tool for cross-comparison. One unique aspect of this liquid phase study is that the same power application technology is applied to fundamentally different types of plasma reactor configurations to evaluate their performance in a single study. In addition, this is the first study to treat nonthermal plasma from microcorona discharges to plasma microchannels. The majority of the data is compiled using uv-vis spectrophotometry. The effect of process parameters such as pulse duration, frequency, power, feed concentrations, flow rates and chemical concentrations are monitored, parameterized and reported. Conclusions were drawn regarding reaction rate and pathway using the traditional chemical engineering toolset.

A finite-element solution is developed so that the four coupled partial differential equations describing plasma systems in air can be simplified to reaction engineering rates and reaction volumes. These are applied to design better plasma microreactors. The computation time and requirements for the developed models are reported. Kinetic

parameters and flow profiles are used to inform meaningful engineering decisions. The most important contribution may be the application of microplasma technology for chemical synthesis and clean water at the microscale. The ability to separate mass transport from previous plasma technologies is only possible at the microscale. This allows this dissertation to generate kinetics without mass transport limitations. New generations of ultra-efficient devices are enabled through the hypothesis addressed in this dissertation.

1.3 – Literature Review

The advent of recent advances in nanoparticle and micro-catalysis offers chemical engineers new catalysts with extremely high surface areas per mass. These catalyst improvements reduce the need for large quantities of expensive and rare catalytic materials.

Microreactor development efforts seek to house these nano and micro-heterogeneous catalysts in a reactor that affords both maximum productivity and processing rate. This can be accomplished when the surface to volume ratio is very high. Many microreactors can be designed with surface to volume ratios of 10,000. That is a large number when compared to conventional chemical tanks which may only have a surface to volume ratio of 3. Design and manufacturing fundamentals allow microreactors to be adapted not only to catalysts but to other surface activated or surface transport dependent reactions. The microreactor platform is also a useful tool for reaction kinetics extraction and for enhanced control of chemical processes. A benefit of microreactors is improved kinetic measurement and mass and heat transport by offering reduced length scales. Microlength scales and their incredible surface to volume ratio often improve the reaction conversion efficiency of reactions that are surface mediated, such as when using solid-phase heterogeneous catalysts or when excellent heat transfer can safely remove the maximum concentration limits for safe chemical processing. This increase in yield is typically accompanied by enhanced productivity. Production rate can be

increased by increasing the number of the devices operating in parallel with each other. In this way, the processing capability of microreactors can match any product demand. “Numbering up” is the term used for increasing production in a microreactor process.

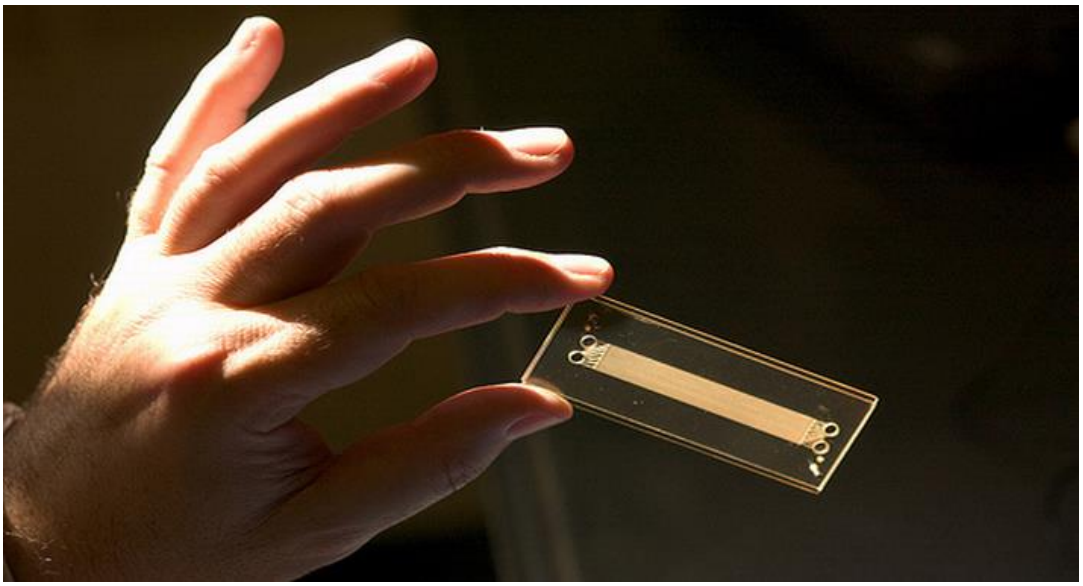

Figure 1: A microreactor design by Oregon State University (CBEE).[2]

The advantages of microtechnologies certainly necessitate exploration and their intelligent design requires a thorough understanding of this technology platform. Many microreactors can reduce reaction times of 1hr to 10s.[3] This is due to enhanced surface mediated reactions by improving concentration gradients near the surface. The micro-width in a microreactor accelerates the diffusion in its shorter dimensions. This leads to uniform residence times and extraordinary product selectivity by eliminating non-uniform concentration profiles which have the potential to aggravate competing reaction pathways. This homogenization is in the direction of the smallest dimensions, allowing the fluid to be converted to product as it proceeds down the length of the reactor. This sequential treatment of the fluid element improves the conversion efficiency since regions of low concentration do not mix with regions of high concentration as in a batch or mixed flow-through reactor. Low concentration fluid at the faster center of the microchannel is prevented from interacting with slower moving high concentration fluid at the wall by microreactor designs which distribute the

velocity of the fluid through geometric path lengths. This allows each flow path to achieve an equal residence time, improving controllability and maximizing the concentration driving force for the rate laws.[4] In this way, yield can be enhanced over batch processing due to controlled flow uniformity that maximizes concentration gradients. Temperature controls allow even higher concentrations of potentially explosive chemicals to be used safely. This increase in concentration makes reactions begin more rapidly. In conclusion, the even residence time offered by microreactors improves product selectivity by eliminating side reactions that would occur in larger scale reactors that do not have excellent flow uniformity or heat uniformity.

In this dc corona microreator study, the electrode gap required to access certain desirable plasma states at atmospheric pressure is only possible at sub-mm separations. Essentially, this means that microtechnology is the only reactor sized to the scale of the plasma. It is demonstrated in this study that the plasma regimes accessible previously only at low pressure are achieved at high pressure using microemitters and microgaps. These microplasma reactors possess unique reaction products based on the uniform residence time, uniform concentration profiles and the reduced electron energy of microplasmas. These unique facets of plasma microreactors result in high selectivity, conversion and energy efficiency. The distribution of electron energies in a plasma determines probabilistically which reactions of the possible several hundred are strongly activated. Microtechnology is necessary to control the plasma discharge energy density itself based on electric field and charge density conditions. This results in new possibilities for controlling the chemical product type and yield of a reactor.

The reactivity of a microplasma diminishes rapidly from the point of initiation. It is therefore useful to treat microplasmas within a microreactor platform that fully utilizes the plasma surface to fluid volume ratio. Atmospheric pressure plasma can drive very useful reactions to high conversion at remarkable efficiencies if it is applied at the microscale. This dissertation contains the first demonstration of large field activation of multiple atmospheric pressure dc microplasmas in series in air and other gases. These large fields are used to activate hydrocarbons, carbon dioxide and water.

It is commonly known that in a methane feed the degree of ionization is determined by the reduced electric field. This degree of ionization is controlled by the electron energy distribution present. The amount of methyl radicals and the degree of dehydrogenation is, in this way, easily controlled by the scale of a dc discharge. The flow velocity through the discharge is another parameter that strongly determines the yield of specific products. For example, the residence time for "successive dehydrogenation" of ethane to ethylene and then to acetylene is ~10^{-6} – 10^{-5}s and 10^{-4} – 10^{-3}s respectively.[5] Rapid flow induced cooling or addition of oxygen can suppress successive dehydrogenation and higher hydrocarbon formation.

Microplasma can be used to deposit metallic or dielectric films, nanotubes or nanoparticles. In the future, these processes may fuel the 3d printing of circuit architecture. These chemistries can operate at atmospheric conditions. Typically, the chemistry involved in these depositions is primarily oxidative. For example, in depositing SiO_2 morphologically pure amorphous films on a substrate, a gas precursor such as BPTEOS (silane or siloxane) is passed over the surface of the material which is to be coated with silicon oxide. Non-thermal atmospheric pressure plasma is highly reactive when compared to low pressure analogs. High conversion of dilute streams containing the silicon precursor is possible. A one weight percent siloxane in air is sufficient for growth rate to be very rapid (0.1 to 1µm/min).

The mechanism for fracturing silanes (which depends on if it is ion or electron mediated-but is most likely ozone mediated under these conditions) results in methyl or siloxane radicals being formed. In air, carbon tends toward CO_2 and H_2 tends to convert to H_2O which forms while silicon is oxidized to SiO.

Plasma discharges into aqueous mixtures of alcohol form smaller molecules tending towards lower molecular weight alcohols, methane, and hydrogen and provide an inexpensive route to fuel a hydrogen economy from transportable fischer-tropsch fuels.

For aqueous environments, plasma discharge is a promoter of radical generated peroxides in aqueous environments. It is desirable to determine the reaction engineering fundamentals of microplasma hydroxyl mediated chemistry. A dye can be used to extract pure kinetics from microreactors which unlike their mixed flow-through reactor counterparts are not hindered by mass transfer limitations which strongly dictate the perceived kinetics that are often reported. Without plasma microreactor studies the potential to reach ultra-high conversion efficiencies is unguided. Using microplasma at the microscale with dc plasma discharges to degrade a common tracer, the author is removing misconceptions about the maximum achievable efficiencies for advanced oxidation processes that utilize plasma. The overall reaction is described by a mechanism which progresses largely via hydroxyl-radical scavenging peroxides for severely mass transport limited systems. At the interface of the plasma and the liquid, hydroxyl radicals themselves persist long enough to directly react with dye. Mass spectrometry can be used to detect the completeness of the mineralization of the dye while uv-spectroscopy detects the destruction of the electron conjugation along the backbone of the main part of the photoactive organic molecule.

Atmospheric pressure plasma can be either self-sustaining or made up of short transient bursts.[6] There are five major types of atmospheric pressure plasma. The type of dc plasma generated is dependent on the current density, pressure, distance and reduced electric field. The lowest current regime is the dark regime which is composed of Townsend streamers. These streamers can be constant or pulsating. The next regime with a higher current density is the corona regime, in which the discharge does not form a complete conduction filament. Following the corona regime is the spark discharge regime. Sparks are intense bursts which are rarely prolonged. After the current density (or distance is diminished) is increased further, the glow discharge region is reached. This region has a very flat current-voltage relationship for gaps less than 1mm.[7] As opposed to a glow, an arc discharge is thermally intense and operates at high currents. Plasma can be generated using dc electric potentials, ac electric potentials, ac inductively coupled fields, microwave gigahertz technologies and even triggered or excited by lasers.

Below are illustrations of a variety of atmospheric pressure plasma types (dc corona, ac DBD, an ac plasma jet and spark).

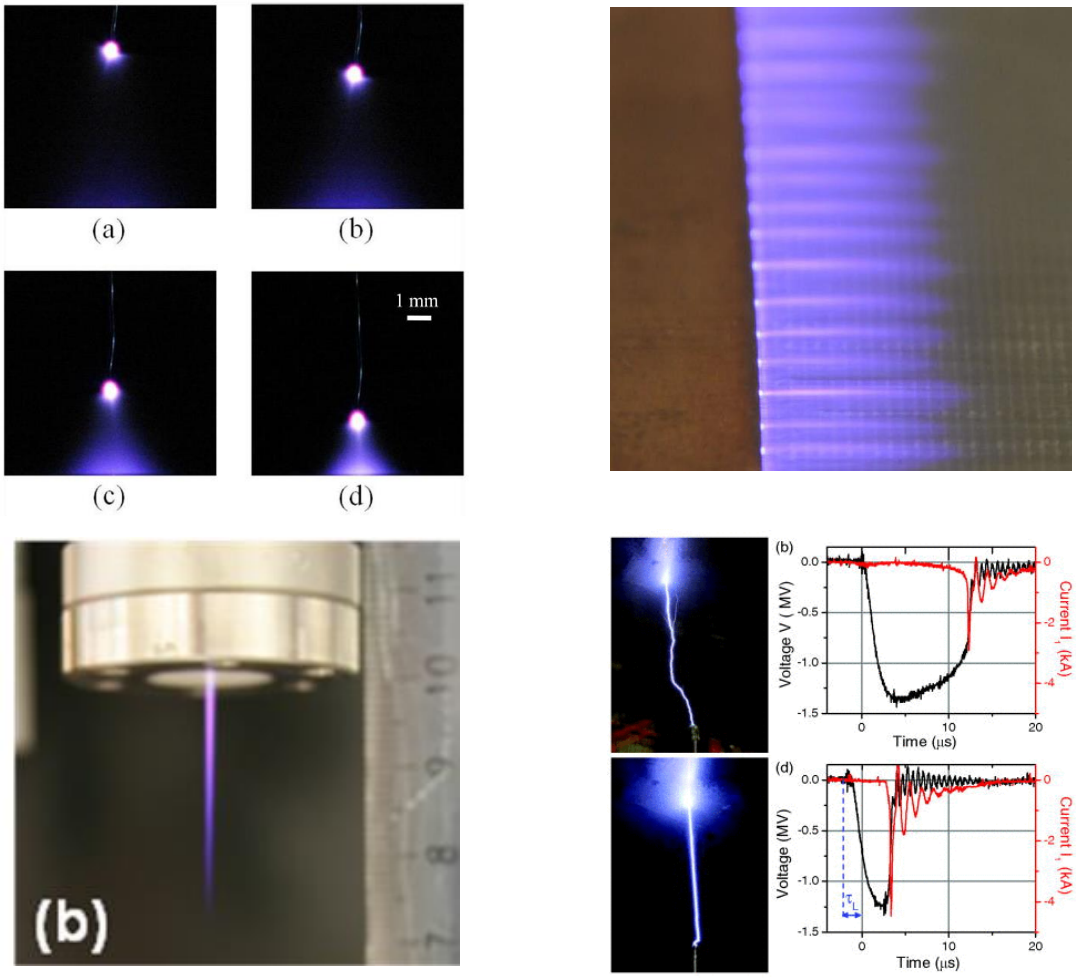

Figure 2: Images of example high pressure plasma. A corona discharge at reduced dimensions (top-left).[8] An ac electric potential driven dielectric barrier discharge plasma at large separation (top-right).[9] A plasma jet (bottom-left)[10] and a spark discharge (bottom-right).[11]

Each of these types of plasmas appear to be visually equivalent but actually can possess very different properties. The structure of each plasma can be fundamentally different based on the driving electric fields. The locations of the plasmas most energetic electrons can be in a physically different locations. For example, only gigahertz plasma creates an oscillating field so fast that heavy charged plasma ions are confined to a narrow zone near the conductor.

All these types of plasma can be encountered in modified combinations depending on the energy input mode. For example, alternating current can be applied to a bare electrode and a shielded electrode in order to supply the needed electric field for plasma formation. While these discharges (termed dielectric barrier discharges) appear to be unlike their dc current counterpart, they actually consist of Townsend streamers that transition to diffuse glow discharges as the waveform for the applied potential changes. At atmospheric pressure, these discharges happen many times a second at the kilohertz frequencies used for most ac plasmas. These rapid but discrete discharges appear to be single silent unique glow-like plasma while in actuality they are plasma which is continually transitioning between the similar types of plasma found in dc discharges. Atmospheric pressure rf plasmas are plasmas undergoing restructuring of the plasma at radio frequencies. Microwave plasma can activate microplasmas from a distant energy source beamed to resonant electrodes. Even more interesting is the superior performance for simple plasma systems when waveforms combining dc and ac modes are employed.

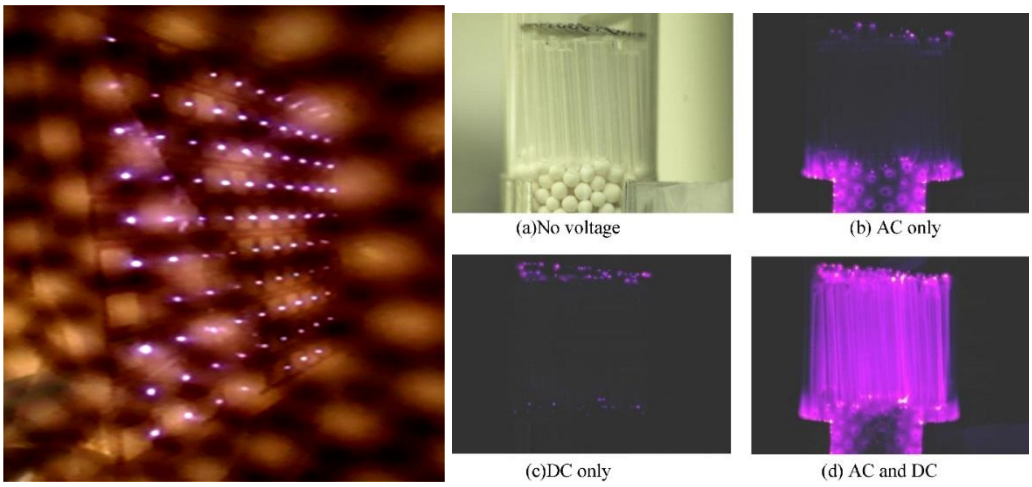

Figure 3: A microwave microplasma array (left) [12] *is shown through a protective grating. Improvements in synergy between plasma excited with dc and ac signals have been recorded in literature for a few limited systems (right).* [13]

Plasma can also be formed at atmospheric pressure by thermally populated higher energy levels, by using chemicals whose rapid reactions invert the electron distribution or by stimulated light emission from coherent monochromatic light amplification technology.

Formation of stable dc non-thermal plasma requires extensive engineering even if microscale and nanoscale emitter electrodes are used. For this reason, non-thermal plasma has almost exclusively been generated in noble gases. Stable plasma is generated at atmospheric pressure above metal holes at fields as low as 10^9V/μm. A natural observation, which regards the transition to microscale reaction engineering, points out that flow can be added to remove the heat generated during discharge that causes instable glow to arc transitions. The erosion of the electrodes during dc rather than pulsed dc operation is reported during observation of metal vapor lines from the cathode emitter electrode on optical intensity spectra.[14]

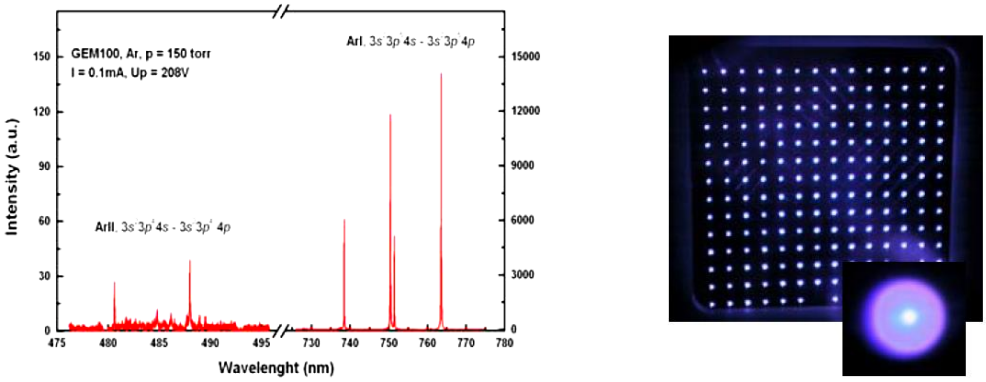

Figure 4: Spectra of argon microdischarge array at 150Torr operates in parallel without individual resistive ballast.

One group is able to take their hot 1000K plasma system and sustain room temperature, non-thermal plasma at pressures up to atmospheric at reduced voltages in Air, Ar, H_2 and H_2/CH_4 for novel lithography electrode microscale systems.[15] The spectral emissive lines of microplasma in a variety of mediums and their spatial distribution in dc pulsed microplasmas are reported.[16, 17]

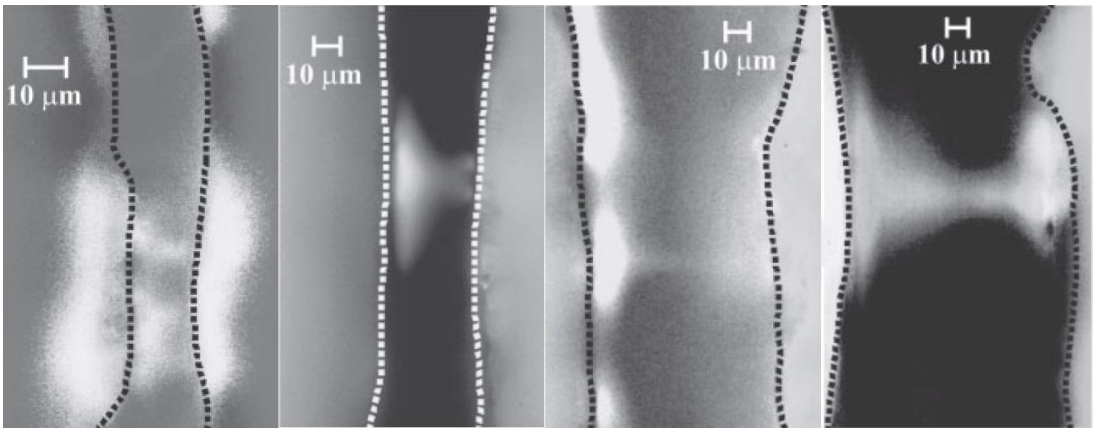

Figure 5: The microplasmas at 20μm, 30μm, 75μm and 100μm in Ar/N_2 use the same applied electric potentials from Reference [17] (© [2013] IEEE).

It has been accurately observed that a single electrode point defines macroscopic breakdown, but collective one-dimensional nanostructures use flux-convergence-effects to intensify local electric fields which interact with lesser space scales through a gain factor which relates the field intensity at the surface to the macroscopic field intensity.[18] Uniform glows 1 cm^2 in area are sustained at 300V to a Paschen minimum of 0.1Torr-cm. Apparent diffuse discharge in an inhomogeneous electric field is easy to realize in atmospheric pressure air, nitrogen, and other gases with voltage pulse durations ranging from nanoseconds to several tens of nanoseconds.[19] During the last decade, microplasma has continued to astound the scientific community with advances in the understanding and applications of microplasma at a rapidly reducing scale and improving pressure limitations. The driving research towards stable microplasma designs in micrometer spacing have demonstrated Penning ionization in plasma at scales of 5μm and below.

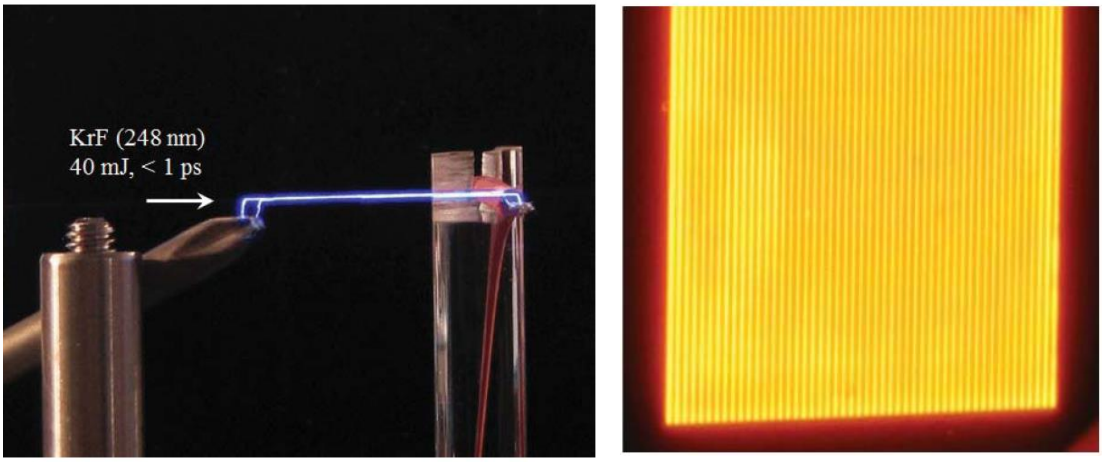

Figure 6: RF voltage plasma microchannel is directed along an ionization path by a sub-picosecond KrF laser at University of Illinois (right). A 760Torr microplasma completely fills the 50 separate, 50μm silicon microchannels (left). [20]

Low voltage atmospheric pressure plasma can be activated in even smaller microgaps that are placed near larger electrode gaps. Afterglow initiation charge carriers from the smaller microgaps stimulate reduced discharge potentials in the large gaps. Stable atmospheric pressure discharge at 270μm is possible at electric potentials below that predicted by Paschen's curve. A 10μm gap seeding plasma in the larger gap produces turn-on electric potentials at 400V and sustaining potentials from 200-300V.

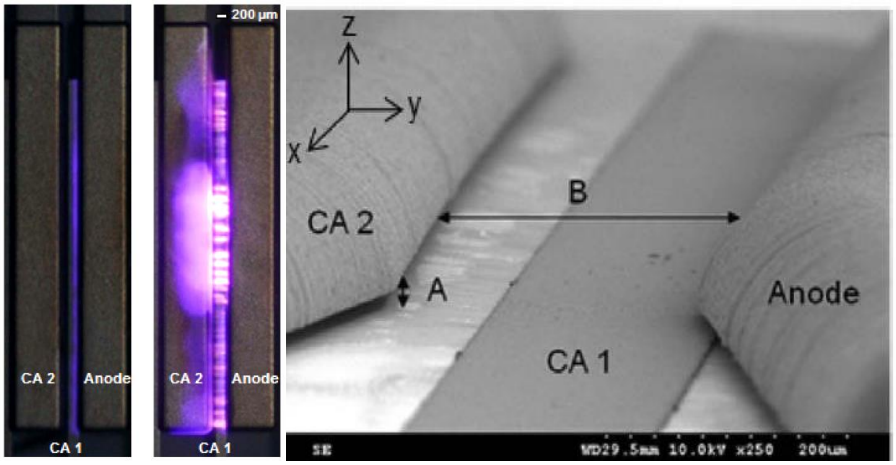

Figure 7: Parallel electrodes separated by distance B are seeded by microdischarge gap A which provides substantially reduced minimum sustaining voltages. [21]

CA1 and CA2 are the two cathodes which are shown next to the anode. Figure is from Reference [21]. Discharge is identified in the 10μm gap before the 270μm channel is seeded and discharges. The smaller gap is pulsed out of phase with the larger electrode gap in order to continuously seed the larger electrode gap. The initiation of non-thermal plasma is demonstrated to occur through the formation of a spark streamer during dc discharge. The current versus voltage characteristic has been reported for 50μm separations between cathode and anode emitter electrodes. The slightly negative voltage response for increasing current during breakdown shows hysteresis if the flat glow regime is traced backward from the subnormal glow regime towards a corona discharge. The electric field for sustained generation of atmospheric non-thermal plasma from rounded wire tips is reported as 7V/μm.[22] The stability of the discharge depends on the external reactance of the circuit. The stability translates into operating in a different regime of discharge while at the same current and voltage effectively shifting the current versus voltage characteristic. The transition from corona to glow and glow to arc modes for non-thermal plasma has been studied using nanosecond pulses at several distances and temperatures even upwards of the electron temperature. This demonstrates that no spark formation occurs during nanosecond pulses and offers great promise for plasma discharge in condensed phases.[23] The flow rate of gas passing over the emitter electrode affects the regime of discharge for non-thermal plasma with higher flow shears injecting instability in the discharge.[24] The distance is not the only defining parameter for inception electric field. The emitter material is subject to cathode column and surface emission barriers which for platinum yield onset potentials of 277V and for copper 370V.[25] Light emission has been reported in silicon metal microgaps of 2-15μm at potentials as low as 30V. Erosion of the cathode and deposits on the anode were reported for silicon surfaces and are thought to vaporize or sputter surface material from interface to interface. Rf plasma has been studied as electrode gap diminishes in size. The electric field of the sheath and bulk are compared to determine for any frequency when the glow regime is reached. An intense increase in sheath electric field is attained somewhere between 102 to 318μm. The sheath thickness occupies nearly the entire 102μm gap almost completely eliminating the bulk thickness. RMS voltage is greatly reduced for substantially higher current densities.[26] This

microplasma regime clearly delineates itself from what is observed with larger atmospheric pressure plasmas. This does not however exclude rf from generating large-area cold atmospheric pressure microplasmas in air at low powers in low flows of inert gas. Rf plasma has been generated between stainless steel mesh and copper plates at 13.56MHz for 3mm separation gaps in open air for tube to plate configuration.[27] At the microscale, plasma inevitably encounters the boundaries of the electrodes and in that spatial confinement loses charge density which must be resupplied to sustain discharge. This can be provided by nanostructured field emission from the cathode if the electric fields are high enough.[28] Unstable glow discharge to arc transition is reported at voltages from 300 to 600V for silicon-metal or silicon-silicon electrodes.[29] Non-thermal plasma also produces solids from the vapor phase. Carbon monoxide is reported to produce suboxides on the surface of the emitter.[30] The stability of the non-thermal microplasma results in a balance of thermal ionization in spots of locally increasing current density and is typically accomplished by reducing the size of the separation or providing external reactance to counter and smooth rapid internal changes in the plasma. Parallel parasitic capacitance is offered as a tool to govern the thermal characteristics of the plasma through changes in the electric field during discharge which are associated with ionization.[31] Microscale and larger scales of dielectric barrier discharge are contrasted and compared in terms of discharge potential, current, reactivity and gas throughput.[32, 33] The stability of nanofibers other than carbon nanotubes has been explored and their resulting current versus voltage characteristics reported. Emission over 1 hour records no change at 13.6V/μm.[34] The minimization of electrode erosion during direct current film deposition is critical for various applications. The analysis of a H_2 plasma jet describes the possible sputter processes in low temperature plasma. EDX is used to identify impurities based on changes in the electrode geometry and SEM determines the presence of microclusters of iron from the stainless steel electrode which are deposition primarily through high speed neutrals and H chemical etching.[35] Studies in ignition using transient plasma have determined that electrode geometry does more to influence discharge than polarity of the discharge. Streamers were observed to consistently leave the electrode with higher electric field even after polarity reversal.

Electrode damage hinders many applications especially during spark discharge. Electrode damage is not observed during nanosecond pulsed plasma used for reactive ignition of a mixture. This leads to the conclusion that nanosecond pulsed transient plasma is non-thermal and will be very useful in many industrial applications including combustion.[36] Nanosecond impulses produce stable macroscopic glow discharges using either controlled pulse durations or duty ratios. Correspondingly, the minimum pulse duration for this behavior in a microplasma discharge should be studied. Also, the frequency of that discharge should be parameterized since a more rapid frequency with yet the same pulse width will certainly affect charge transport in the intracavity region.

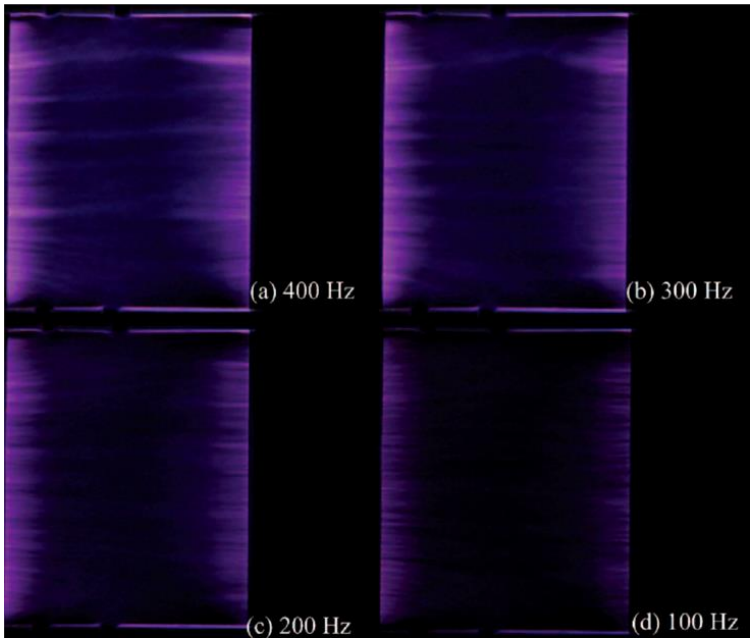

Figure 8: Nanosecond pulses from a dual spark gap transformer at 65kV for wires 4cm apart.[37]

A dielectric barrier non-thermal atmospheric pressure plasma jet has also been ignited from a smaller dielectric barrier parallel ring discharge. More than 56% of the system energy is consumed by the first discharge in the dielectric barrier discharge and the time required to develop the peripheral plasma jet depends upon the applied electric potential. Rapidly-pulsed dielectric barrier plasma from the first discharge generates

the plasma jet from which detaches a plasma bullet traveling away from the parallel rings of the dielectric barrier discharge source in the direction of the helium gas flow. The plasma frequency, which is related to pulse duration, is different in that it describes the repetition rate of the pulses and in part defines a pulse duration. Pulse duration is the time for which a single pulse is applied and does not indicate the pulse repetition frequency. The frequency response of dc and ac breakdown processes in micro and nano gaps is of interest for high speed electronics operating at the GHz to THz range and has implications in microplasma generation applications. Traditional vacuum relationships between frequency and distance between electrodes do not hold for atmospheric pressure microplasmas. At very high frequencies the breakdown voltage is usually three times lower than predicted. This is an effect of trapped ions whose low drift velocity cannot transverse the distance of the gap within the time frame of the rapidly reversing field. Nitrogen for example commonly displays dc breakdown voltages of 130V at 19μm with copper electrodes and has its predicted critical frequency at 6.3GHz.[38]

It is also possible to replace one of the plasma electrodes with conductive water. A potential can be applied to the fluid with one electrode in the fluid and the other a charged column of plasma or by two immersed electrodes both in the liquid. An electric potential difference in a liquid drives plasma electrochemistry. How rapidly the electric potential changes its peak intensity defines the electric overpotential and the electroactive species that will be generated in largest quantity.

A schematic that demonstrates the most common electric discharge configuration is shown below. The reactor consists of a metal tank. An electrode is charged to the opposite polarity of the liquid. Plasma forms at the interface and can penetrate into the liquid once the peak applied voltage is sufficient for streamer propagation. The gas head space overhead is frequently charged with oxygen or argon or air. The electrode itself is often sharp in order to reduce breakdown voltages. The liquid itself is well mixed in terms of stable chemical species.

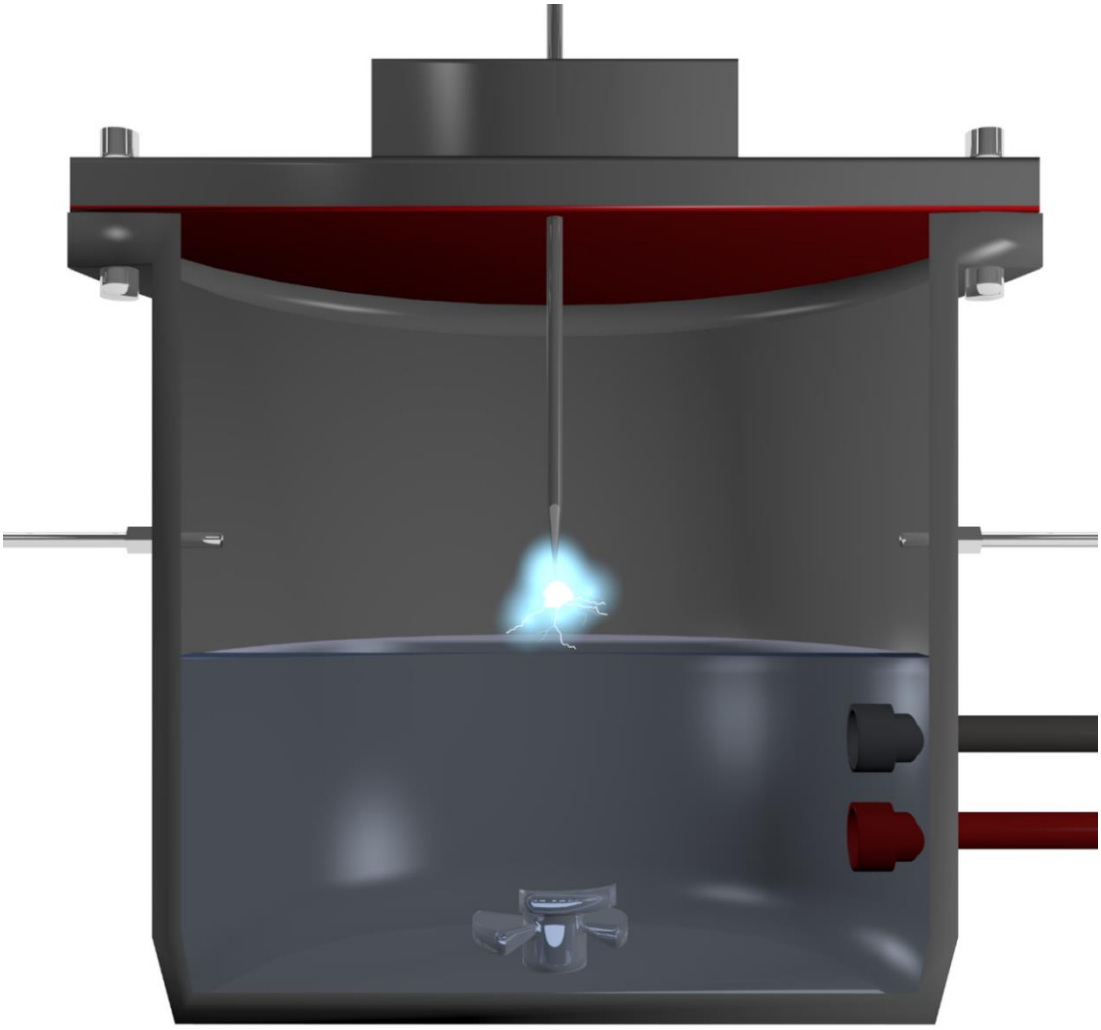

Figure 9: A commonly studied reactor type for liquid interface plasmas is the mixed flow tank reactor.

Energy efficiency is typically reported in terms of the energy required to remove a certain percentage of contaminant. A G factor of $G_{50\%}$ indicates that 50% of the starting concentration of an organic toxin has been degraded. In the case of an organic dye, it is usually colorimetrically deactivated.

There are a variety of combined systems which have high reported efficiencies.[39, 40] A reasonable point of division between different non-thermal plasma technologies is due to the differing types of air/water interfaces. Jets, bubblers, droplet exchangers can replace the plasma interface and affect surface discharge mass transport or even the

discharge type itself. Examples of discharge types are immersed glow discharge electrolysis, gliding arc discharge, corona discharge, interfacial glow discharge, dielectric barrier discharge, and immersed electric discharge and plasma jets. The reaction kinetics associated with pulsed partial discharge in the direct injection configuration achieved 4.3 g/kWh^{-1} using a 57kV peak impulse and ferrous sulfate and carbon particles.[41, 42] Pulsed corona discharge, which is typically more efficient than discharge electrolysis, has been surpassed by a non-pulsed diaphragm glow discharge reactor in which conductive solution is separated from anode to cathode by a high dielectric diaphragm with microscale hole. The 200μm deep hole allows discharge at the microscale with conductive water on either side of the diaphragm acting as the electrodes so that there is no damage to the actual electrodes.[43] Pulsed signals would likely have caused discharge from the real electrodes since there is an effective macroscopic time delay for charge to move from the metal electrode to the discharge diaphragm unless the discharge could be limited by pulse duration. Glow discharge has been improved by the addition of multiple anodes.[44] The direct mineralization of certain sulfonates has been demonstrated.[45] Fenton's reaction has been studied with respect to glow discharge and the COD was found to decrease rapidly.[46] A vapor sheath typically forms around the discharge at the platinum electrode which is responsible for the metal vapor emission spectra which are orange-red.

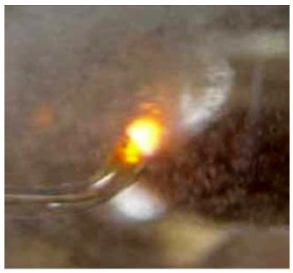

Figure 10: Contact glow discharge electrolysis is depicted at a platinum electrode with fully developed vapor sheath surrounding the electrode.

The discovery of contact glow discharge electrolysis was made in liquid ammonia and is one of the first studies that summarizes quite well the phenomena of contact electrolysis.[47]

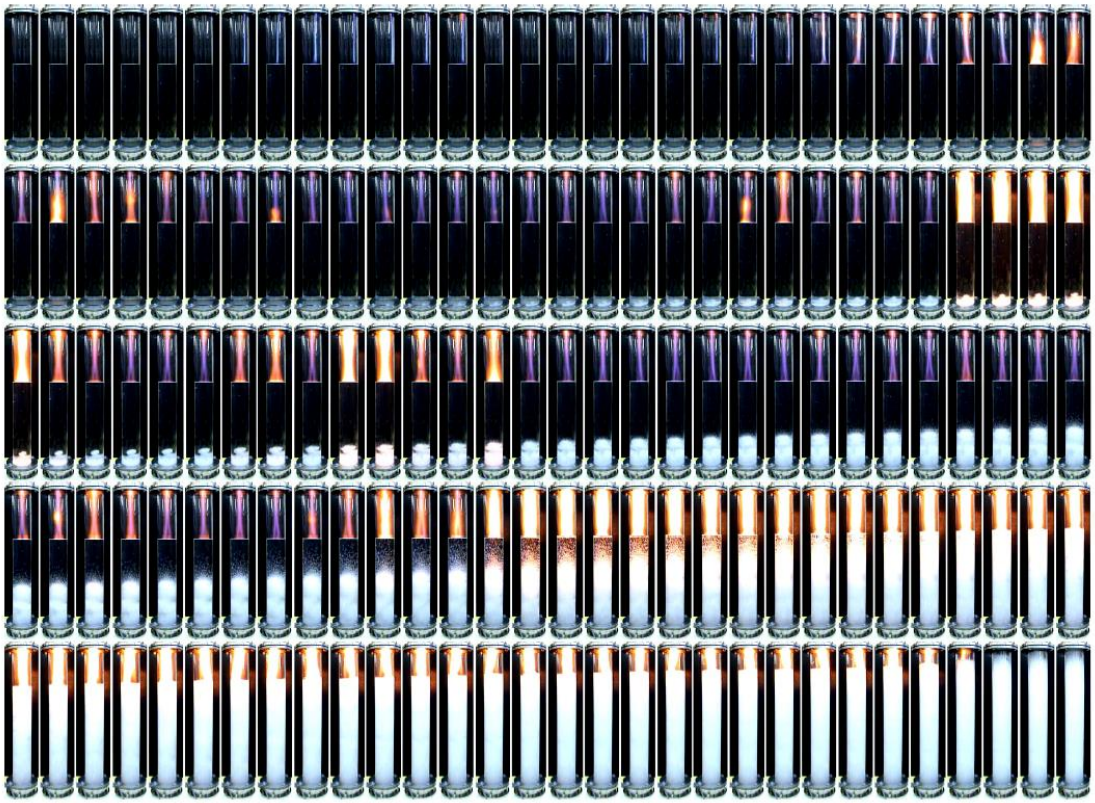

Figure 11: The frame by frame development of a noble gas discharge above and entering the liquid from the reverse electrode at 25Hz frame rate. Figure is from Reference [50].

The gas-liquid reactors are treated thoroughly in literature. Typically one electrode is in the gas above the liquid.[48] The generation of peroxide is recorded and monitored during operation of non-thermal plasma in an air/water system.[49] An excellent study which shows dc glow discharge extending throughout the gas and liquid even records the formation of the glow at the electrode using a 25Hz frame rate.[50] The desulfurization process has been performed using pulsed plasma in a quartz tube gas-liquid packed bed.[51] The kinetics of non-thermal plasma desulfurization are explored at reduced temperature.[52] Several atypical reactors have been developed and some possess a very high efficiency. Non-thermal plasma electrospray pin to plate electrode

configuration separated by 4cm and discharging with G factor of 2.5g/kWh can completely remove phenol. This is the highest reported G factor in literature currently.[53] A wetted-wall reactor attempted to incorporate carbon nanotubes for improved phenol degradation using non-thermal discharges.[54] Drupe shaped discharges were studied in a non-thermal plasma suspended capillary drip discharge reactor.[55] Air bubbles, injected into discharge capillaries, provide stable low voltage discharge at microscale anode-to-cathode separations. The discharge current is 0.6mA and the discharge voltage is 500V. The typical energy per pulse is 60nJ.[56] The study of sodium emission spectra seems to require large amounts of vaporized fluid for long discharge times.[57] The ability to generate plasma in condensed phase at low power is largely due to the application of pulsing technology. The yields of peroxide using 0.3 microsecond pulse technology can be much lower than at larger scales wherein the formation of gas on the emitter during the onset of slower pulses of applied voltage made possible streamer formation within the gas bubbles. The G_{H2O2} factor of 8.2E-9mol/J has been achieved at large and microscale electrode gaps using 20kV peak waveforms with 3μs pulse durations involving gas/liquid systems at microsecond pulse durations. The gradient in radical concentration drops off very rapidly from the discharge streamer. Researchers have endeavored to determine if streamers can be widened so that their produced electrons can reach higher efficiencies in the production of free radicals. The energy yield for plasma reactors ranks pulsing, air/water mediums, and reduced scale (thin films of water) as the most critical when improving efficiency.[58] Microtechnology employs scales which are on the order of normal discharges which promotes efficient utilization of non-thermal plasma. Mass and heat transfer improvements increase the reaction rate and reduce electrode damage. This not only means a shorter space residence time but longer performance lifetime. The majority of plasma applications in microreactors pertain to purely gas phase studies.[59] The design of microreactor plasma systems depends on the flow, non-thermal plasma interaction, material constraints and separation distance of the anode and cathode. The distribution of ozone in a gas liquid microreactor is performed for reactivity.[60] Very recently, the benefits of microtechnology been realized with regard to plasma formation at the microscale; however, the successful application of the technology at high efficiencies was not.[61]

The lifetime of an unprotected sharp metal emitter is typically 10 to 20 minutes.[62] The slow microsecond discharges are fast enough to prevent arc formation by preventing the streamer from propagating the full distance between the cathode and anode before the applied voltage is removed. This can be seen best in a time resolved image of a pulsed electrode. The separation distance is specifically selected for the 600 ns pulse duration using a Marxbank generator so that the discharge was just beyond the anode. The arc does not form and the fluid is treated entirely.[63] If the scale is reduced to say microscale, it is obvious the pulse duration must decrease linearly since the plasma velocity fronts for streamer formation are linearly related to distance.[64] The negative discharge is much slower than the positive discharge and would most likely be very useful at the microscale if larger voltages are needed for non-thermal plasma formation on short non-arcing time scales since voltage like gap distance also affects streamer propagation speed.

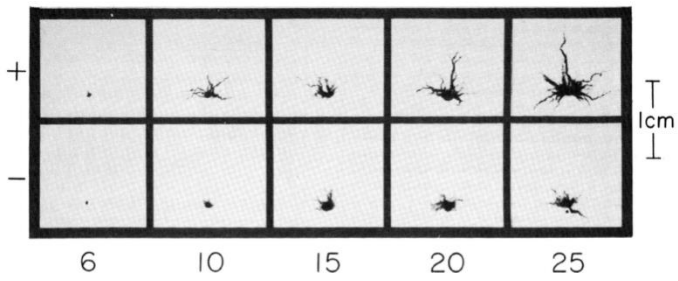

Figure 12: The time scale for discharge in water at macroscopic scales shows slightly different development rates for reversed polarity discharge from sharp electrode points. [65]

The electric potential for streamer formation at 10mm separation gaps is approximately 5kV. The corresponding point for 100mm is 20kV. The brightness of the discharge is proportional to the water resistivity.[66]

A detailed experimental study of non-thermal plasma generated between two tungsten filaments specifically focuses on the growth and compression of the bubble formed during discharge in aqueous media. The study relates well to laser induced chemical reactions that produce bubbles by clearly describing partition energies throughout each

phase of bubble development. Accurate monitoring of radiative waveform from photodiode and hydrophone with simultaneous 10MHz sampling and high-speed camera records at frame rates near 3000frames/s allows a clear picture of the discharge event to be characterized energetically. Small and large bubbles behave differently. During the growth phase, intense heat is generated as the optical intensity rises. Internal temperatures are deduced from the Stefan-Boltzmann Law regarding surface temperature and thermal radiation. Estimates of this surface temperature peak at 18,000K which is relatively low compared to most studies. Temperatures and energy partitions during each phase are reported.[67]

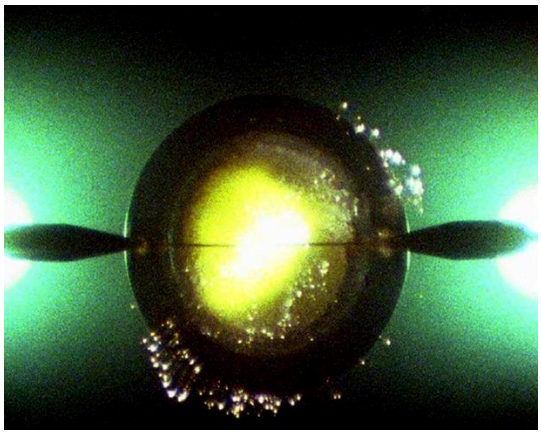

Figure 13: The image of a bubble at its first maximum radius of 51.5mm from Reference [67].

Pulsed plasma formation in water can be enhanced by the addition of carbon nanotubes within the condensed phase for pulses of 300 ns duration during 40kV peak applied electric potentials. The streamer is twice as long as when no nanofiber is present subject to the same impulse potential.[68]

Not frequency but duration of the pulse controls the development of the non-thermal plasma. The frequency causes interaction between pulses by chemical means since it is not on the time scale of the phenomena of interest. The pH, radical concentration or local temperature may affect the next pulse but does not provide a direct effect on the electronic emission. For pulse times much less than 50ns, it can be observed from previous work that the discharge can be highly localized around the emission point to

a distance of 600μm for a 20mm separation using a 32kV peak electric potential. In fact, it might be stated that the complete environment of the emitter is bathed in a controlled homogenous glow.

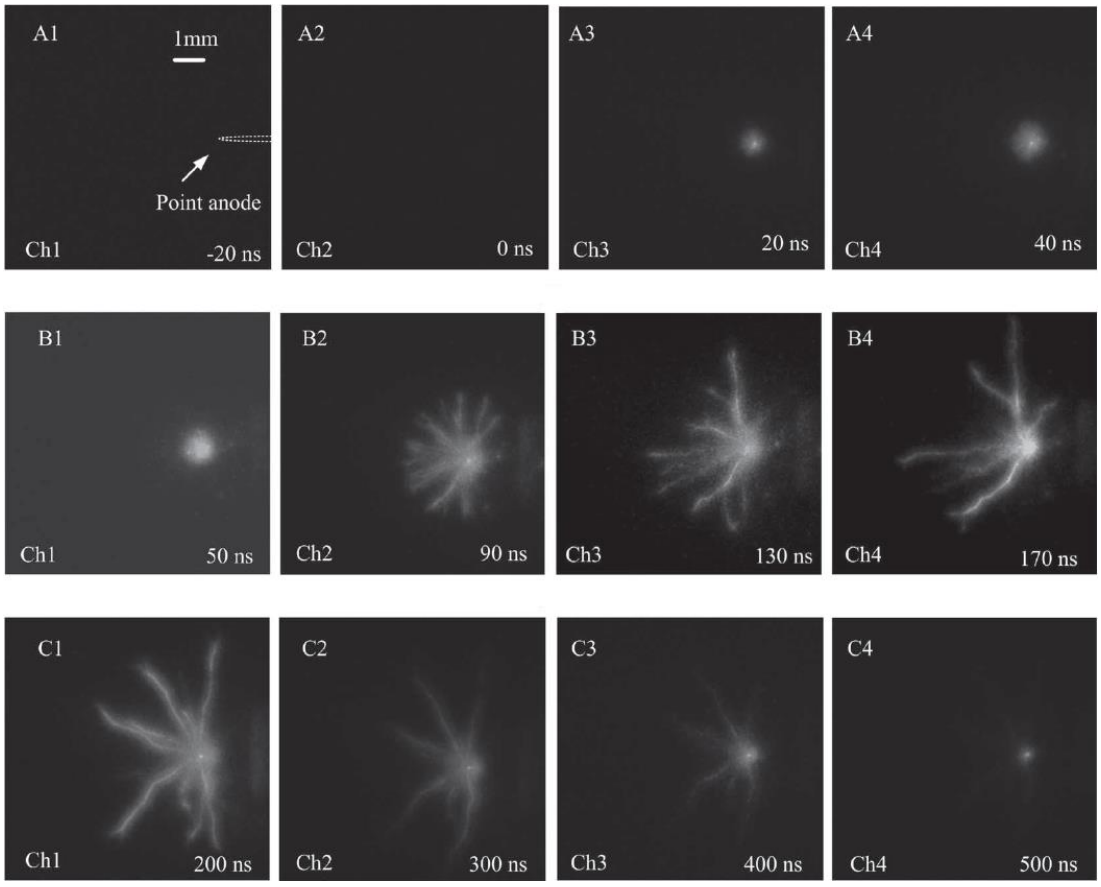

Figure 14: Sharpened point discharge shows glow characteristics at confined temporal scale. Secondary mode branching of multiple streamers occurs after 90ns. [69]

Research performed independently and concurrently with Oregon State has produced similar findings. In 2008, the Drexel group began studying non-thermal plasma around very sharp tips for spectroscopy.[70] Later that year, it is observed that "field-emission-initiated negative coronas require nanoscale electrodes and are not observed when macroscale electrodes or positive polarities are used." [71] Supporting photographs of the emission are supplied. The non-thermal plasma is generated with greatly reduced

electric potentials. The non-thermal plasma around the carbon nanotube electrode tips was chemically reactive for the production of gold nanoparticles. It was also observed that the pulse durations as low as 3-15ns were required to initiate the glow.

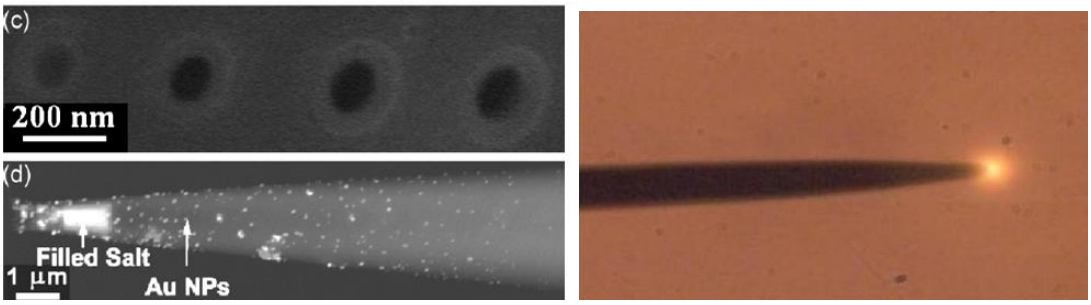

Figure 15: Carbon nanotube pipets and probes have activated aqueous mixtures for nanogold particle synthesis at 1kV and spectroscopic 3-30μm sized discharges at microseparations between two probes at electric potentials down to 300V as observed under optical microscopy. [72]

Electrodes erode when microsecond pulsed non-thermal plasma is used to create discharges in fluids. This erosion is not observed when using microscale, nanosecond pulsed plasma. It is postulated that bubble formation and breakdown within generated bubbles leads to greater electrode damage in microsecond discharges.[73] The best evidence, that electrode damage is caused by bubble formation, is measurements of positive ion scattering during field emission in liquid noble gases. These noble gases are completely inert and still damage the electrode during discharge. Assuming ionic current is frictional in the discharge, experimental calculations demonstrate a reasonable agreement between the onsets of electrode damage at the theoretical point in time during pulsing experiments when enough heat could be generated at the tips by this frictional ionic current.[74] While ion back bombardment has been offered as the source of electrode erosion due to experiments with low fields in N_2, it is noted that bombardment of electrons on N_2 covered electrodes could erode from chemically formed N_2^- or N^-.[75] Lower onset voltages do occur in air over water. Bubbles are often introduced rather than formed by the discharge to take advantage of this energy savings. This may also reduce the damage that the electrode system experiences when submerged in a liquid phase for microsecond pulsed discharges.

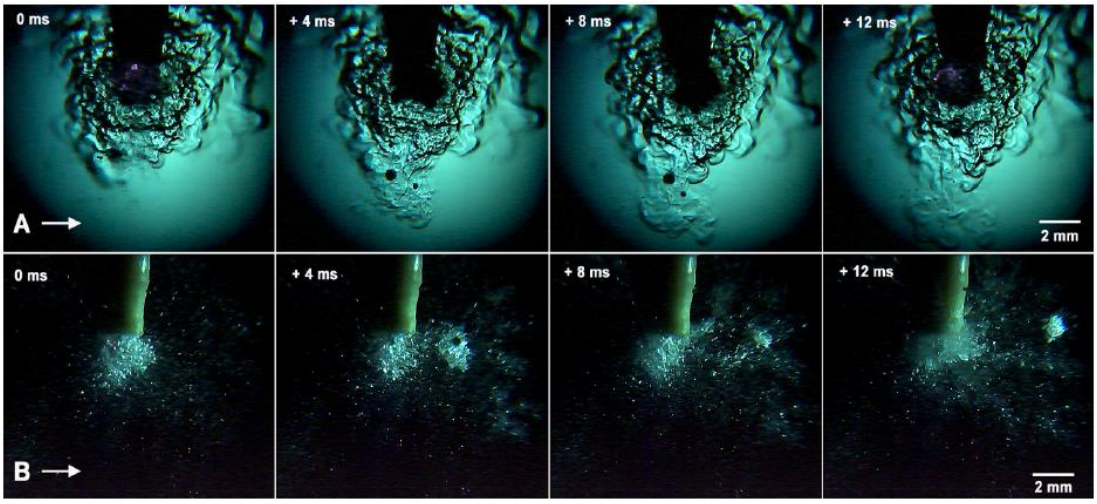

Figure 16: Shadowgraph images of thermal instabilities near pulsed discharge emitter electrodes at 700Hz without external cooling. [76]

Bubble formation is not observed during plasma formation using high voltage nanosecond pulsing in large electrode gaps.

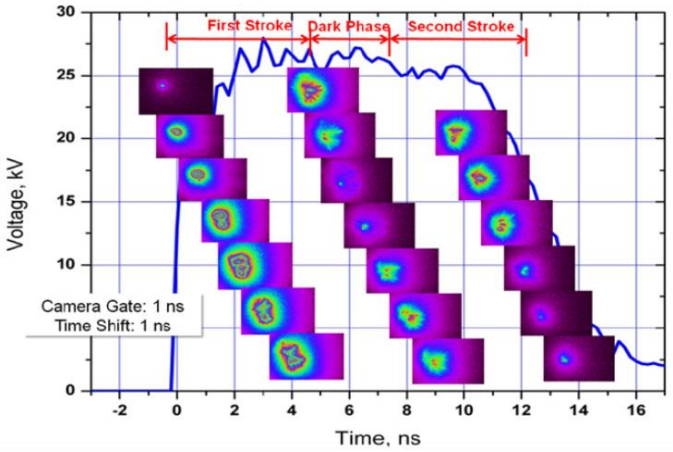

Figure 17: The 27kV discharge over macroscale separations at sharp emitter electrodes shows on a 1ns camera gate time frame the spectral response from 250-750nm for bubbleless discharge dynamics. [77]

Explanations for the lack of bubble formation seem to indicate an alternative streamer formation event. This has been hypothesized to occur based on the creation of nano-sized pores in the liquid during application of intense electric fields. It is known that

streamer formation can be triggered by focused lasers which greatly reduce the inception electric potential perhaps through the same extension of natural liquid voids via resonance.[78] The only other group to suggest the lack of bubble formation lacking breakdown events but possessing electrode damage was during the use of 2000 nanosharp tips at 2 to 50mm separation distances with pulses 2.5μs in duration.[79] Interesting enough is the extension of this technology beyond water as the only condensed phase of interest. If non-thermal plasma can be generated in water without bubble formation, perhaps it could also be initiated at very low currents in non-polar, dielectric liquids without vaporization of the medium. Enhanced current injection has long been known for sharp metal emitters in non-polar hydrocarbons.[80] Recent work confirms that dc corona regime discharge can activate silicon oil from nanoemitters.

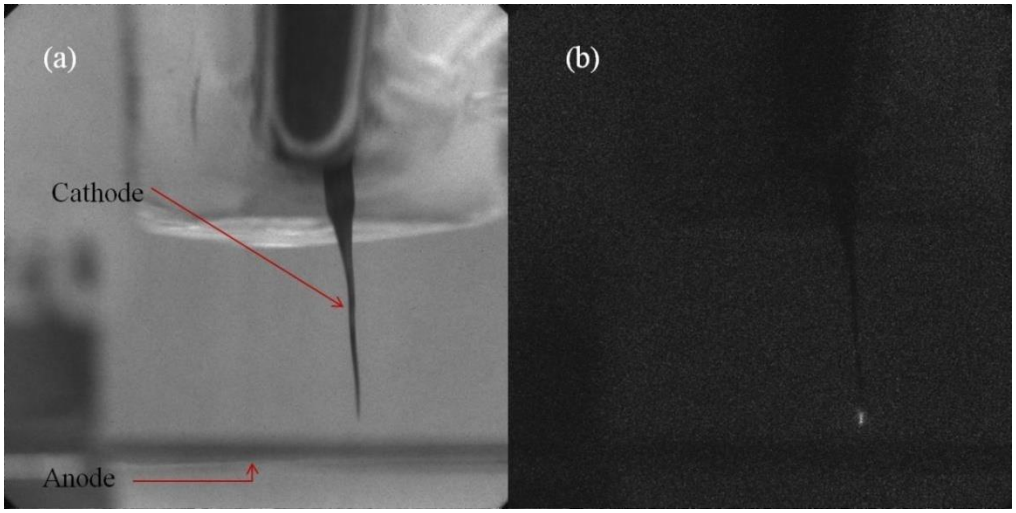

Figure 18: Images of the electrode setup in silicon oil for a discharge gap of ~ 1.0 mm (cathode is a stainless-steel wire) for (a) No-discharge, ambient lights on and (b) Discharge current of 2 μA and an exposure time of 50 msec. [81]

The streamer discharge is localized to the point and pin in these dielectrics before streamer formation just as it was shown to be in the water system.

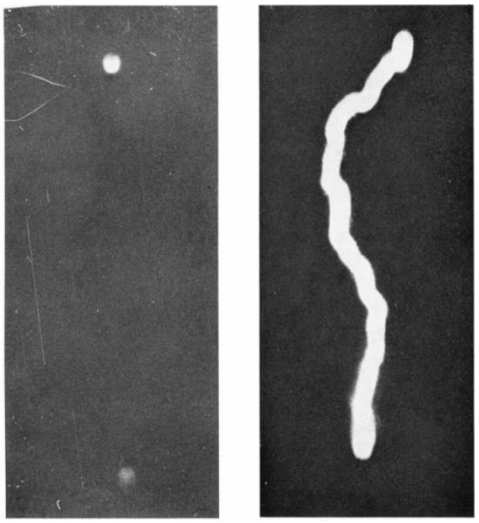

Figure 19: Pin to point discharge in high dielectric liquid which appears localized during at least part of the discharge process prior to streamer formation. [82]

If the pulse time is short enough, an area of reactive liquid in a plasma discharge around carbon nanotube emitters or fields of sharp crystals or metal tips may be possible. The photochemical activity of the discharge has long been reported.[83] This discovery necessarily mandates extensive characterization and scrutiny.

The non-equilibrium environment of non-thermal plasma yields the advantage of promoting non-kinetically favored reactions at ambient temperature and atmospheric pressure. Correspondingly, diverse applications for the many discussed modes of non-thermal plasma exist.[84] Not in the least is the ability to generate stable plasma at atmospheric pressure avoiding high cost <1mTorr operations. Continuous flow production of the smallest nanoparticles (1-5nm) during flow through microplasma synthesis is a promising option for nanoparticle production. Homogeneous nucleation is favored in high pressure plasmas. Additionally, the non-equilibrium conditions allow for spatially distinct electron driven chemistry to occur within the same plasma which makes processes tunable both by structure and energetics.

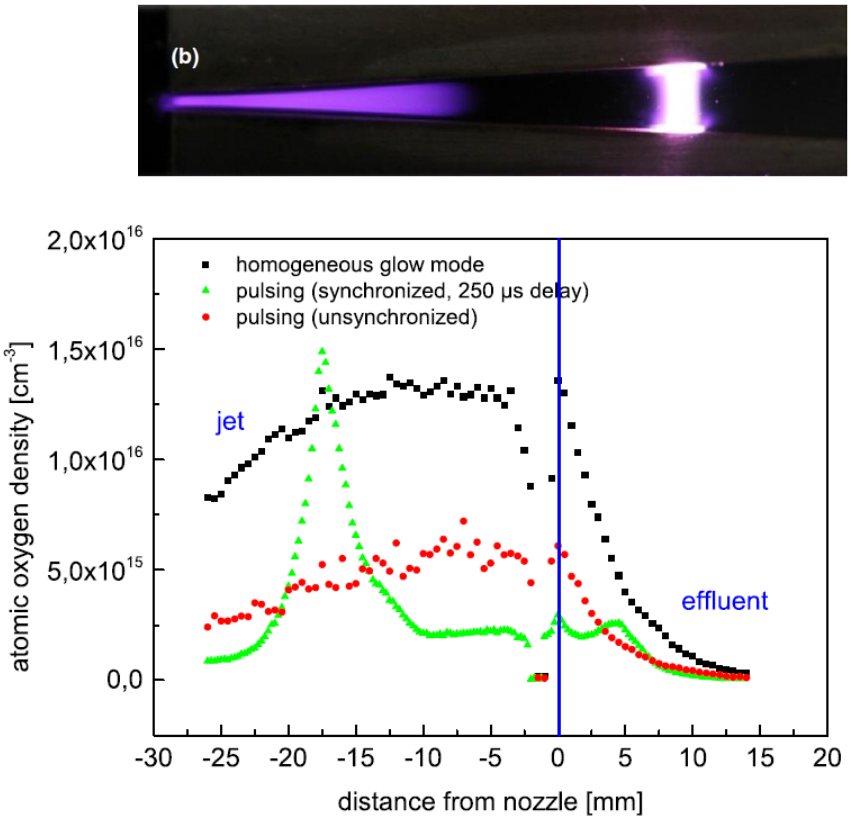

Figure 20: Coexistence of glow and constricted discharges. [85]

Solid state growth and epitaxy

Advances in nanoscience utilizing this decade's innovation in atmospheric pressure plasma are extensive. The advantage of microplasma arrays and self-organization of oxides and carbon along surface electric field lines are pointed out as very promising applications of non-thermal plasma.[86] Copper oxide thin films such as vertically aligned wires, needles, leaves, trees and fans can be grown at pressures of 10-50Torr. [87] Reasons for the necessary operation at low pressure and for the use of noble gases are likely the non-microspatial scales employed in these technologies which treat as much as 20mm^2 of a sample from distances of 5-40mm. The uniformity of the carbon film depositions in the atmospheric pressure non-thermal plasma section has already determined what precision is involved in deposition processes at these reduced scales. Vertically aligned metal oxide nanostructures are grown at distances of 5-50mm at

pressures up to 100Torr. These metal oxide structures varied from CuOtoPdO and NiO.[88] Atmospheric pressure arc discharge synthesis of TiO_2 nanorods is possible at a gas-liquid interface.[89] Etching of transmitting conductive oxide F:SnO_2 can produce a significantly enhanced topography. Triangular features trap light in photovoltaic devices at the interface of these transparent conducting oxide layers.[90] Non-thermal 10mTorr, 13.56MHz plasma at 7cm is capable of producing very high quality 5-10nm silicon nanocrystal production with 50% utilization from flow through silane.[91] Europium doped yttria red phosphor used in light emitting devices can be synthesized through sintering non-thermal plasma at vacuum pressures.[92] This reactive spark plasma sintering is capable of densifying the microstructure of ZrB_2-SiC to yield ultrahigh-temperature ceramics. The nanoparticle size for spark plasma sintering is three times smaller than when using more traditional reactive hot pressing which leaves secondary phases at the grain boundaries reducing high-temperature mechanical properties.[93] Thermoelectric power generation from heat difference fluxes can be accomplished using Mg_2Si. It possesses good electrical conductivity and low thermal conductivity. Ball milling can produce dense nanocrystalline powders of Mg_2Si; however, spark sintering plasma increases compaction densification up to 98% which is critical to utilize Mg_2Si as a thermoelectric material.[94] Diamond-like carbon thin films can be deposited in controlled shear patterns based on the direction of plasma flow through microchannels at interfacial areas between the plasma ionized inert and the film precursor.[95] While it is possible to disperse reactive ions in gas surface deposition. It is the ability to disperse atmospheric pressure monodisperse plasma bubbles in microfluidic chips for possible nanomaterial synthesis that is truly exciting.[96] Thin films of SiO_x films have been reported similar to the carbon suboxide films already discussed and although impure represents the possibility of atmospheric pressure microplasma to generate Si films.[97, 98] The impurity of the films could easily be remedied at the microscale with nanostructured emitters using field emission dominated breakdown stimulated by external light emission. This strong photoionization and electron emission regime may eliminate the formation of charge pairs undergoing backwards ion bombardment by supplying ejected electrons at the boundary of the emitter. Backward ion bombardment is responsible for electrode

sputtering and has also been eliminated in nanosecond pulse plasmas. These two techniques have never been proposed to improve film purity deposition to the author's knowledge. Glow discharge non-thermal plasma can oxidize gold nanoparticles on silicon as determined by XPS. The treatment was characterized using the $4f_{5/2}$ and $4f_{7/2}$ binding energies which changed over time providing rates for oxidation at the surface during 80μA discharge. The transient glow to arc regime which is self-pulsing was studied during microhollow cathode discharge. Ammonia is dissociated to nitrogen and hydrogen for 1.5sccm of ammonia at 480V and 9.2mA.[99] CeO_2-doped Ni/Al_2O_3 plasma treated nanocatalyst is able to dry reform methane at higher production rates with the plasma treatment. A stronger base NiO and $NiAl_2O_4$ interaction, smaller size distribution and reduced agglomeration and more uniform morphology is reported with reduced deactivation during 550-850°C reaction steps. BET surface area is increased substantially for all catalyst samples above that of the wet impregnation technique. The catalyst shows improved coke formation resistance after plasma treatment and may be the effect of the produced spinel.[100]

Nanocrystal functionalization with polymer using two phase non-thermal plasma above a liquid interface achieved induced liquid chemistry that phenomenally impacted current density during illumination.[101]

Switching technology

The MOSFET has a switching analog in microplasma technology. MOPFET are microplasma field effect transistors which utilize ionized helium gas as the charge source needed at the gate in order to have switching in extremely high temperature conditions, typically higher than 1000°C, and under ionizing radiation encountered in space exploration. Currently, the mobility of the ions is too slow for rapid switching but electron emission at smaller scales of plasma would increase the mobility of the charge carrier which would promote rapid switching responses.[102]

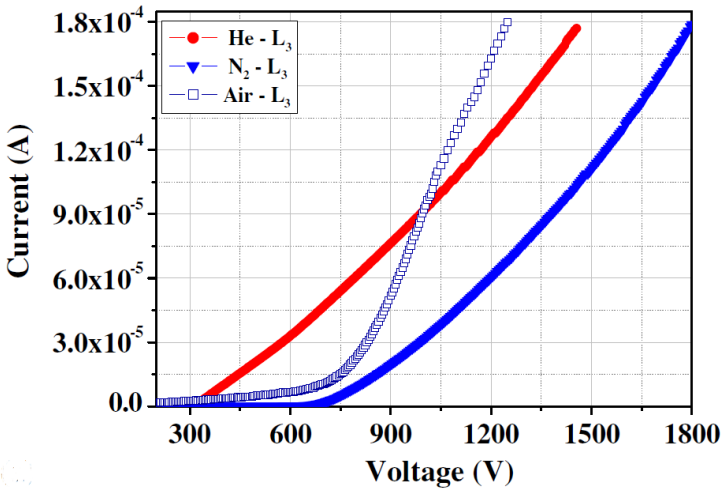

Figure 21: The light amplification under high electric field in 50μm gap at low currents from Reference [105].

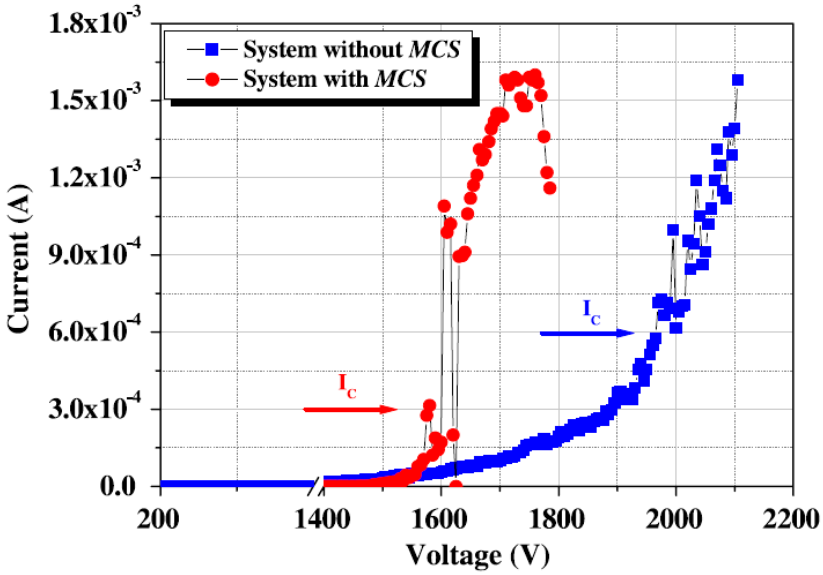

Figure 22: The distinct transition from light amplification with microcapillaries from Reference [105].

The reversal of energy consumption between townsend discharge and glow discharge for atmospheric pressure air discharges is interesting. The power of atmospheric glow discharge being ten times less than townsend discharges. Gain values for light amplification of the input can reach twenty. Microfabricated glow discharge plasma

has been coupled with desorptive ionization mass spectroscopy for efficient and robust detection of molecular substances 1.5kDa and less at the femptogram per square mm.

Sensing and light generation

Novel devices utilizing the flexibility of low power atmospheric pressure microplasma can be made through screen printing on paper substrates with line tolerances of 50μm for selected silk screens. These devices can sample liquid salt solutions with multiple metallic vapor emission lines using plasma spectroscopy.[103] Microwave activation of plasmas can be achieved with only 10V for switchable microplasma array resonators.[104] Light amplification of LED IR beams in microcapillary channels between GaAs semiconductor, Kapton and nickel electrode system under high dc electric field shows remarkable increase through avalanche, yielding a continuous discharge characteristic up to 1.5mA at 700Torr for a 50μm gap.[105]

Fuel reforming

Dielectric barrier discharge operates with alternating current and a non-conductive membrane or dielectric barrier. Microdischarges from aluminum electrodes have upgraded methane and methane/ethane mixtures to propane and butane at 10-15% selectivity. Gases with reduced ionization coefficients improves conversion.[106] Macroscopic dc discharges form ethane and ethylene even at room temperature. Streamer propagation versus the gentle primary glow maintained at the emitter electrode are offered as explanations for low yields.[107] Application of the gentle non-thermal, non-equilibrium plasma to achieve greater upgrading yields deserves attention. The application of nickel oxide ceramic fibers to dielectric barrier discharge at separations of 10mm increases emission stability and decreases the required electric potential by several times.[108] Hydrogen is produced almost exclusively at temperatures under 600°C at the thermodynamic equilibrium conversion rate for this non-equilibrium process.

Oxygen dissociation and oxidation reactions

Carbon dioxide decomposition is possible at atmospheric pressure at the separations near Paschen's minimum. Conversions reach 7.7% at flow rates of 3ml/min. The plasma shows instabilities and negative average trend in electric potential versus current despite constant average electric potential across the reactor of 340V. [109] The instabilities arise from local overheating or inadequate external stabilization by circuit reactance. Wastewater treatment is possible using ac dielectric-barrier, non-thermal plasma with mineralization rates as high as 47.3% for energy consumptions as low as $20.5 gkW^{-1}h^{-1}$. Cerium oxide catalyst was introduced to obtain synergistic effects.[110]The glow discharge to arc discharge transition has been used to provide large-volume, slow streamers which efficiently and rapidly combust methane and air during ignition as opposed to the small-volume, high current spark plug.[111] The optimization of non-thermal plasma is as equally interesting as its gentle glow counterpart. Trichel pulses, transient sparks and glow discharge were all used to evaluate sanitation of water samples sprayed and in water. The plasmas were all non-thermal and the spark regime was 2-3 orders of magnitude more efficient due to uniform and complete treatment of the liquid which flowed over the ground electrode or completely covered both electrodes during streamer discharge.[112] The scale of the discharge is listed as the governing factor related to efficiency and completeness of the remediation. This well-performed study points to the advantage of microscale technology as an enabling tool for stable gas and condensed phase non-thermal plasma reaction engineering. Dielectric barrier discharge has also been used to partially oxidize methane to methanol using added water which was demonstrated not to participate in the reaction kinetics expect for radical transport or to sequester liquid oxygenates as they are formed.[113] Pulsed corona discharge also has oxidation potential in air for low concentrations of aromatics using nanosecond pulsing technology at the industrial scale.[114]

A variety of approaches exist which can be used to extract useful information from complex chemical systems undergoing non-thermal plasma. There are mechanistic computational simulations which rely on experimentally determined wave functions,

photo-ionization and attachment coefficients to predict charge transport at a near fundamental level. Time based simulations match streak-diagrams from simulation to experiments to evaluate the corresponding accuracy of prediction for different streamer formation geometries and fields. Robust finite element solvers can fit charge transport physics for electrohydrodynamic flow without solving the non-thermal plasma charge distribution or time phase development of the discharge if the discharge is stable and at steady state in a dc field.[115] In simulations which rigorously treat ion-ion or ion-electron recombination during the development of the photo-ionizing streamer, a Boltzman equation solver like ELENDIF and a conservation law solver such as the monotonic upstream-centered scheme are required. [116] Critical to the proper development of the streamer dynamics is the introduction of photo-ionization. However photoionization is treated analytically during the simulation routine, being essentially based on experimental measurements such as from Penney and Hummert.[117]

Limiting cases for the dimensionless kernel for photo-ionization are not tractable except at limiting extremes.[118] The development of the discharge near the onset condition for non-thermal plasma streamer formation in air has been treated in the finite element solver COMSOL coupled with a MATLAB environment and corroborated reasonably with discharge at 5kV.[119] The onset potential can be accurately predicted from established experimentation for cylindrical anodes.[120] The finite difference time domain simulation method has been used to accurately model the current versus voltage characteristic of 6mm ball to plate non-thermal plasma discharges.[121] Integro-differential interface equations provide accurate contour predictions for complex geometries to generate explicit solutions including small symmetry-breaking perturbations.[122] An example of streak diagrams used for evaluation of time dynamic streamer formation coupled to charge transport with classical drift, diffusion and reaction for the prediction of chemical specie formation.[123]

The differences between negative ac and dc partial discharges are detailed succinctly with respect to mathematical formulation.[124] Alternatives to complete solution to temporal dynamic simulations of non-thermal plasma are dimensionless analyses

which can be an efficient and often a more useful tool in engineering applications. The fundamental parameters which have been inserted into computationally demanding software, that do not even offer explicit solutions frequently, still rely on experimental wave function measurements for the photo-ionization absorption function. If the same parameters that impact the coupled systems of partial differential equations for both electrostatics and conservation of momentum and mass are inserted into dimensionless quantities and fit to experimental data, a better understanding of the parameters is achieved.[125] While macroscopic breakdown has been traditionally well characterized by the development leading to the formulation of Paschen's curve, microplasma assisted breakdown events have been demonstrated to be highly dependent on field emission from the cathode emitter to the positive space charge region. For this the Townsend avalanche criterion is modified to obtain a modified Paschen curve.[126]

$$\left(\gamma_{se}-\gamma^{'}\right)\left(e^{\alpha d}-1\right)=1$$

Where the well-known criterion has been modified to include the ion-enhancement coefficient ($\gamma^{'}$) depicting the influence of field emission and its enhancement due to positive space charge. The secondary electron emission coefficient (γ_{se}) being in this way diminished by considering the one-dimensional microdischarge behavior. Also, α is the microscale ionization coefficient. The total steady state current density and ion-enhancement coefficient of interest can be found after assumptions in the scale of the change in the positive space charge electric field (E^{+}).

$$\gamma^{'}=\frac{1-\left[1-\gamma_{se}\left(e^{\alpha d}-1\right)\right]e^{-D_{FN}E^{+}/E^{2}}}{\left(e^{\alpha d}-1\right)\left(1+2E^{+}/E\right)}-\gamma_{se}$$

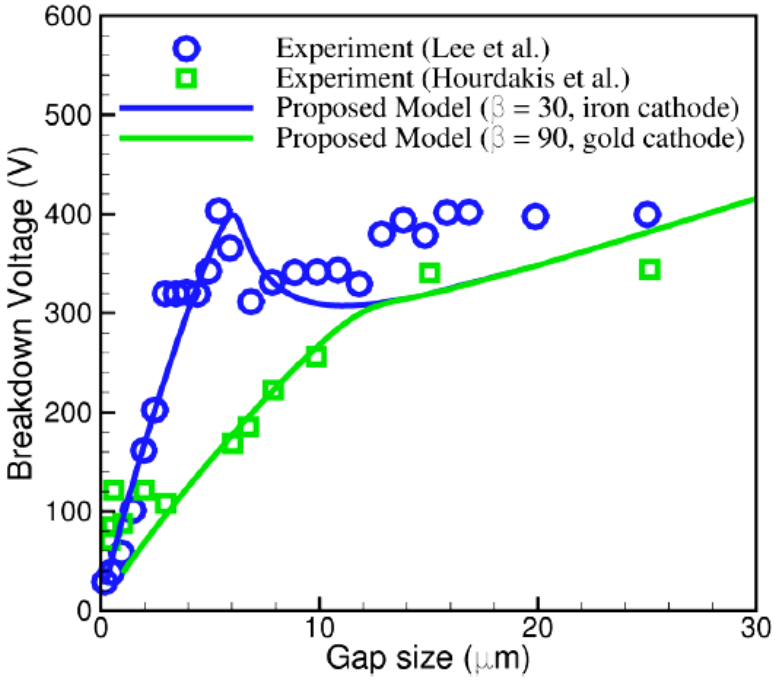

Figure 23: The scaling model developed for field emission enhanced microplasmas compared to experimental data from Reference [126].

Simulations have been performed for inverse pyramidal microcavity plasmas at 10μm with each cavity operating at atmospheric pressure in dielectric barrier discharge at 10kHz. The interaction between extremely dense arrays of microcavities through photoionization and sequential drift of ions between cavities influences the overall discharge pattern. The initial plasma seed for the simulation is a 10μm Gaussian plasma.[127]

Step by step methods employing independent reaction time techniques for liquids exposed to ionizing radiation can be used to calculate radiolytic yields. This technique tracks the radiolytic species. Classical drift diffusion equations ignore these species spatially. Monte-Carlo SBS LET Fricke dosimetry has been used to determine G factors for radiolytic yield in the most mechanistic models available in the liquid phase.[128]

Higher order mechanistic models and dimensional analyses can be complemented with kinetic models of dc non-thermal discharges or pulsed dc discharges. These models ignore spatial transfer of charged species in ionizing streamers by attempting to relegate the reactive zone to a certain part of the reactor. The rate kinetics absorbs the differences in reactive energy for different plasma powers and scale with changing conditions. The trends in rate kinetics and the reaction volume are fit using sensitivity analysis and Chi squared approach. The effective volume for reactive species impacts reaction engineering design and provides useful chemical conversion pathways for non-thermal plasma processes. Reaction engineering compartment modeling and Navier-Stokes simulation, which treats drift-diffusion transport with finite element modeling, compare very closely while providing different information.[129]

There are a variety of mathematical techniques with which to deal with the conservation equations either in compartment modeling or for the actual system. Variational iterations and decompositions including double or modified decompositions can rapidly produce results identical to finite element modeling with substantially lower computational time. Since new mathematical techniques are continually being developed, the discussion will be limited to some of the simplest and most efficient analytical approximation techniques having the widest applicability for both linear and non-linear reacting systems. Several examples will be offered building up to a comparison with COMSOL, a finite element modeling tool. The Adomian polynomial decomposition technique has been used to treat the simplest transport problems in heat transfer being elegantly compared to separation of variables.[130] The efficiency of the technique has been studied for parabolic equations and suggestions made for improvement in the recursion relationship offered in certain cases where the exact solution is not found in the zeroth component.[131] Great versatility is available using the Adomian decomposition method since the Adomian polynomial can be replaced by a variety of other polynomials which offer select and impressive advantages especially in non-linear cases arising in reaction engineering.[132] The chemical reaction-diffusion model of Brusselator has been treated sufficiently with the decomposition technique.[133] He’s variational iteration method solves a non-linear reaction diffusion Michaelis-

Menton kinetic enzymatic reaction with moving boundaries.[134] He's variational iteration method has also been used for the Cauchy reaction-diffusion problem avoiding discretization, linearization and pertebations which significantly reduces error and computation time.[135] The reaction-diffusion equation is offered using the Adomian decomposition method and summary of the development of these techniques stemming from 1986.[136] Fluid dynamic applications such as Blasius solution are easily treated by analytic approximates using the Adomian decomposition method.[137]

References

[1]P Rumbach, D M Bartels, R M Sankaran, D Go, "The solvation of electrons by an atmospheric-pressure plasma." Nat. Commun. (**2015**) 6, 7248

[2]A R Tuhy, E K Anderson, G N Jovanovic, "Urea separation in flat-plate microchannel hemodialyzer; experiment and modeling." Biomed Microdevices. (**2012**) 14, 595

[3]B P Mason, K E Price, J L Steinbacher, A R Bogdan and D T McQuade, "Greener Approaches to Organic Synthesis Using Microreactor Technology." Chem. Rev., (**2007**) 107, 2300-2318

[4]J Yoshida, A Nagaki, T Iwasaki and S Suga, "Enhancement of Chemical Selectivity by Microreactors." Chem. Eng. Technol., (**2005**) 28, 259-266

[5]D H Lee, K-T Kim, Y-H Song, W S Kang, S Jo, "Mapping Plasma Chemistry in Hydrocarbon Fuel Processing Processes." Plasma Chem. Plasma Proc. (**2013**) 33, 249

[6]E M van Veldhuizen and W R Rutgers, "Corona discharges: fundamentals and diagnostics." Invited Paper, Proc. Frontiers in Low Temp. Plasma Diagn. IV. (**2001**) 40

[7]V I Arkhipenko, A A Kirillov, Y A Safronau, L V Simonchik and S M Zgirouski. "Plasma nonequilibrium in self-sustained normal DC atmospheric pressure glow discharge in noble and molecular gases." ISPC confer., 191.

[8]Dion Savio Antao, "A study of Direct Current Corona Discharges in Gases and Liquids for Thin Film Deposition." PhD Thesis, Drexel University (**2009**)

[9]Z Zijie, L Jiun-ming, Z Jianguo, C Yongdong, K B Cheong, "Study Of Shock And Induced Flow Dynamics By Pulsed Nanosecond DBD Plasma Actuators." Asia J. (**2014**) 52nd Aerospace Sciences Meeting

[10]C Jiang, M T Chen, M A Gundersen, "Polarity-induced asymmetric effects of nanosecond pulsed plasma jets." J Phys. Appl. (**2009**) 42, 232002

[11]B Forestier, A Houard, I Revel, M Durand, Y B Andre, B Prade, A Jarnac, J Carbonnel, M Le Neve, J C de Miscault, B Esmiller, D Chapuis, A Mysyrowicz, "Triggering, guiding and deviation of long air spark discharges with femtosecond laser filmament." AIP Adv. (**2012**) 2, 012151

[12]Pramod K Singh, Jeffery Hopwood and Sameer Sonkusale. "Metamaterials for remote generation of spatially controllable two dimensional array of microplasma." Nature (**2014**) 4, 5964.

[13]Akira Mizuno. "Generation of non-thermal plasmas combined with catalysts and their application in environmental technology." Catalysis Today (**2013**) 211, 2-8

[14]C Penache, ABrauning-Demain, L Spielberger and H Schmidt-Bocking. "Experimental Study of High Pressure Glow Discharges Based on MSE Arrays." Confer.: Plasma Sci., (**2000**) 10, 1109

[15]T Ito, T Izaki and K Terashima. "Application of microscale plasma to material processing." Thin. Sol. Films (**2001**) 386, 300-304

[16]Marius Blajan and Kazuo Shimizu. "Spatial and temporal distribution of microplasma in small discharge gaps."IEEE trans. Indust. Appl. (**2013**) 49, 1787-1792

[17]Marius Blajan and Kazuo Shimizu. "Spatial distribution of light emission in microplasma under 100μm gaps."Jap. J. Appl. Phys. (**2012**) 51, 08HC031-5

[18]ZhongyuHou, BingchuCai and Hai Liu. "Mechanism of gas breakdown near Paschen's minimum in electrodes with one-dimensional nanostructures." Appl. Phys. Lett. (**2009**) 94, 163506

[19]Tao Shao, Victor F. Tarasenko, Cheng Zhang, Mikhail I. Lomaev, Dmitrii A. Sorokin, Ping Yan, Andrei V. Kozyrev and EvgeniKh. Baksht, "Spark discharge formation in an inhomogeneous electric field under conditions of electron generation," J. Phys. D: Appl. Phys. (**2012**) 111, 023304

[20]J G Eden, S J Park, J H Cho, M H Kim, T J Houlahan, B Li, E S Kim, T L Kim, S K Lee, K S Kim, J K Yoon, S H Sung, P Sun, C M Herring and C J Wagner. "Plasma Science and Technology in the Limit of the Small: Microcavity Plasmas and Emerging Applications." IEEE trans. Plasma Sci. (**2013**) 41, 661

[21]Lury Lee and Youngmin Kim."Low-voltage atmospheric-plasma generated by utilizing afterglow initiation carrier." IEEE trans. Plasma Sci. (**2013**) 41, 155-158

[22]David Staack, Bakhtier Farouk, Alexander Gutsol and Alexander Fridman."Characterization of a dc atmospheric pressure normal glow discharge." Plasma Sources Sci. Technol. (**2005**) 14, 700-711

[23]David Z Pai, Deanna A Lacoste and Christophe O Laux. "Transitions between corona, glow, and spark regimes of nanosecond repetitively pulsed discharges in air at atmospheric pressure." J. Phys. Appl. Phys. (**2010**) 197, 093303

[24]Jichul Shin, V Narayanaswamy, Laxminarayan L Raja and Noel T Clemens."Characterization of a Direct-Current Glow Discharge Plasma Actuator in Low-Pressure Supersonic Flow." AIAA J. (**2007**) 45, 1596-1605

[25]Zdenko Machala, Emmanuel Marode, Christophe O Laux and Charlses H Kruger. "DC Glow Discharges in Atmospheric Pressure Air." J. Adv. Oxid. Technol. (**2004**) 7, 133-137

[26]A J Wagner, D Mariotti, K J Yurchenko and T K Das. "Experimental study of a planar atmospheric-pressure plasma operating in the microplasma regime." Phys. Rev. (**2009**) 80, 065401

[27]Qiang Chen and Hajime Shirai, "Large-area cold atmospheric pressure discharges realized by mesh covered tube-plate electrodes in open air." IEEE trans. Plasma Sci. (**2013**) 41, 421-424

[28]David B Go and Daniel A Pohlman, "A mathematical model of the modified Paschen's curve for breakdown in microscale gaps." J. Appl. Phys. (**2010**) 107, 103303

[29]Takahito Ono, Dong YounSim and Masayoshi Esashi, "Micro-discharge and electric breakdown in a micro-gap." J. Micromech. Microeng. (**2000**) 10, 445-451

[30]Robert Geiger and David Staack, "Analysis of solid products formed in atmospheric non-thermal carbon monoxide plasma." J. Phys. D: Appl. Phys. (**2011**) 44, 274005

[31]D Staack, B Farouk, A Gutsol and A Fridman, "Stabilization of the ionization overheating thermal instability in atmospheric pressure microplasmas." J. Appl. Phys. (**2009**) 106, 013303

[32]StanislavPekárek, "Experimental study of surface dielectric barrier discharge in air and its ozone production," J. Phys. D: Appl. Phys. (**2012**) 45, 075201

[33]Anil Ağiral, Tomohiro Nozaki, Masahiko Nakase and ShuheiYuzawa, "Gas-to-liquids process using multi-phase flow, non-thermal plasma microreactor," J. Chem. Eng. (**2011**) 167, 560-566

[34]Anil Agiral and J.G.E. Gardeniers, "On chip microplasma reactors using tungsten oxide nanowires and carbon nanofibers as electrodes," J. Phys. Chem. C: (**2008**) 112(39), 15183

[35]Federica Causa, Francesco Ghezzi, David Dellasega, Roberto Caniello and Giovanni Grosso, "Analysis of cathode geometry to minimize cathode erosion in direct current microplasma jet." J. Appl. Phys. (**2012**) 112, 123302

[36]B Shukla, V Gururajan, K Eisazadeh-Far, B Windom, D Singleton, M A Gundersen and F N Egolfopoulos, "Effects of electrode geometry on transient plasma induced ignition." J. Appl. Phys. (**2013**) 46, 205201

[37]L Li, Y-L Liu, Y-F Ge, Y Bin, J-J Huang, F-C Lin, "Generating diffuse discharge via repetitive nanosecond pulses and line-line electrodes in atmospheric air." Rev. Sci. Instrum. (**2013**) 84, 105105

[38]Abbas Semnani, Ayyaswamy Venkattraman, Alina A Alexeenko and Dimitrios Peroulis, "Frequency response of atmospheric pressure gas breakdown in micro/nanogaps." Appl. Phys. Lett. (**2013**) 103, 063102

[39] John Foster, Bradley S. Sommers, Sarah Nowak Gucker, Isaiah M. Blankson and Grigory Adamovsky, "Perspectives on the interaction of plasmas with liquid water for water purification," Trans. Plasma Sci.(**2012**) 40(5), 1311-1323

[40]Jufang Zhang, Jierong Chen and Xiaoyong Li. "Removal of phenolic compounds in water by low-temperature plasma: a review of current research." J. Water Res. Protect. (**2009**) 2, 99-109

[41]David R. Grymonpré, Amit K. Sharma, Wright C. Finney and Bruce R. Locke, "The role of Fenton's reaction in aqueous phase pulsed streamer corona reactors," Chem. Eng. J. (**2001**) 82, 189-207

[42]David R. Grymonpré, Wright C. Finney and Bruce R. Locke, "Aqueous-phase pulsed streamer corona reactor using suspended activated carbon particles for phenol oxidation: model-data comparison," Chem. Eng. Sci. (**1999**) 54, 3095-3105

[43]Yong Jun Liu and Xuan Zhen Jiang, "Phenol degradation by a nonpulsed diaphragm glow discharge in an aqueous solution," Environ. Sci. Technol. (**2005**) 39, 8512-8517

[44]Xinglong Jin, Hongmei Zhang, Xiaoyan Wang and Minghua Zhou, "An improved multi-anode contact glow discharge electrolysis reactor for dye discoloration," Electr.Acta (**2012**) 59, 474-478

[45]Ryo Amano and Meguru Tezuka, "Mineralization of alkylbenzenes in water by means of contact glow discharge electrolysis," Water Res. (**2006**) 40, 1857-1863

[46]Jinzhang Gao, Jie Yu, Yan Li, Xiaoyan He, Lili Bo, Lumei Pu, Wu Yang, Quanfang Lu and Zhiming Yang, "Decoloration of aqueous Brilliant Green by using glow discharge electrolysis." J. Hazard. Mat. (**2006**) B137, 431-436

[47]A Hickling and M D Ingram, "Contact Glow-Discharge Electrolysis," (**1964**), 783-793

[48]Petr Lukes and Bruce R Locke, "Plasmachemical oxidation processes in a hybrid gas-liquid electrical discharge reactor," J. Phys. D: Appl. Phys. (**2005**) 38, 4074-4081

[49]A M Anpilov, E M Barkhudarov, Yu B Bark, Yu V Zadiraka, M Christofi, Yu N Kozlov, I A Kossyi, V A Kop' ev, V P Silakov, M I Taktakishvili and S M Temchin. "Electric discharge in water as a source of UV radiation, ozone and hydrogen peroxide." J. Phys. D: Appl. Phys. (**2001**) 34, 993-999

[50]Dmitry V. Vyalykh, Alexander E. Dubinov, Igor L. L'vov, Sergey A. Sadovoy and Victor D. Selemir, "Making and Study of Moderate Pressure Glow Discharge on the Basis of Electrolytic Foamy Cathode, Prepared as the Aqueous Solution of $NaHCO_3$," J. Mod. Phys. (**2010**) *1*, 236-243

[51]Heejoon Kim, Akira Mizuno, Yuhei Sakaguchi, Guoqing Lu and Masayoshi Sadakata, "Development of a new dry-desulfurization process by a non-thermal plasma hybrid reactor," Energ.Fuels. (**2002**) 16(4), 803-808

[52]Wan-Ying Liu, Zheng-Lan Lei and Jin-Kun Wang, "Kinetics and Mechanism of Plasma Oxidative Desulfurization in Liquid Phase," Energy & Fuels (**2001**) *15*, 38-43

[53]Mohammed Elsawah, Hany H. Abdel Ghafar, Nasser N. Morgan, Safwat Hassaballa, Ahmed Samir, Farouk F. Elakshar and Abdou A. Garamoon, "Corona discharge with electrospraying system for phenol removal from water," IEEE Trans. Plasma Sci. (**2012**) 40(1), 29-34

[54]Noriaki Sano, Yuichi Yamane, Yoshio Hori, Takuya Akatsuka and Hajime Tamon, "Application of Multiwalled Carbon Nanotubes in a Wetted-Wall Corona-Discharge Reactor To Enhance Phenol Decomposition in Water," Ind. Eng. Chem. Res. (**2011**) 50, 9901-9909

[55]Qusay A Abbas, Fadhil Y Hadi, Majid H Dwech and Falah A-H Mutlak, "Comparison the Formation of Spark Corona Discharge between Tap and distilled Waters at Liquid Electrode." J. Baghdad Sci. (**2013**) 10, 237-242

[56]Sven Tombrink, Saskia Muller, Richard Heming, Antje Michels, Peter Lampen and Joachim Franzke, "Liquid analysis dielectric capillary barrier discharge."Anal.Bioanal. Chem. (**2010**) 397, 2917-2922

[57]P. Bruggeman, J. Degroote, C. Leys and J. Vierendeels, "Plasma characteristics in air and vapor bubbles in water." 28th ICPIG (**2007**) 10

[58]Muhammad Arif Malik, "Water purification by plasmas: which reactors are most energy efficient," Plasma Chem. Plasma Proc. (**2010**) 30, 21-31

[59]U. Kogelschatz, "Applications of Microplasmas and Microreactor Technology." Contrib. Plasma Phys. (**2007**) 47, 80-88

[60]Yasuhiro Wada, Martin A. Schmidt and Klavs F. Jensen, "Flow Distribution and Ozonolysis in Gas-Liquid Multichannel Microreactors." Ind. Eng. Chem. Res. (**2006**) 45, 8036-8042

[61]M MSein, Z Bin Nasir, U Telgheder and T C Schmidt, "Studies on a non-thermal pulsed corona plasma between two parallel-plate electrodes in water." J. Phys. D: Appl. Phys. (**2012**) 45, 225203

[62]Pavel Sunka, "Pulse electrical discharges in water and their application." Phys. Plasmas (**2001**) 8, 2587-2594

[63]A Abou-Ghazala, S. Katsuki, Karl H. Schoenback, F.C. Dobbs and K.R. Moreira, "Bacterial Decontamination of Water by Means of Pulsed-Corona Discharges." IEEE Trans. Plasma Sci. (**2002**) 30, 1449-1453

[64]H Akiyama, "Streamer Discharges in Liquids and their Applications."IEEE Trans. Dielectrics and Electr. Insulation (**2000**) 7, 646-653

[65]J Sidney Clements, Masayuki Sato and Robert H. Davis, "Preliminary Investigation of Prebreakdown Phenomena and Chemical Reactions Using a Pulsed High-Voltage Discharge in Water." IEEE Trans. Ind. Appl. (**1987**) 2, 224-235

[66]Jong-Hyuk Choi and Bok-Hee Lee, "Electrical Properties Associated with Discharge Developments in Water Subjected to Impulse Voltages," J. Elect. Eng. Tech. (**2010**) 5, 156-162

[67]Karel Vokurka and Jaroslav Plocek, "Experimental study of the thermal behavoir of spark generated bubbles in water." Experim. Therm. Fluid Sci. (**2013**) 51, 84-93

[68]Kiminobu Imasaka, Wei Sun, Hironari Tomita, Yuki Kato, Usama Khaled and Junya Suehiro, "Enhancement and Stabilization of Pulsed Steamer Discharge in Water by Adding Carbon Nanotubes," Jap. J. Appl. Phys. (**2010**) 49, 086203

[69]Xiao Qiong Wen, Gui Shi Liu and Zhen Feng Ding, "Temporal Evolution of the Pulsed Positive Streamer Discharge in Water," IEEE Trans. Plasma Sci. (**2012**) 40(2) 438-443

[70]David Staack, Alexander Gutsol, Gary Friedman and Alexander Fridman, "Preliminary Evaluation of Low Power Pulsed Corona Discharge for Characterization of Liquids." Plasma Assist. Decontam. Biolog. Chem. Agents. (**2008**) NATO Sci. Peace Security: Chem. and Biology, 79-86

[71]David Staack, Alexander Fridman, Alexander Gutsol, Yury Gogotsi and Gary Friedman, "Nanoscale Corona Discharge in Liquids, Enabling Nanosecond Optical Emission Spectroscopy," Angew. Chem. (**2008**) 120, 8140-8144

[72]Sayan Bhattacharyya, David Staack, Elina A. Vitol, RijuSinghal, Alexander Fridman, Gary Friedman and Yury Gogotsi, "Localized Synthesis of Metal Nanoparticles Using Nanoscale Corona Discharge in Aqueous Solutions." Adv. Mater. (**2009**) 21, 4039-4044

[73]M E Pinchuk, V A Kolikov, Ph G Rutberg, A G Leks, R V Dolinovskaya, V N Snetov and A Yu Stogov, "Dynamics of bubble generated by low energy pulsed electric discharge in water." J. Phys. Conf. Series (**2012**) 406, 012035

[74]Bret Halpern and Robert Gomer, "Field Emission in Liquids," J. Chem. Phys. (**1969**) 51, 1031-1047

[75]Bret Halpern and Robert Gomer, "Field Ionization in Liquids," J. Chem. Phys. (**1969**) 51, 1048-1055

[76]B S Sommers and J E Foster, "Nonlinear oscillations of gas bubbles submerged in water: implications for plasma breakdown." J. Phys. D: Appl. Phys. (**2012**) 45, 415203

[77]Danil Dobrynin, Yohan Seepersad, Mikhail Pekker, Mikhail Schneider, Gary Friedman and Alexander Fridman, "Non-equilibrium nanosecond-pulsed plasma generation in the liquid phase (water, PDMS) without bubbles: fast imaging, spectroscopy and leader-type model." J. Phys. D: Appl. Phys. (**2013**) 46, 105201

[78]Anders Sunersson, Peter Barmann, Stefan Kroll and Lars Walfridsson, "Laser Triggering of Electric Breakdown in Liquids." IEEE Trans. Dielect. Elect. Insulat. (**1994**) 1, 680-691

[79]V S Teslenko, A I Zhukov, V V Mitrofanov and A P Drozhin, "A multispark electric discharge in a liquid." 5th Intern. Conf. Korea (**1997**) 03P20

[80]G Coe, J F Hughes and P E Secker, "High-current injection into liquid hexane using field emitters." Brit. J. Appl. Phys. (**1966**) 17, 885-890

[81]Dion Savio Antao, "A study of Direct Current Corona Discharges in Gases and Liquids for Thin Film Deposition." PhD Thesis, Drexel University (**2009**)

[82]N Shammas, C.W. Smith and J.H. Calderwood, "Coronas in insulating liquids," J. Phys. D: Appl. Phys. (**1974**) 7, 2587-2592

[83]Horst Metzler and Werner F. Schmidt, "On corona light emission in dielectric liquids," J. Phys. D: Appl. Phys. (**1976**) 9, 198-200

[84]Davide Mariotti and R Mohan Sankaran, "Perspectives on atmospheric pressure plasmas for nanofabrication." J. Appl. Phys. (**2011**) 44, 174023

[85]Daniel Schroder, Sebastian Burhenn, Dennis Kirchheim and Volker Schulz-von der Gathen, "Enhanced oxygen dissociation in a propagating constricted discharge formed in a self-pulsing atmospheric pressure microplasma jet." J. Appl. Phys. (**2013**) 46, 464003

[86]T Belmonte, G Arnoult, G Henrion and T Gries, "Nanoscience with non-equilibrium plasmas at atmospheric pressure." J. Appl. Phys. (**2011**) 44, 363001

[87]T Koh, E O'Hara and M J Gordon, "Growth of nanostructured CuO thin films via microplasma-assisted, reactive chemical vapor deposition at high pressures." J. Cryst. Growth. (**2013**) 363, 69

[88]Travis L Koh, Evan C O'Hara and Michael J Gordon, "Microplasma-based synthesis of vertically aligned metal oxide nanostructures."Nanotechnol. (**2012**) 23, 425603

[89]E Acayanka, A TiyaDjowe, S Laminsi, C CTchoumkwe, S Nzali, A PoupiMbouopda, P T Ndifon and E M Gaigneaux, "Plasma-assisted synthesis of TiO_2 nanorods by gliding arc discharge processing at atmospheric pressure for photocatalytic applications." Plasma Proc. (**2013**) none

[90]J L Hodgkinson, M Thomson, I Cook and D W Sheel, "Non-thermal atmospheric pressure plasma etching of F:SnO_2 for thin film photovoltaics." J. Nanosci. Nanotechn. (**2011**) 11, 8403-8407

[91]Ozgul Yasar-Inceoglu, Thomas Lopez, Ebrahim Farshihagro and Lorenzo Mangolini, "Silicon nanocrystal production through non-thermal plasma synthesis: a comparative study between silicon tetrachloride and silane precursors." Nanotechn. (**2012**) 23, 255604

[92]Piotr Psuja, Wieslaw Strek and Ihar Yelkin, "Non-thermal plasma-driven synthesis of Eu^{3+}:Y_2O_3nanosized phosphors." J. Nanopart. Res. (**2014**) 16, 2176

[93]Wen-Wen Wu, Guo-Jun Zhang, Yan-Mei Kan, Pei-Ling Wang, Kim Vanmeensel, Jozef Vleugels and Omer Van der Biest, "Synthesis and microstructural features of ZrB_2-SiC based composites by reactive spark plasma sintering and reactive hot pressing." ScriptaMaterialia. (**2007**) 57, 317

[94]M Saleemi, M S Toprak, S Fiameni, S Boldrini, S Battiston, A Famengo, M Stingaciu, M Johnsson and M Muhammed, "Spark plasma sintering and thermoelectric evaluation of nanocrystalline magnesium silicide (Mg_2Si)." J. Mater. Sci. (**2013**) 48, 1940-1946

[95]Masahiro Hashimoto, Ryoto Sato, Shinya Kumagai and Minoru Sasaki, "A microplasma reactor chip: using interface in micro/nanochannels towards material processing." IEEE (**2013**) none

[96]Y Yamanishi, S Sameshima, H Kuriki, S Sakuma and F Arai, "Transportation of monodisperse microplasma bubble in microfluidic chip under atmospheric pressure." IEEE (**2013**) none

[97]J Benedikt, R Reuter, D Ellerweg, K Rugner and A von Keudell, "Deposition of SiO_x films by means of atmospheric pressure microplasma jets." None (**2010**)

[98]R Reuter, K Rugner, D Ellerweg, T de los Arcos, A von Keudell, J Benedikt, "The role of oxygen and surface reactions in the deposition of silicon oxide like films from HMDSO at atmospheric pressure." arXiv:1105.5899v3 (**2011**) none

[99]David D Hsu and David B Graves, "Microhollow cathode discharge stability with flow and reaction," J Phys. D: Appl. Phys. (**2003**) 36, 2898-2907

[100]Nader Rahemi, Mohammad Haghighi, Ali Akbar Babaluo, Mahdi FallahJafari and PooyaEstifaee, "CO_2 reforming of CH_4 over CeO_2-doped Ni/Al_2O_3nanocatalyst treated by non-thermal plasma." J. Nanosci. Nanotechnol. (**2013**) 13, 4896-4908

[101]Somak Mitra, Steffan Cook, Vladimir Svrcek, Ross A Blackley, Wuzong Zhou, Janez Kovac, Uros Cvelbar and Davide Mariotti, "Improved optoelectronic properties of silicon nanocrystals/polymer nanocomposites by microplasma-induced liquid chemistry." J. Phys. Chem. (**2013**) 117, 23198

[102]Faisal K Chowdhury, Yuying Zhang and M Tabib-Azar, "Fabrication and characterization of 3D microplasma field effect transistors." MEMS (**2013**) 669-672

[103]Cheng-Che Hsu, Jheng-Han Tsai, Yao-Jhen Yang, Ying-Chih Liao and Yen-Wen Lu, "A foldable microplasma-generation device on a paper substrate." J. Microelectromech. Syst. (**2012**) 21, 1013-1015

[104]Alan R Hoskinson, Pramod K Singh, Sameer Sonkusale and Jeffrey Hopwood, "Low-voltage switchable microplasma arrays generated using microwave resonators." IEEE Electron. Device Lett. (**2013**) 34, 804-806

[105]B G Salamov, S Ozcelik, AInaloz and T S Mammadov, "Study of light emission amplification in a semiconductor gas discharge system." J. Appl. Phys. (**2007**) 40, 6657-6668

[106]K Thanyachotpaiboon, S Chavadej, T A Caldwell, L LLobban and R G Mallinson, "Conversion of Methane to Higher Hydrocarbons in AC Nonequilibrium Plasmas."AIChE J. (**1998**) 10, 2252-2257

[107]Changjun Liu, Abdulathim Marafee, Bobby Hill, Genhui Xu, Richard Mallinson and Lance Lobban, "Oxidative coupling of methane with ac and dc corona discharges," Ind. Eng. Chem. Res. (**1996**) 35, 3295-3301

[108]Zhou ZhiPeng, Zhang JiMin, Ye TaoHong, Zhao PingHui and Xia WeiDong. "Hydrogen production by reforming of methane in a corona inducing dielectric barrier discharge and catalyst hybrid reactor."Chinese. Sci. Bulletin (**2011**) 56, 2162-2166

[109]Peter J Lindner, Sang Youp Hwang and R S Besser, "Analysis of a Microplasma Fuel Reformer with a Carbon Dioxide Decomposition Reaction."Energy Fuels. (**2013**) 27, 4432

[110]Pathpireddy Manoj Kumar Reddy, Allumolu Dayamani, Shaik Mahammadunnisa and Challapalli Subrahmanyam, "Mineralization of Phenol in Water by Catalytic Non-thermal Plasma Reactor – An Eco-Friendly Approach for Wastewater Treatment." Plasma Process. Polym. (**2013**) 10, 00084

[111]M Bellenoue, S A Labuda and M Engles, "Corona discharge ignition and combustion promotion of methane/air mixtures." European Combustion Meeting (**2005**)

[112]Z Machala, I Jedlovsky, B Pongrac, L Chladekova, D Giertl and L. Sikurova, "Various dc discharges for sterilization at atmospheric pressure." 11th Intern. Symp. High Temp. Low Pressure Plasma (**2008**) 8, 530

[113]S A Nair, Tomohiro Nozaki and Ken Okazaki, "Methane oxidation conversion pathways in a dielectric barrier discharge reactor-Investigation of gas phase mechanism," Chem. Eng. J. (**2007**) 132, 85-95

[114]W F L M Hoeben, F J C M Beckers, A J M Pemen, E J M van Heesch and W L Kling, "Oxidative degradation of toluene and limonene in air by pulsed corona technology," J. Phys. D: Appl. Phys. (**2012**) 45, 055202

[115]Nels E Jewell-Larsen, Sergey V Karpov, Igor A Krichtafovitch, ViviJayanty, Chih-Peng Hsu and Alexander V Mamishev, "Modeling of corona-induced electrohydrodynamic flow with COMSOL multiphysics," Proc. ESA Ann. Meeting on Electrostatics (**2008**) Paper E1

[116]YounTaeg Kim and Ki WoongWhang, "Two-Dimensional Numerical Simulation of Radical Generation in the Positive Corona Discharge," IEEE Trans. Plasma Sci. (**2000**) 28(1), 261-267

[117]A A Kulikovsky, "The role of photoionization in positive streamer dynamics," J. Phys. D: Appl. Phys. (**2000**) 33, 1514-1524

[118]Manuel Arrayás, Marco A Fontelos and José L Trueba, "Photoionization effects in streamer discharges," PACS arXiv (**2006**) 1-17

[119]Nam-Kyung Kim, Se-Hee Lee, G.E. Georghiou, Dong-Wook Kim and Dong-Hun Kim, "Accurate Prediction Method of Breakdown Voltage in Air at Atmospheric Pressure," J. Electr. Eng. & Tech. (**2012**) 7(1), 97-102

[120]Yuesheng Zheng, Bo Zhang and Jinliang He, "Onset conditions for positive direct current corona discharges in air under the action of photoionization," Phys. Plasmas (**2011**) 18, 123503

[121]Baris Baykant Alagoz, Hafiz Z. Alisoy, Serkan Alagoz and Fevzi Hansu, "A space charge motion simulation with FDTD method and application in negative corona electrostatic field analysis," Appl. Math. Comp. (**2012**) 218, 9007-9017

[122]Manuel Arrayás and Marco A. Fontelos, "Electric discharge contour dynamics model: the effects of curvature and finite conductivity," PACS arXiv (**2011**) 1-23

[123]O Eichwald, O Ducasse, D Dubois, A Abahazem, N Merbahi, M Benhenni and M Yousfi, "Experimental analysis and modeling of positive streamer in air: towards an estimation of O and N radical production," J. Phys. D: Appl. Phys. (**2008**) 41 234002

[124]R J Van Brunt, "Physics and Chemistry of Partial Discharge and Corona." IEEE Trans. Dielect. Elect.Insulat. (**1994**) 1, 761-784

[125]J E Jones, A Boulloud and R T Waters, "Dimensional analysis of corona discharges: the small current regime for rod-plane geometry in air." J. Phys. D: Appl. Phys. (**1990**) 23, 1652-1662

[126]A Venkattraman and A A Alexeenko, "Scaling law for direct current field emission-driven microscale gas breakdown." Phys. Plasmas. (**2012**) 19, 123515

[127]Alexander Wollny, Torben Hemke, Markus Gebhardt, Ralf Peter Brinkmann, Henrik Boettner, Jorg Winter, Volker Schulz-von der Gathen, Zhongmin Xiong, Mark J Kushner and Thomas Mussenbrock, "Ionization wave propagation on a microcavity plasma array." arXiv:1104.5579v2 (**2013**)

[128]Ianik Plante, "A Monte-Carlo step-by-step simulation code of the non-homogeneous chemistry of the radiolysis of water and aqueous solution-Part II: calculation of radiolytic yields under different conditions of LET, pH, and temperature," Radiat. Environ. Biophys. (**2011**) 50, 405-415

[129]E V Rebrov, M H J M de Croon and J C Schouten, "Development of the kinetic model of platinum catalyzed ammonia oxidation in a microreactor," Chem. Eng. J. (**2002**) 90, 61-76

[130]Alice Gorguis and Wai Kit Benny Chan, "Heat equation and its comparative solutions," Comput.Math. Appl. (**2008**) 2973-2980

[131]Bongsoo Jang, "Exact solutions to one dimensional non-homogeneous parabolic problems by the homogeneous Adomian decomposition method," Appl. Math.Comput. (**2007**) 186, 969-979

[132]M M Hosseini, "Adomian decomposition method with Chebyshev polynomials," Appl. Math.Comput. (**2006**) 175, 1685-1693

[133]Abdul-MajidWazwaz, "The decomposition method applied to systems of partial differential equations and to the reaction-diffusion Brusselator model," Appl. Math. Comput. (**2000**) 110, 251-264

[134]G Rahamathunissa and L Rajendran, "Application of He's variational iteration method in nonlinear boundary value problems in enzyme-substrate reaction diffusion processes: part1. The steady-state amperometric response." J Math. Chem. (**2008**) 44, 849-861

[135]Mehdi Dehghan and Fatemeh Shakeri, "Application of He's variational iteration method for solving the Cuachy reaction-diffusion problem." J Comp. Appl. Math. (**2008**) 214, 435-446

[136]Rahul Bhadauria, A.K. Singh and D.P. Singh, "Solution of Reaction-Diffusion Equation by Adomian Decomposition Method," Int. J. Eng. Sci. Technol. (**2012**) 4(6), 2626-2630

[137]Sonia M Holmquist, "An examination of the effectiveness of the Adomian decomposition method in fluid dynamic applications." PhD Thesis, University of Central Florida (**2007**)

Chapter 2- Electrical Characterization of DC Corona Microplasma Generated from Micropoints at Room Temperature and Ambient Pressure

Justin Pommerenck, Jordan Pommerenck, Jacob Lum, Yousef Alanazi, Peter Kreider, Yu Maio, Goran Jovanovic, Alexandre F T Yokochi, Nick AuYeung

(to be submitted)

2.1 - Abstract

Nonthermal plasma is investigated in micron to millimeter gaps. By reducing the plasma discharge gap from 2mm to 400μm, more than a twofold reduction in operating voltage is accomplished at the same current. This savings in energy arises from the intensified electric field that depends on the microplasma spacing. The full voltage versus current curve for dc microplasma is compared to that of classical low pressure plasma. Similarity in shape and appearance are demonstrated for both dc corona and glow discharge between plasma in both of these regimes at microspacings at high pressure and large spacings at low pressure. The conditions necessary to confine a 100-400μm active electron plume of a dc microcorona within a microchannel is successfully determined. Fields of active microcoronas are established in a single microreactor device for the first time at atmospheric pressure in air and an air mixture with hydrocarbons. This is the first report of fields of activated microcoronas confined to a microreactor platform for high efficiency chemical conversion. These electrical measurements are critical for informing the engineering design of high performance plasma microreactors for chemical synthesis.

Keywords:
Corona, microplasma, glow discharge, dc, microgap, current, voltage, atmospheric pressure plasma

2.2 – Introduction

Corona discharge has been electrically identified as a luminous partial discharge from wires, rods or other conductors when held at high electric potential relative to a geometrically opposing conductor. It has the disadvantage of only activating a small region of space directly at the emitting conductor and possibly at the opposite electrode as well. The term *corona discharge* is nearly always used exclusively for high pressure plasma discharges.

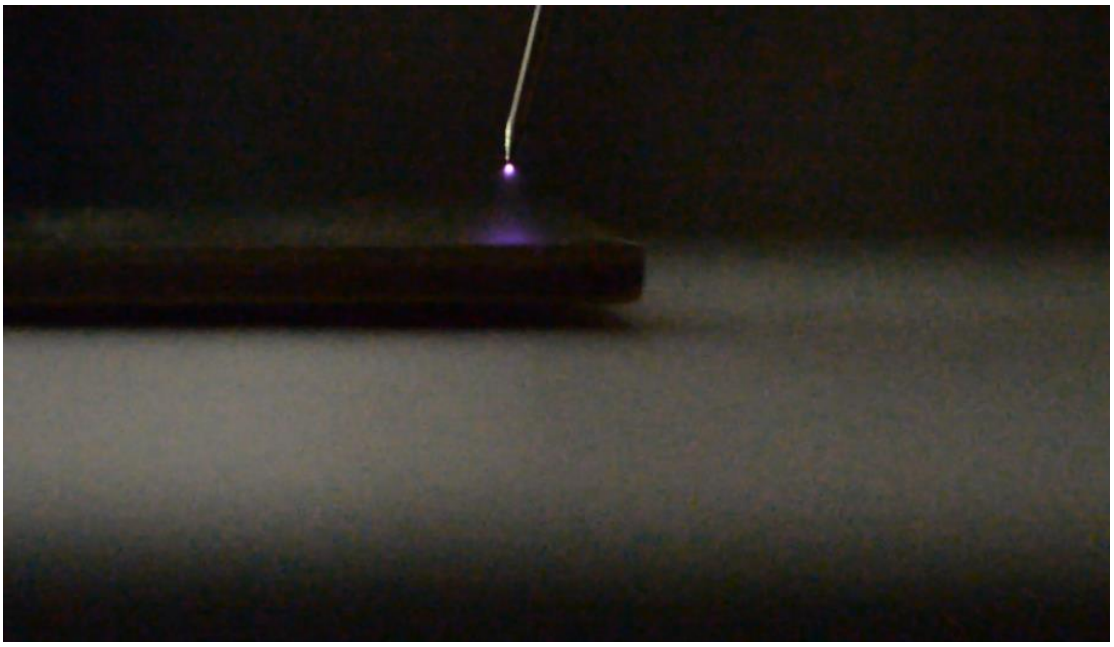

Figure 24: An example self-sustained corona discharge from a pin held 1.3mm from a brass plate.

The conditions for corona discharge to occur include the following: a large resistance from the dark space, a high aspect ratio for the corona to occur around, and a threshold current and voltage requirement for breakdown must meet the Townsend criteria which defines the conductivity of the dark space that is operating in the dark discharge regime. The electric field required to produce a corona of a certain diameter (d_c) has been estimated from Paschen's law calculations using air as the medium.

$$< E > \approx \frac{438}{ln(1340\ d_c)} \left[\frac{kV}{cm}\right]$$

For more than a century, the current distribution in a corona discharge has been commonly known to follow a Warburg distribution. A Warburg distribution has a higher current directly in line with the sharpest emission point.

$$j(\theta) = \frac{1}{2\,d^2} cos^5(\theta)$$

The resistance, provided by the bulk neutral air in the drift region of electric field intensity that is away from the corona, is highly non-linear. When the ionization front produces plasma faster than can be absorbed by the micropoint, a spark discharge occurs. A spark discharge has a higher electron energy and shorter duration than a corona discharge. A corona discharge can be formed which has a positive column and anode glow (AG) while still possessing a drift space.

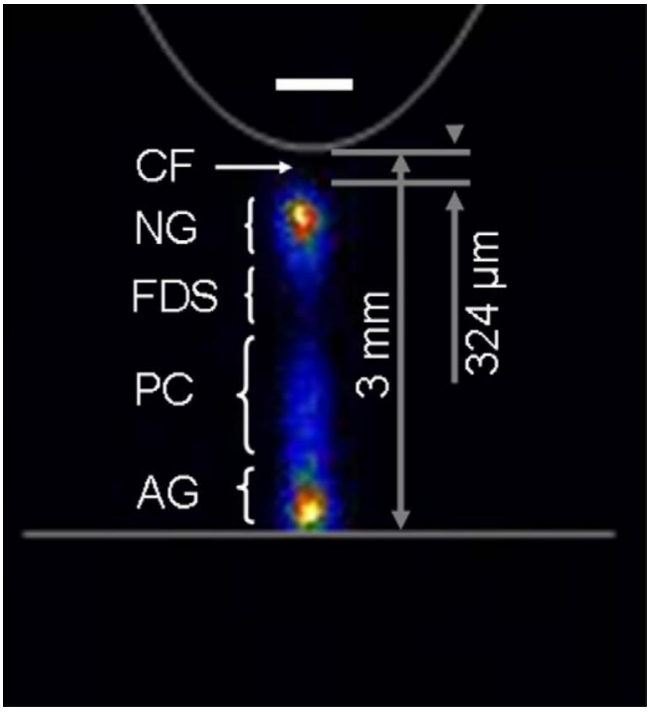

Figure 25: CCD image of a corona developed into a glow discharge.[138]

Under the condition that the dark space is bounded by the negative and positive charge column, the dark space is termed a Faraday dark space (FDS). This is a region which shows high voltage drop due to charge cancellation of negative and positive ions in the bipolar drift region. This entire discharge type is termed a glow discharge. It requires a lower overall voltage to sustain since its dark space is correspondingly reduced by the balancing of the extended positive column (PC) and negative glow (NG).

2.3 – Low pressure plasma versus high pressure microplasma

The pressure, at which a plasma exists, fundamentally alters its properties. The proximity of gas molecules and the electric field determines the free space charge density. At low pressure, the mean free path between gas molecules is high and charge interaction is reduced. At high pressure, charge interaction is magnified. The mean free path sets the electric field threshold for the current density at which columns of charge grow or rearrange. It is more useful to formulate the electric field as a reduced electric field. This is the electric field divided by pressure. In microplasma, the length scale separating the charged surfaces is fundamentally decreased in order to increase the electric field formed between the two electrodes. This increase in the electric field, similar to the increase to high pressure, makes the reduced electric field much closer to that which exists in low pressure plasma.

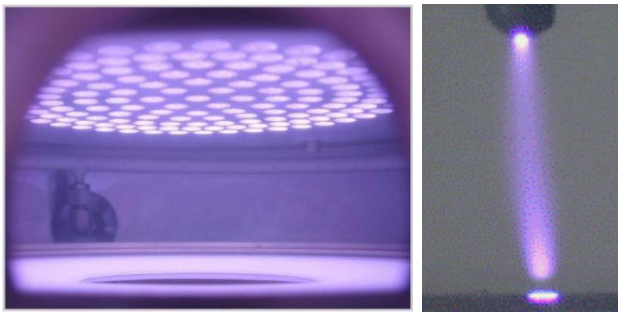

Figure 26: An industrial application of inductively coupled plasma (gas ring and gas transmission plate inside the process chamber of an Oxford Instruments PlasmaPro 100 ICP180 system during a plasma process) [139] *[left] and a recent experiment that is replicated in a small electrode gap* [140] *[right].*

As either the electrode separation gap or the pressure increases, it is possible to have both plasma in several stable states from the same set of electrodes merely by altering gas composition or gap separation.

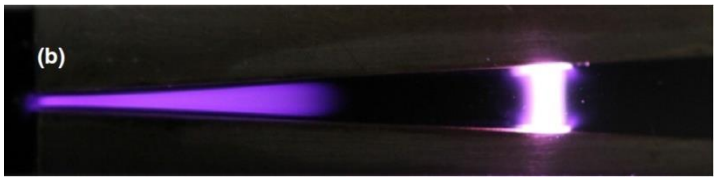

Figure 27: Simultaneous existence of two discharge types at different gap separations and gas compositions.[141]

In addition to the plasma distance and pressure, gas composition has a similar effect on the type of plasma that is formed. Each gas has its own ionization energy requirements and probabilities for its chemical activation network. The plot of voltage versus pressure multiplied by distance shows different voltage minimums for each gas. Noble gases show lower voltage minimums than gases which have diatomic.

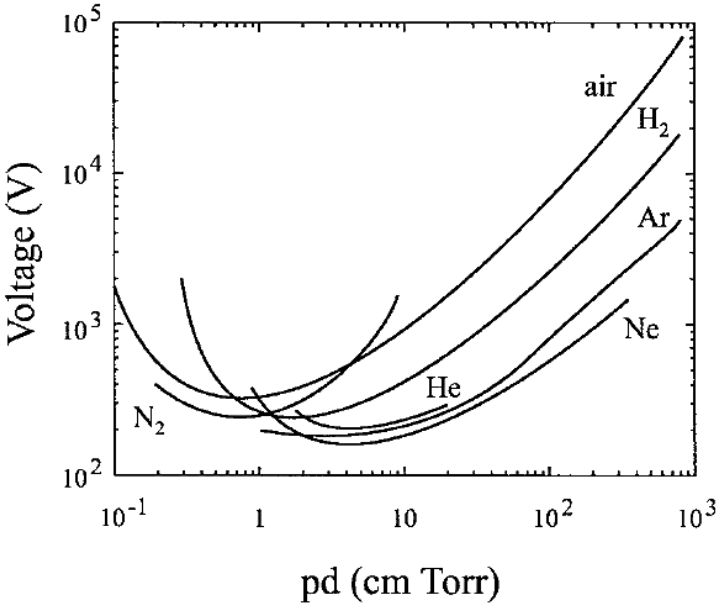

Figure 28: An example Paschen curve for several possible gases in parallel flat plates.[142]

It is useful to plot voltage versus current. The current, if increased, relates to the space charge density by increasing charge density the electrode gap distance. As current is increased the dark discharge region transitions to a glowing region with distinct partially illuminated to fully illuminated glow discharge region. Once the inner-electrode region becomes charge saturated and overheats (determined by the operating pressure), a glow to arc transition occurs.

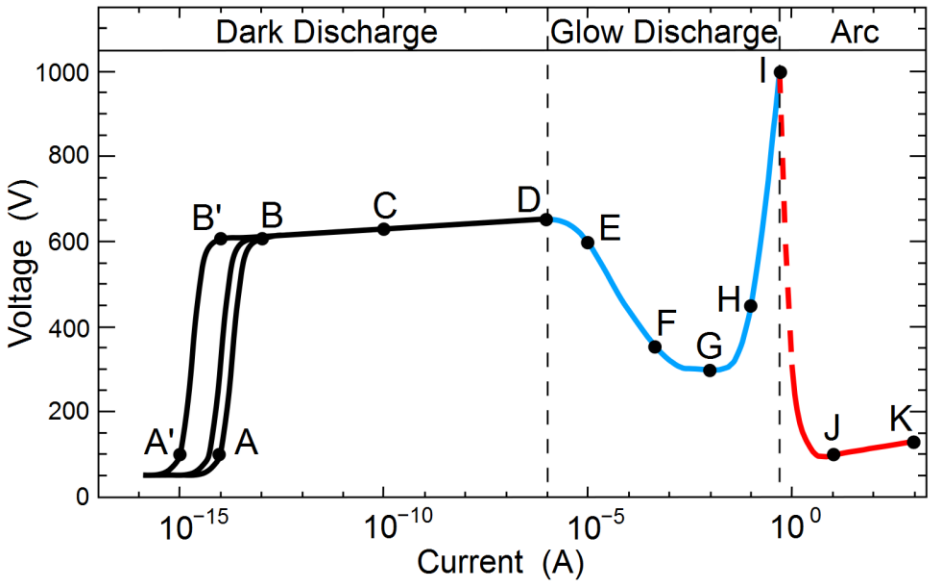

Figure 29: A current-voltage plot showing Townsend, glow and arc regimes (© [1975] IEEE).[143]

2.4 – Comparison of dc, ac, DBD, microwave and thermal to dc microplasma

The structure of dc, ac, DBD, microwave and thermal plasmas all differ based on its applied field. The location of its space charge and the distribution of energy in electrons, ions and neutrals define the properties and electronic characteristics for each type of plasma. For example, a schematic of a dc corona discharge shows the production of electrons near the discharge electrode and follows their interaction in the plasma region with gas molecules. The unipolar region shows the dark discharge transport of negative ions completing the electrical pathway.

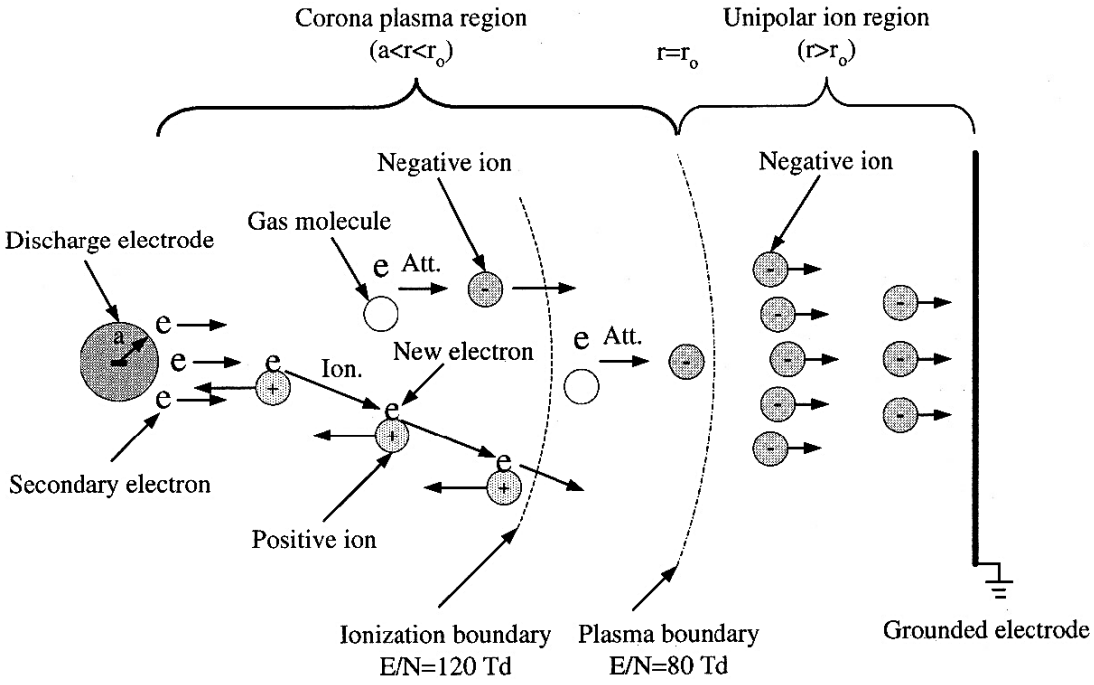

Figure 30: The negative corona discharge from wire to plate.[144]

The gas molecules can be activated in a variety of ways that imparts complexity when studying reactive mixtures. The charge density distribution for a corona discharge in a coaxial configuration in an oxygen atmosphere shows 10^{19} number density for ozone at moderate voltages.

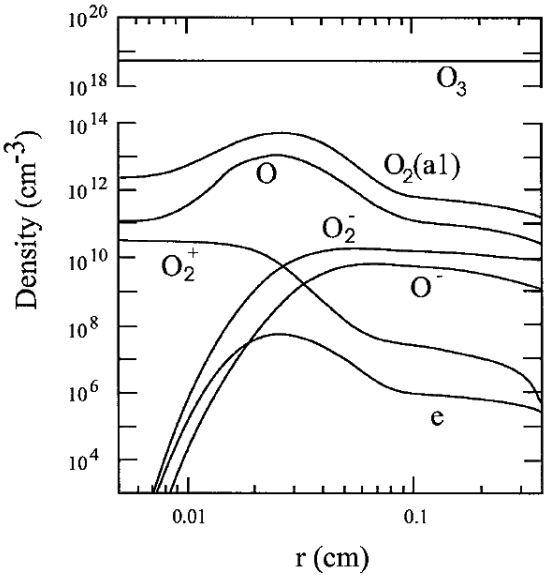

Figure 31: The electron plume extends from the negative electrode at the left side of the graph.[145]

Perhaps more interesting than the density of charged atoms is the electron energy distribution responsible for generating those species. Optimizing the electron average energy toward the activation energy of the desired reaction increases the efficiency of the process. Maxwell or Druyvesteyn prediction can be used for higher or lower degrees of ionization in many types of plasma.

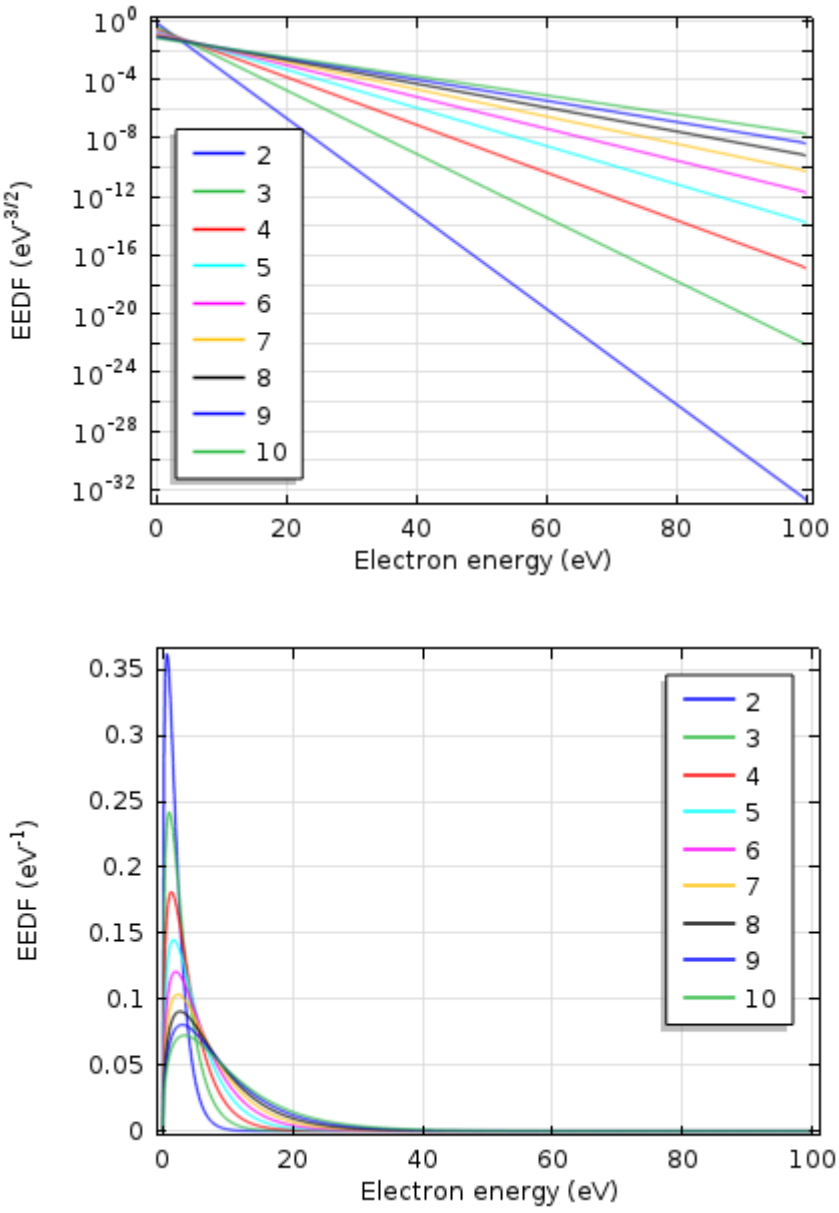

Figure 32: The Maxwell calculated electron energy for 2-10eV in a FEM package [Comsol].[146]

The reduced electric field E/N determines the electron distribution function and can range from 300 Td to 500 Td for DBD. Alternatively, the electron energy probability

function can be multiplied by the density to shift the EEDF from units of [$eV^{-3/2}$] to units of [$eV^{-3/2}$ m^{-3}].

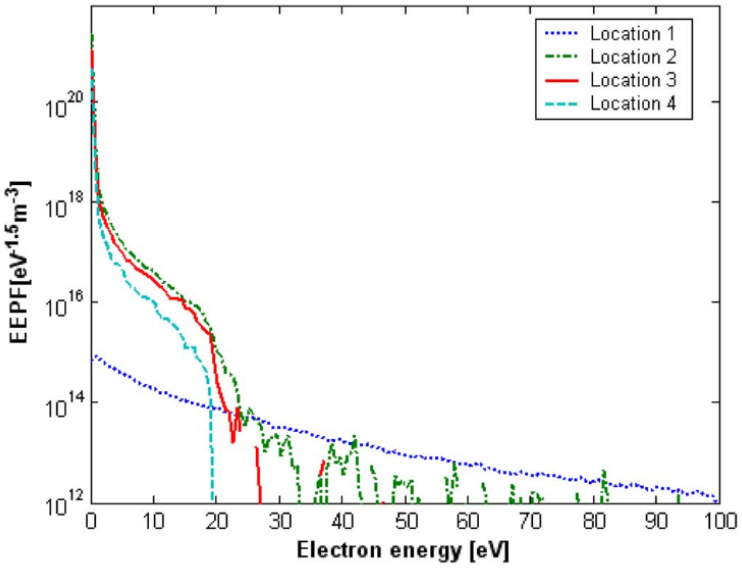

Figure 33: The electron energy distribution function for a dc microplasma in a 200μm gap. [147]

One conclusion from electron energy distribution measurements and calculations is that similar low pressure plasma can likely be generated in microgaps at high pressure.

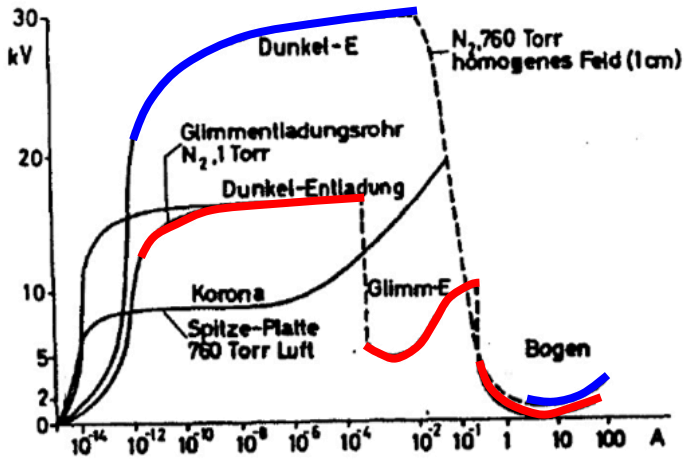

Figure 34: The differences in low and high pressure discharges in nitrogen are observed as an absence of the regime labeled Glimm-E (glow) under high pressure discharges.

The ability to reproduce classical low pressure voltage versus current plots and demonstrate similarity to high pressure microplasma voltage versus current plots is one

of the objectives of this electrical study. It can be seen from the previous figure that at high pressure (760 Torr) [blue], even in as small as 1cm gaps, the only plasma that can be generated is in the regime called Dunkel-E (dark) and Bogen (arc). At low pressure (1Torr) [red], Glimmentladungsrohr (smoldering glow), Glimm-E (glow) and Bogen (arc) are accessible.

2.5 – High pressure electrical measurement setup and discharge geometry

The equipment that is used for electrical measurement includes a Glassman High Voltage unipolar positive power supply, two Keithley 6-1/2-digit precision multimeters for continuous analog readings from the high voltage probes, several Agilent differential probes limited to under 10kV and resolving to 70MHz and a Hewlett-Packard HP54542A 2Gs/s oscilloscope is used to average pulsed discharges.

A schematic is included of the pin to plate geometry for the measurement of high pressure plasma in each of the fundamentally different E/N regions.

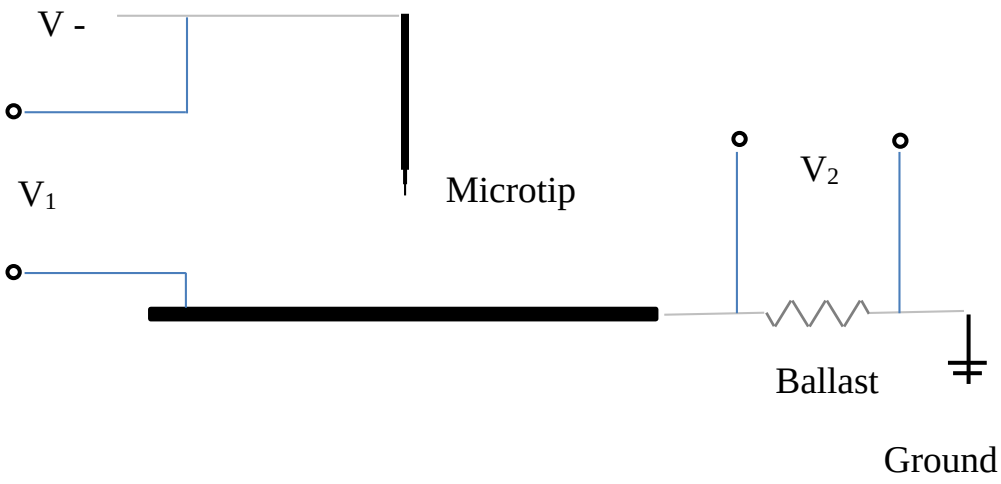

Figure 35: The schematic is illustrated with the V- potential indicating the lower potential from the unipolar power supply (ground) and the ground indicating the higher potential (positive) so that the relative potential is correct.

The microtip is an electrochemically etched Ni or Wu wire that is inserted in a microhole that is drilled in a flame proof fiberglass sheet.

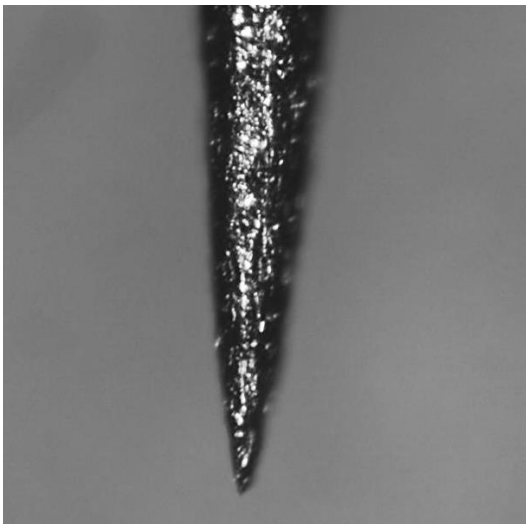

Figure 36: An optical micrograph showing the etched microtip has a <10µm tip.

For the multiple microtip experiment, 0.5mm nickel plated stainless steel sequin needles are used in arrays. These pins are set in 0.5mm holes drilled using a microCNC stage which defined the pattern based on G-code written during this study.

2.6 – Results from dc corona microplasma from single micropoints

The discharge current from a pin to the surface of a stainless steel and brass plate in air is recorded for 1.3mm (full curve) and 0.1-2mm (glow only) distances. The regime shown below is the glow discharge regime only. The dark discharge, corona and spark discharge are omitted before the curve. The arc regime is never attained and would have begun at the rightmost end of the data section. The discharge process is controlled by incrementally increasing the current limit at the power supply which has both voltage and current control limits with digital display. The minimum possible potential achievable in air is 371V.

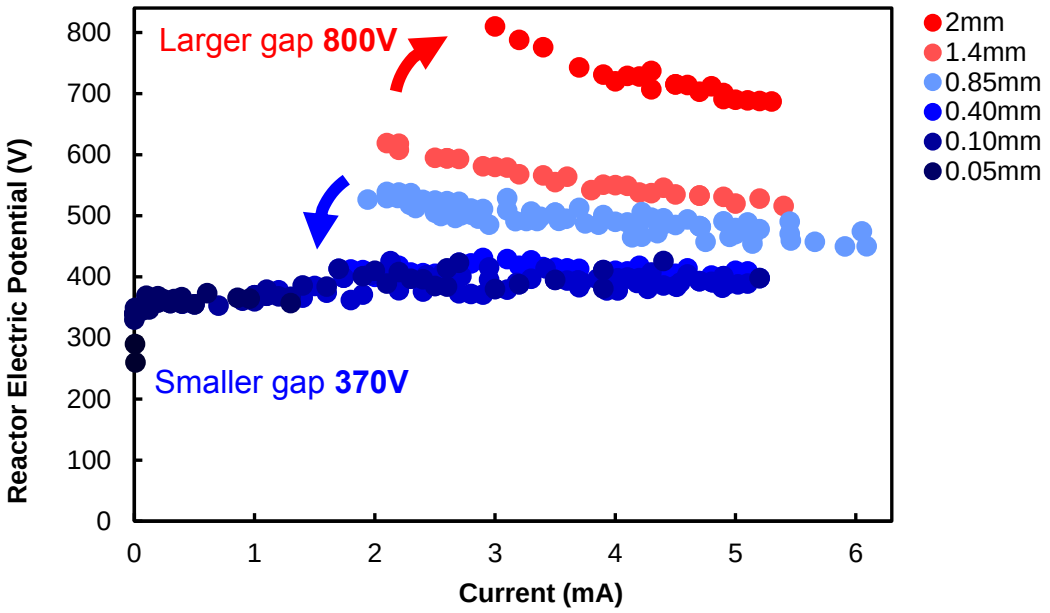

Figure 37: Smaller separation gaps results in lower sustaining potentials for dc glow discharge. A minimum in voltage reductions is encountered at 400µm of under 400V.

Since the same number of current flows at each separation gap, the smaller gap on average has either a lower electron energy distribution or is more efficient at creating the same number of charge carriers with lower electrical potentials. Since the reduced electric field changes it is more likely that the electron energy distribution changes. Measurements of the microplasma glow in pure nitrogen flow can be taken using ultraviolet-visible spectroscopy and the excited nitrogen states inferred. Calculations of the average electron energy distribution could be made but would not be direct spatial measurements such as should be made within each of these microplasmas to determine exactly from what source are the reductions in required electric potential derived.

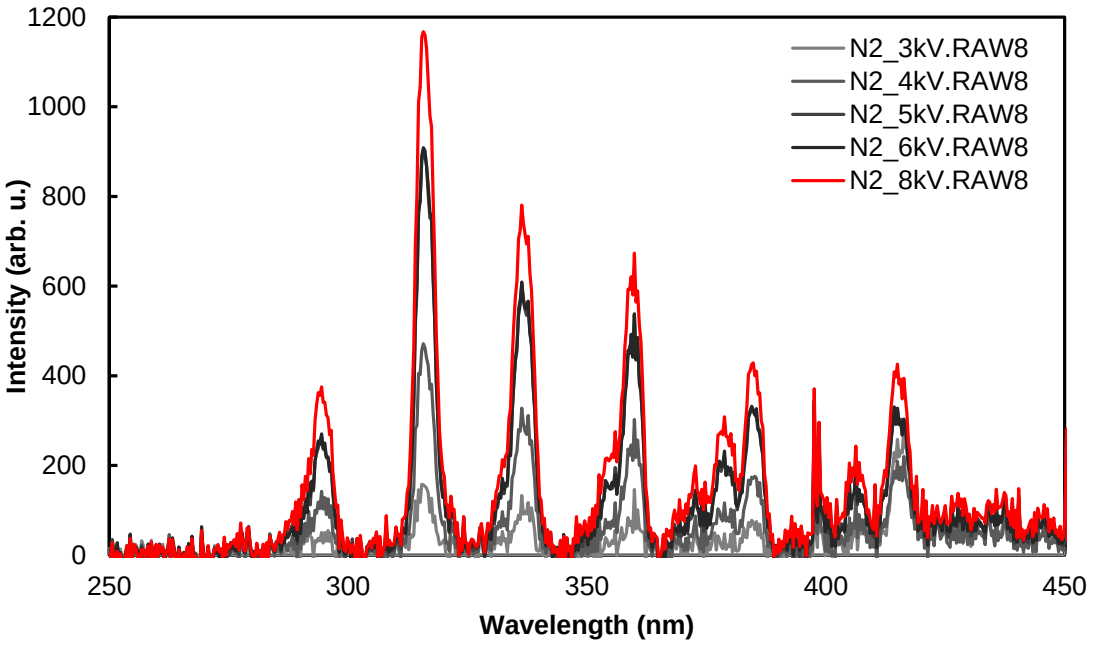

Figure 38: The spectral measurement from a single glow discharge in a nitrogen atmosphere (1.5mm).

The larger peaks correspond to vibrational state transitions for N_2 C-B (1-0), N_2 C-B (0-0), N_2 C-B (0-1), N_2 C-B (0-2) and N_2 C-B (0-3). These transitions have an associated energy requirement in electron volts and indicate by their abundance the energy distribution of the electrons. The same electrical and optical measurements can be made for multiple substrate material and surface roughnesses.

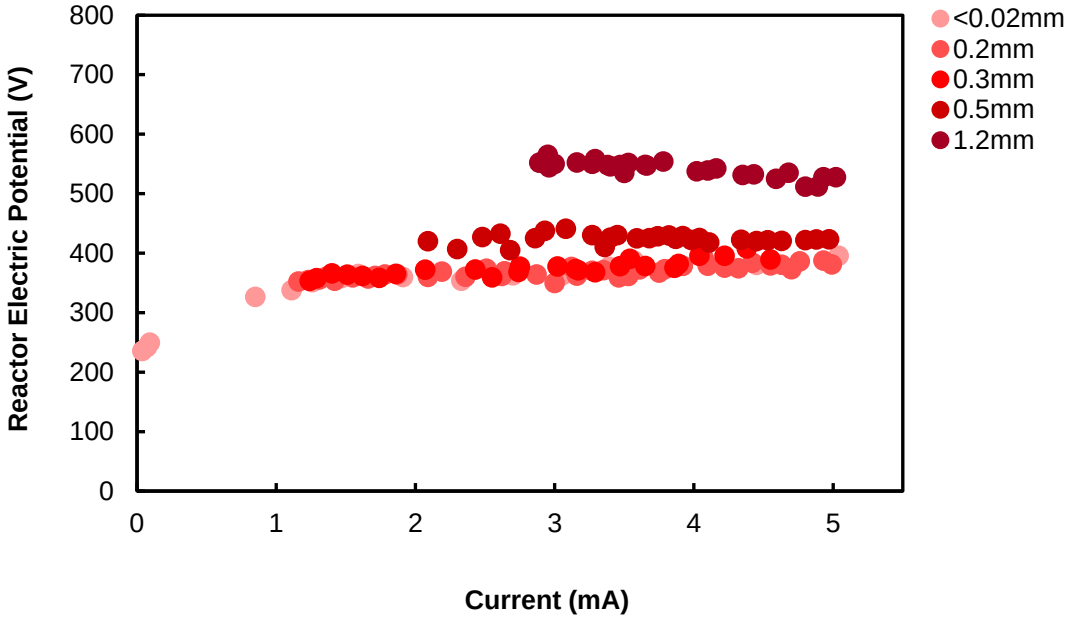

Figure 39: The same study is performed for a variety of different metal substrates and roughnesses.

The development of a single pin from a corona into a glow filament is shown as current is progressively increased from left to right and top to bottom.

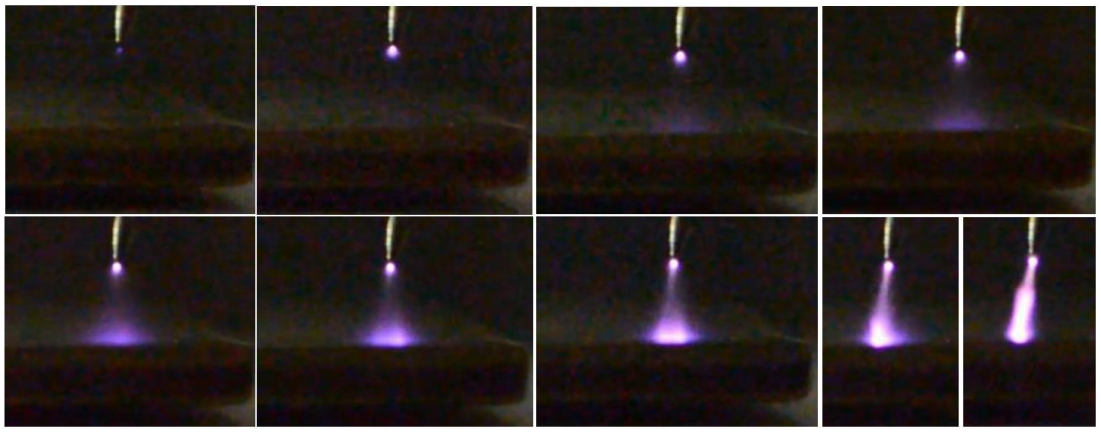

Figure 40: The gradual development of a corona discharge from a smoldering glow into a bright glow filament. The separation gap is 1.3mm and tip sharpness is 50µm.

The current voltage characteristic which shows the undeveloped corona region in more detail than the previous experiments has the corona onset potential (red), end of the corona regime (light pink) and beginning of the glow regime.

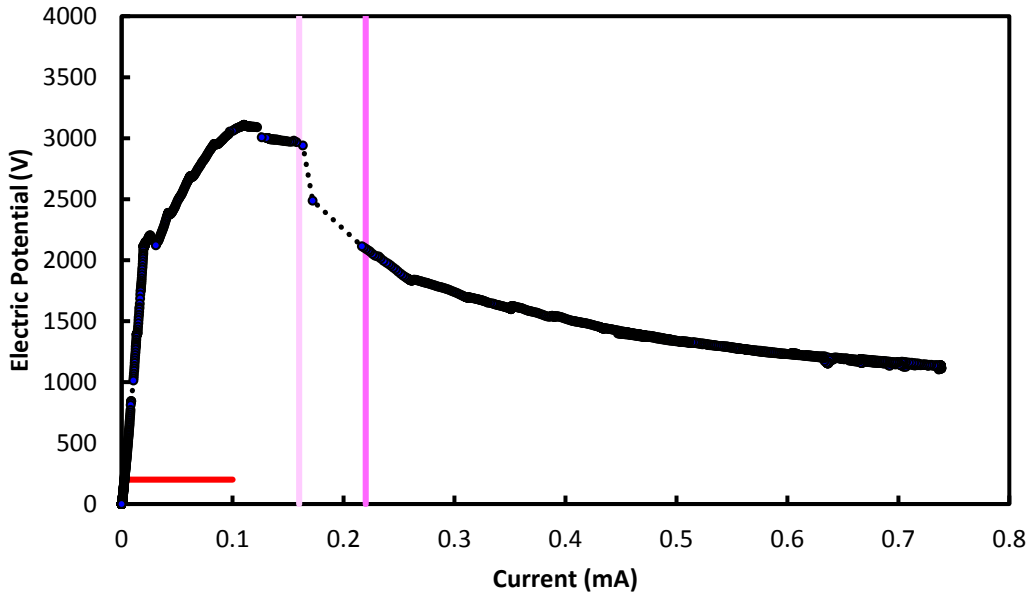

Figure 41: The current-voltage characteristic for a developing corona from an unsharpened pin.

The discharge current from a single electrochemically etched tip to the surface of a conductor is recorded for 5mm distance.

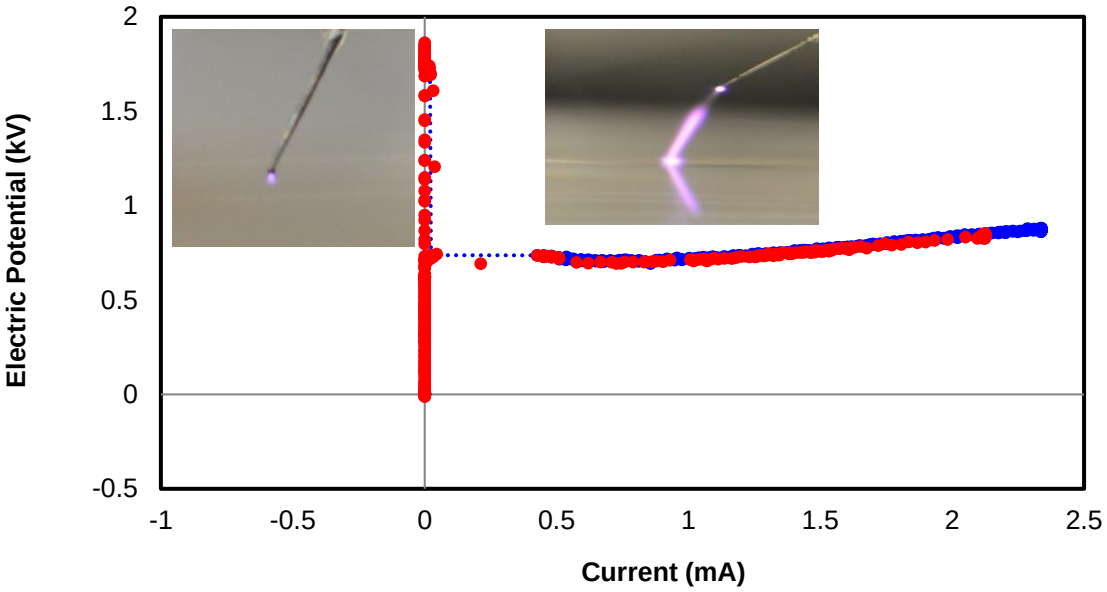

Figure 42: The corona and glow discharge curves that are generated also reveal relative microneedle sharpness at a specific distance when comparing several emitters.

The above plot can be transformed onto a logarithmic scale and overlaid with the classical low pressure plasma voltage versus current curve.

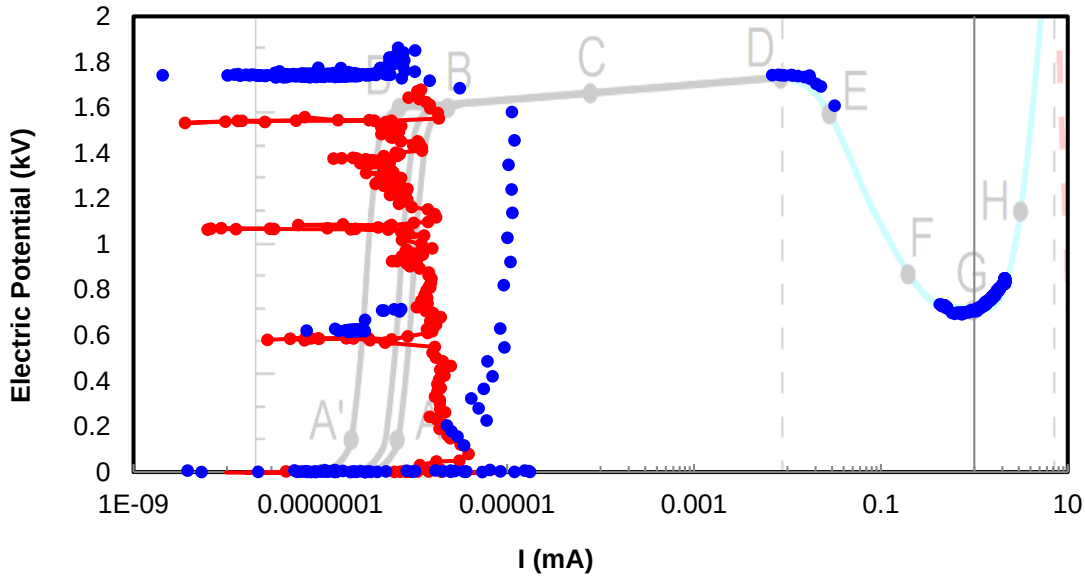

Figure 43: A strong similarity is demonstrated between the data and classical theory for all the regimes.

Additionally, it is demonstrated that the sharpness of the microtip can allow for strong reductions in the required onset voltage and minimum sustaining glow discharge voltage.

2.7 – Results from dc corona microplasma from fields of micropoints

Previous to this study no report of fields of microplasma exists for 2mm and smaller electrode gaps and certainly none wherein the useful portion of plasma occupies an entire 400µm microchannel. As many as 70 pins, have been activated using an electrical path of 1.5mm. The geometrical construction of the device that is used for chemical microcorona synthesis is shown below.

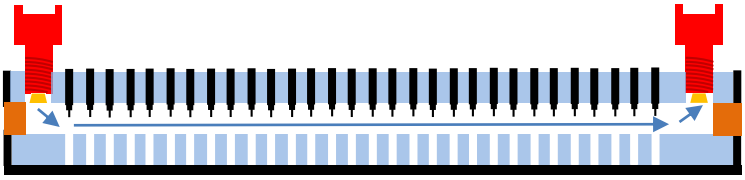

Figure 44: A dual spacer system defines a 400µm flow path for gas to travel through the plasma region of the microcoronas at the tip of the metal points. An additional 1mm of electrical path is added by milling or laser cutting fiberglass microholes opposite of the needles only.

More than 20 pins were not easily ignited from a single power supply since the differential resistance for the glow phase is negative during the normal glow discharge regime and the current threshold for a corona is approximately 20µA. The sum of the necessary current is limited by the current density transition to this negative differential resistance regime at approximately 0.3-0.7mA depending on the electrical gap that is selected. If this minimum glow discharge current is surpassed only one pin activates with the entire current in that single microgap. As the gap is increased multiple tips will ignite again in the corona regime. The gap is minimized to reduce power consumtion per unit of current that passes through the plasma to soften the electron energy distribution and prevent high electron energies that cause coking or waste energy upon initiating reactions. An expanded view of a microdevice operating with the nominal 20

pins per power supply (2kV, 1mA). The power supplies cost $20-$200 for variable digital current control. A row of manually inserted electrochemically etched W tips or 0.5mm shaft sequin pins can easily ignite under 2kV. A ballasting system is being constructed that will allow higher currents to be used based on toggling between the two regimes actively.

Figure 45: The series of 20 activated microcoronas in an expanded cross-sectional view.

2.8 – Conclusion

The benefit of a complete electrical characterization of microplasma in each of the potential regimes (townsend, corona, spark, glow) is useful since each of these phenomena will possess different electron energy distributions and contact a different volume of the gas as well as obtain different selectivity pathways. The electron energy distribution which is controlled by microgap separation will lead to different reaction pathways even at atmospheric pressure (based on the available electron volts required for activation of chemical energy barriers of direct or indirect chemical activation). This is reflected in the product distribution and certainly influence yields toward desired products. Microcorona and glow are continuous discharges. Microcorona has an incomplete ionization column while glow has a completed column which is reflected in its negative differential resistance in the electric potential versus current plot. Not

only does the slope and magnitude of the electric potential versus current characteristic change, but the minimum sustaining current is reduced for smaller gaps and high aspect ratio structured emitters. A knowledge of the stability of the glow discharge regime based on electrode separation distance and plasma current is useful when designing devices for high conversion and good energy efficiency. An entire network of reactor designs for microcorona or glow placement is necessary to optimize the chemical conversion based on the acquired electrical performances.

References

[138] P Bruggeman, J Liu, J Degroote, M G Kong, J Vierendeels and C Leys, "Dc excited glow discharges in atmospheric pressure air in pin-to-water electrode systems." J. Appl. Phys. (**2008**) 41, 215201

[139]O Thomas, "Inductively coupled plasma chemical vapour deposition (ICP-CVD)" Oxf. Instrum. Plasma Technol. (**2010**) white paper

[140]David Staack, Bakhtier Farouk, Alexander Gutsol and Alexander Fridman."Characterization of a dc atmospheric pressure normal glow discharge." Plasma Sources Sci. Technol. (**2005**) 14, 700

[1413]Daniel Schroder, Sebastian Burhenn, Dennis Kirchheim and Volker Schulz-von der Gathen. "Enhanced oxygen dissociation in a propagating constricted discharge formed in a self-pulsing atmospheric pressure microplasma jet." J. Appl. Phys. (**2013**) 46, 464003

[142]A Schutze, J Y Jeong, S E Babayan, J Park, G S Selwyn and R F Hicks, IEEE Trans. Plasma Sci., (**1998**) 6, 1685

[143]C. F. Gallo, "*Coronas and Gas Discharges in Electrophotography: A Review*," IEEE Trans. on Indust. Applications, (**1975**) 6, 739

[144]Junhong Chen, "Model of the Negative DC Corona Plasma: Comparison to the Positive DC Corona Plasma." Plasma Chem. Phys., (**2003**) 20, 83

[145]F Pontiga, C Soria, A Castellanos. "Electrical and chemical model of negative corona in oxygen at atmospheric pressure." J Electrostatics, (**1997**) 40:41, 115

[146]A Meiners, "Electron Energy Distribution Function." COMSOL (**2014**)

[147]J Choi, F Iza, J Lee and C-M Ryu, "Electron and Ion Kinetics in a DC Microplasma at Atmospheric Pressure." IEEE Trans. Plasma Sci., (**2007**) 35, 1274

Chapter 3- Methane Coupling Observations and Microplasma Reactor Design

Justin Pommerenck, Peter Kreider, Jordan Pommerenck, Joel Pommerenck, Yu Maio, Yousef Alanazi, Goran Jovanovic, Alexandre F T Yokochi, Nick AuYeung

Industrial and Engineering Chemistry Research

ACS Publications
1155 Sixteenth Street N.W.
Washington, DC 20036, US

(to be submitted)

3.1 - Abstract

A plasma microreactor using dc corona and glow discharge has successfully converted methane flows to C_2 and C_3 hydrocarbons. Products include ethylene, acetylene, ethane, propane, propene, and propyne. The microplasma reactor reaches 80% conversion with 80% selectivity to C_2 unsaturated hydrocarbons. The operating power is between 1-5W and treats 10-100sccm. The inlet feed is 50-90% N_2 and 10-50% CH_4. The plasma has been studied in reactors using a single discharge, a series of single discharges and a hexagonal arrangement of multiple plasma discharges. Optimization in reactor performance requires narrow hundred micron gas inlets to reach the ultrafast residence time for maximum selectivity and conversion. Multiple plasmas in series or hexagonal arrangement reduce bypass. Series plasma reactors reduce bypass by mixing of the unreacted and reacted bypass from the first plasma prior to it being entered into the second plasma in the series reactor. Hexagonal arrangement reactors incorporate multiple plasmas in a pattern that maximizes the number of flow lines that pass through plasma. This hexagonal pattern improves selectivity by creating a uniform residence time for all of the gas. This study reduces bypass from approximately 50% to 20% based on the maximum achievable conversion that is possible during residence time studies. Efficiency of conversion of electrical energy to the standard energy of formation reaches 45%.

Keywords:
Methane, hydrocarbon coupling, ethylene, microreactor, microplasma, corona

3.2 – Introduction

Excellent research has been conducted on hydrocarbon plasma processing for decades. Much of the focus for value added hydrocarbon production has targeted the conversion of methane by plasma to higher hydrocarbons or carbon dioxide conversion to synthesis gas. There are many types of plasma driving technologies which give arise to ac "gliding" arc discharges[148], ac dielectric barrier discharges[149], ac or dc corona discharge (at large separation gaps)[150, 151] microwave or rf discharges[152], and spark discharges (for H_2 production). The driving technology determines the mixture of plasma modes (Townsend, corona, spark, glow, arc).

Corona discharge is successful in converting entire streams of methane to C_2 hydrocarbons.[153] This specific corona discharge has its electron energy and spatial scale determined by 40kV and 1cm length dimension. As the electrode separation is reduced, smaller conversion of methane is observed. The electric field is intensified and the energy distribution is increased which led to higher complete dehydrogenation of methane to coke. The higher electron energy can be reduced even at microscale electrode separations since the electric field inception requirements are also reduced to 500-1000V. This gives rise to an unstudied regime of soft/low energy plasma (1-5eV) for a variety of chemical applications. A study of this plasma regime has been successfully performed in microscale ac and dielectric barrier plasmas which are easy to homogenize within a chemical reactor since the formation and collapse of plasma channels is frequent and the differential resistance is changing from positive in the corona regime to negative in the diffuse glow regime. This has a drawback in that the energy is deposited on a short time scale which leads to higher than average pulse energies in constricted filaments (this is a disadvantage for low activation energy hydrocarbon processing since coke formation is promoted by higher average energy; higher average energy is desirable when efficiently forming and densifying nanoparticle morphology). Depending on the power supply technology, a DBD or ac plasma can possess different ratios of streamer to diffuse behavior.[154]

This dissertation is the first to inclusively relate the difference in chemical efficiency and conversion based on the dc microplasma regime for ultrafast flow velocities. This fundamental understanding of the chemical yields from both corona and glow regimes can assist DBD and ac plasma studies by informing researchers of the type of chemical products from plasmas regimes, in which the plasma is more filamentary or diffuse in nature and based on the plasmas expected space charge density and electron energy distribution. This unification of the expected plasma chemical yield should depend only of the spatial and temporal measurements of plasmas. This topic will be the focus of a future publication and should be investigated through electron density measurements in single reactor systems for a variety of plasma types with comparable chemimetrics.

3.3 – Methane coupling reactor types

Non-thermal plasma reactors for methane conversion have been studied using a variety of reactor types. Industrial reactors typically process flows as high as several hundred cubic meters per hour. There are several examples of plasma reactors including the microwave jet, gliding arc reactor, dielectric barrier discharge reactor (DBD), rotating arc reactor. The majority of these reactors are studied at large electrode gap separations. Some research has been done in microscale reactors using arc discharge and dielectric barrier discharge.[155, 156] The results in terms of retaining processing capacity to several hundred standard cubic centimeters per device is promising in terms of numbering up of the devices when finally sizing to fit the needed capacity of the feed stream. Also, the efficiencies tend to increase as the electrode separation gap of the plasma decrease. This has already been accurately characterized for dc microplasma reactors during the electrical portion of this study.

Microwave jets are one of the examples offered above as being evaluated for industrial application in a variety of commercial reactions. Microwave jets utilize microwave energy directed by a waveguide to a nozzle to activate gas which is ejected at very high

flow rates. This process has several advantages in which the gas flow is treated to high conversion since the entire stream is usually activated. The process is usually used to study production of hydrogen from biomass solids or methane.

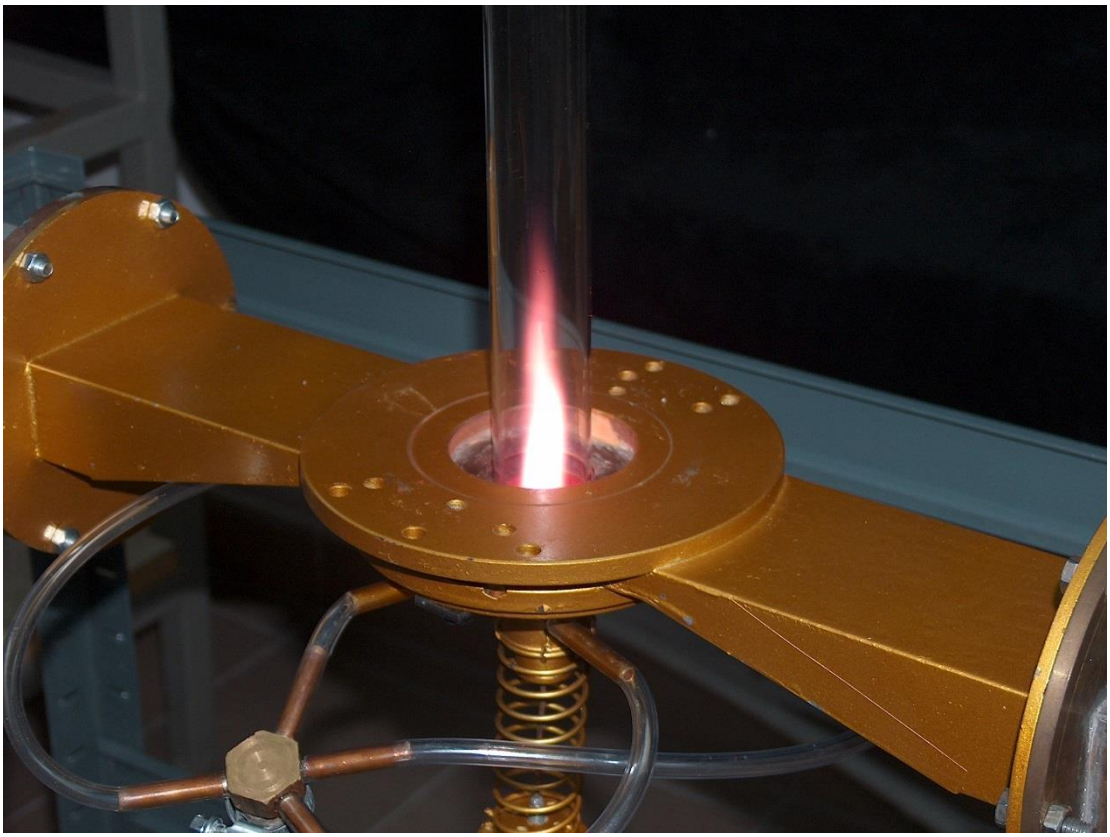

Figure 46: A microwave jet methane reformer for hydrogen production. [Dept. Hydrogen Energy][157]

Microwave plasma reactors usually reach at least 70% efficiency in hydrogen production and continue to reduce the operating energy consumption through improvements in plasma reactor design. They have also been used to reprocess landscape waste, rubber tires and other waste to valuable fuel products.

The gliding arc reactor uses arc level currents of several amperes at near 1kV electric potentials. Gas is rapidly passed through a 2D plasma discharge from a charged injector to both grounded wedges. Gas contacting is typically poor in these devices and higher than 40% conversion is difficult to obtain. The figure below illustrates that a jet of gas

if forced between two narrow thin electrodes. The gas flow forces the formed arcs down the length of the thin conducting electrodes which enlarges the reaction length. This is one of the earliest reactor configurations used to study the conversion of methane in an argon diluent. Because of the bypass which in turn results in low conversion, the flow rates are reduced and process efficiency suffers. A diagram of an industrial 2D gliding arc discharge reactor is depicted below.

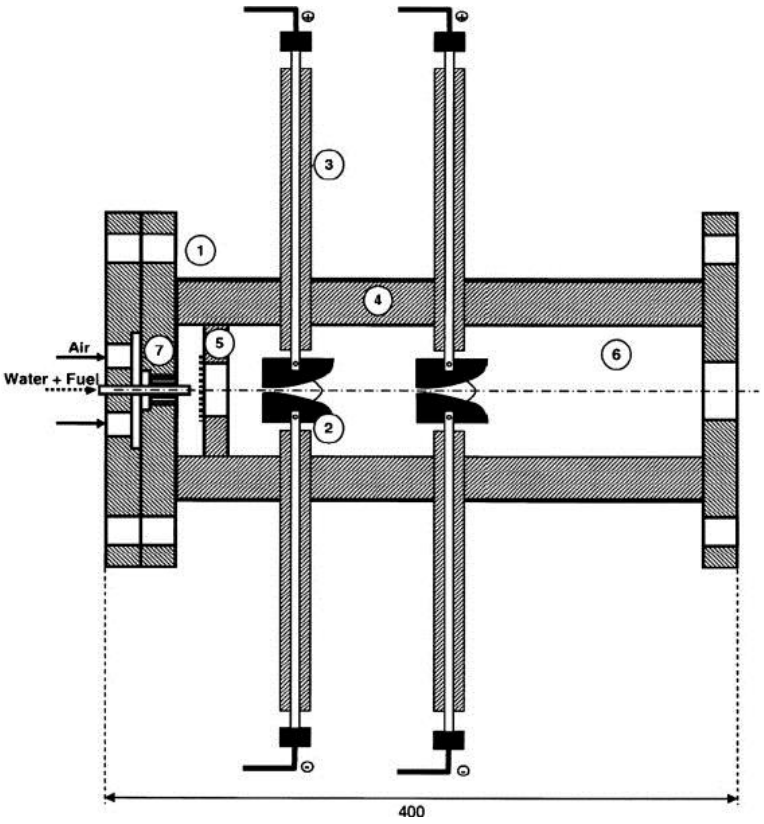

Figure 47: The diagram of an industrial gliding arc reactor is a 2D plasma reactor that has been used to process methane.[158]

The DBD reactor uses a dielectric barrier to prevent charge flow during the application of an alternating potential. Streamers repeatedly form at several kilohertz and create a homogeneous plasma space with each filament typically lasting a short amount of time.

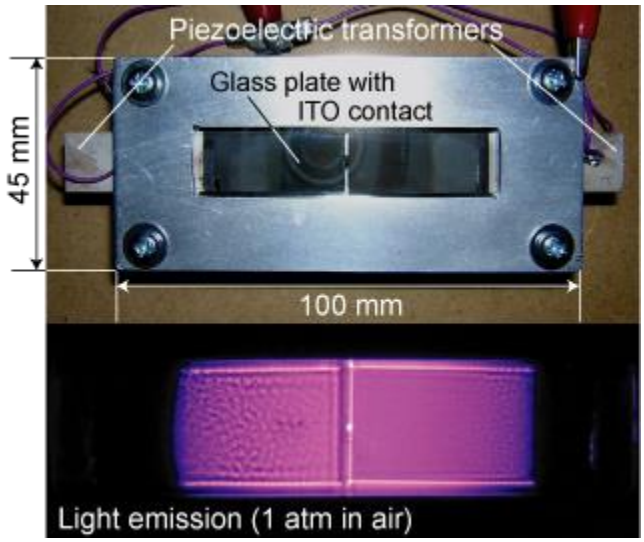

Figure 48: A compact dielectric barrier discharge reactor using piezoelectric transformer.[159]

Arguments in favor of plasma chemical reactors usually center on energy efficiency, product selectivity and reductions in capital investment. Reductions in capital cost are due to processing ultrafast flows in a single device. Processing times are fast since only millisecond residence times are necessary for complete reaction of the feed gas.

3.4 – Methane coupling experimental setup and reactor geometry

Two 200 sccm Brooks™ mass flow controllers, which are operated by a single microcontroller, are fed methane and nitrogen by gas cylinders regulated to 25 psi. The mass flow controllers are calibrated volumetrically. A 20ml vial is filled with water and glass spheres. The inlet gas is sparged through the water to obtain a consistent water vapor content based on the flow velocity and ambient temperature. This mixture of methane, nitrogen and water vapor reaches a typical flow velocity of 0.5m/s in the inlet tubing which forms a jet into a perpendicular dc non-thermal plasma. The effluent is sampled using either an in-line 150μL sampling loop or 1μL Hamilton Syringe via the front port of a SRI model 6100 gas chromatograph using HID detection after a Hayesep D column. Mass spectrometry is used to identify products. The 150μL

sampling loop is used for minor species while major species are measured using the 10μL Hamilton Syringe. A simple illustration for the setup is shown below.

Figure 49: The gas cylinder regulator and mass flow controller output flow to the microplasma device which is sampled by both a manual 150μL sample injection loop and 10μL syringe.

The power supplied to a single discharge is 1 - 6W. Higher powers and conversion are reached by increasing the number of discharges in series or reducing the bypass through the single microplasma or fields of microplasmas. Higher residence times and conversion are reached by increasing the number of discharges in parallel. The effect of changing power does unfortunately also change the residence time of the gas in the plasma not via the flow rate or by a path length dependence but by either encountering more directly the inlet jet or by not entirely treating the stream since the size of the plasma is highly dependent on power (although it is the goal to isolate these factors to the greatest extent possible). The plasma regime is dependent on the pressure, plasma electrode separation and the power supplied and follows the typical atmospheric pressure voltage-current characteristic. These modes, in order of increasing current density, are Townsend, corona, spark, glow and arc (which is not attained in this study which never utilizes more than 5mA per microplasma). The reaction conditions are kept dilute in methane to simulate biogas conversion (10-30% methane in nitrogen).

This has the added advantage of reducing the equilibrium conversion of $carbon_{(g)}$ to $carbon_{(s)}$ at 3:1 ratios of nitrogen to methane. Nitrogen is explored as a diluent so that the conditions encouraging hydrocarbon upgrading are investigated prior to investigating the promoting of liquid oxygenation of hydrocarbons in dilute oxygen or water vapor streams.

3.5 – Results from single microplasma microreactors

Conversion, of up to 80% of methane, in a methane and nitrogen feed is accomplished using microscale technology with plasma regime and ultrafast flow velocity controlling the selectivity of the products. Selectivity to C_2 hydrocarbons reaches 80% with the remainder being a mixture of propane, propene, and propyne along with carbon solid formed in the inner electrode region. The primary products in the glow regime show strong selectivity toward hydrocarbon couplings with MW < C_6. The geometrical layout of the simple device is diagramed below.

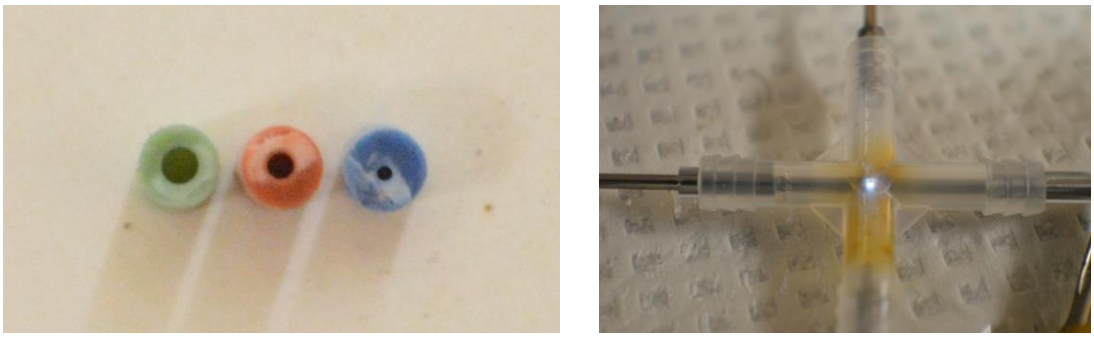

Figure 50: The inlet diameters of the PEEK tubing that are selected for each study (left). These tubes send flow directly into the center of the microplasma in the cross type reactor (right). The small orange PEEK tubing is used for the first study.

The inlet feed is 25% methane and 75% nitrogen. The flow rate is 13sccm. The reactor begins to thermalize the plasma at powers greater than 5W.

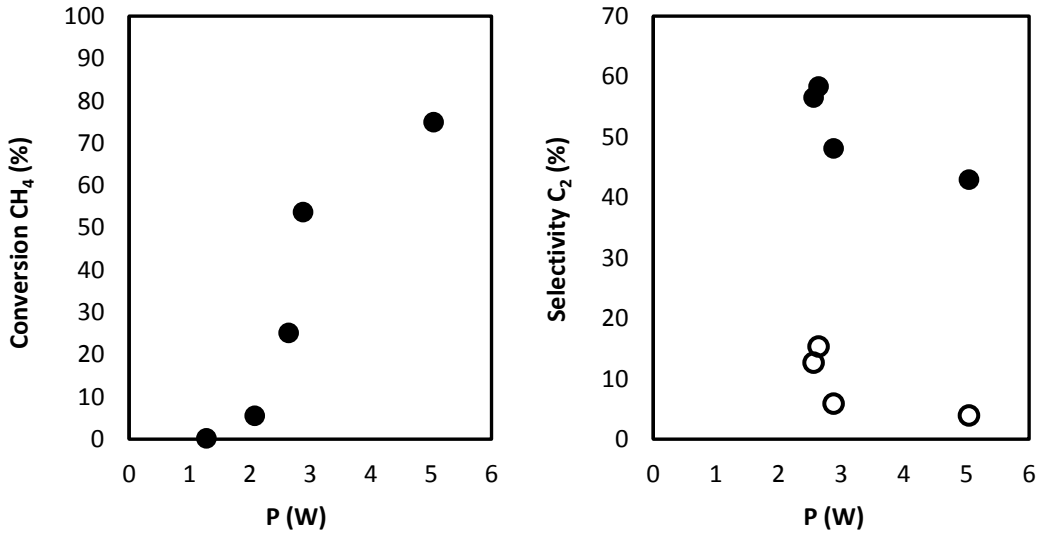

Figure 51: In a plasma reactor, the conversion of methane and the selectivity to C_2 hydrocarbons both reach 80% for 5W of power.

The selectivity is strong toward C_2H_4 and C_2H_6 at ultrafast residence times. The power required to convert 60% of the inlet methane is less than 3W. The power data shows that the trend in conversion and selectivity relates more closely to which regime of plasma the reactor is using. The regime has already been demonstrated to be dictated by current density within the plasma (whether filamentary as in Townsend > spark > arc or diffuse such as in corona > glow). Thus, current density, which relates to plasma type, puts conversion on a single trend despite being at a variety of powers based on voltage changes. These voltage changes do affect efficiency which directly relates to power usage. It is also possible that the current density which relates to size of the plasma plume, until the positive column is saturated with its maximum space charge, may actually be describing the improved transport of the methane jet into the larger plasma plume at higher current densities.

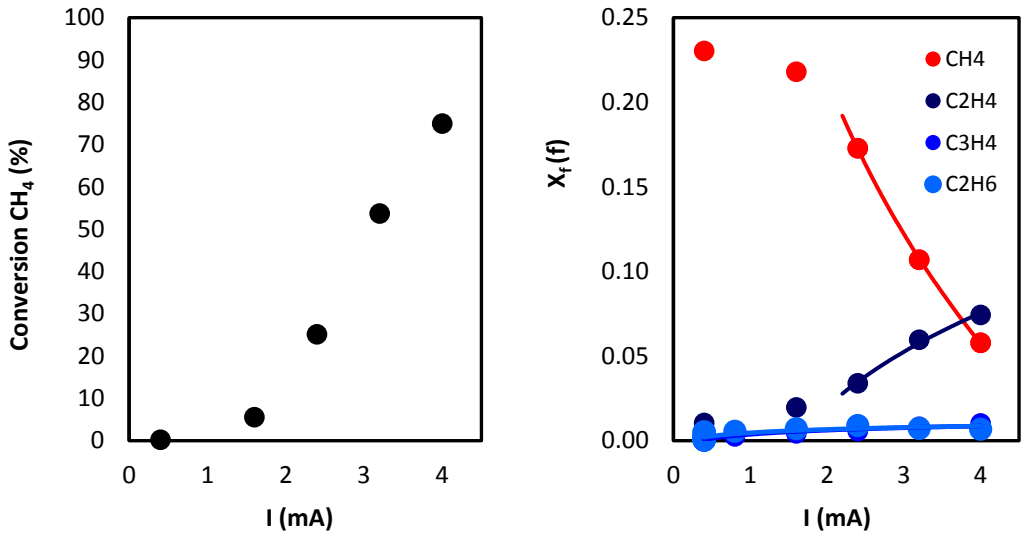

Figure 52: The current is strongly related to conversion within the glow regime.

Without this methane jet (1.58mm OD PEEK with 400µm ID for the methane jet), a 1.58mm OD PEEK with 750µm ID tubing gives a much higher average residence time (not in the reactor which is the same for identical flow rates) but within the plasma plume itself (which sees a slower methane jet through the center of each plasma filament). This higher residence time leads to molecular coupling of C_2 hydrocarbons. The modified inlet and its geometrical arrangement are shown below.

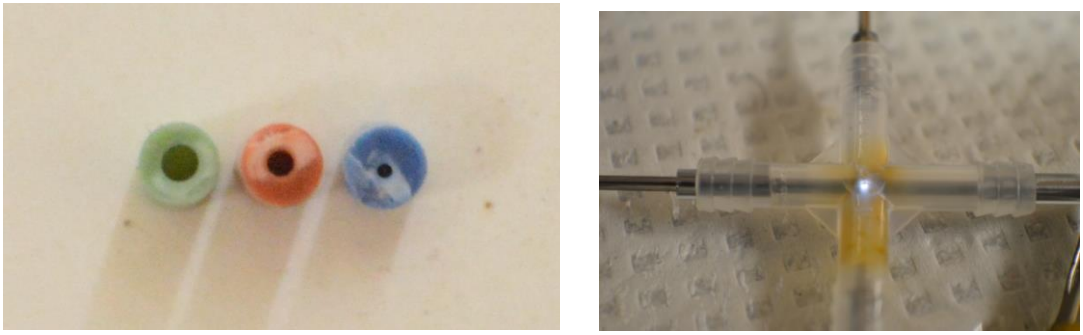

Figure 53: The orifice diameter of the inlet tube is increased to 750µm to change the flow path through the plasma discharge (left). The assembled reactor is shown processing methane (right). This change in the orifice diameter is used demonstrate that selectivity changes based on that change in flow path.

The inlet feed is set at 10% methane and 90% nitrogen. The 80% selectivity to C_2 hydrocarbons is replaced with 50% selectivity to C_2 and 45% to C_3 hydrocarbons.

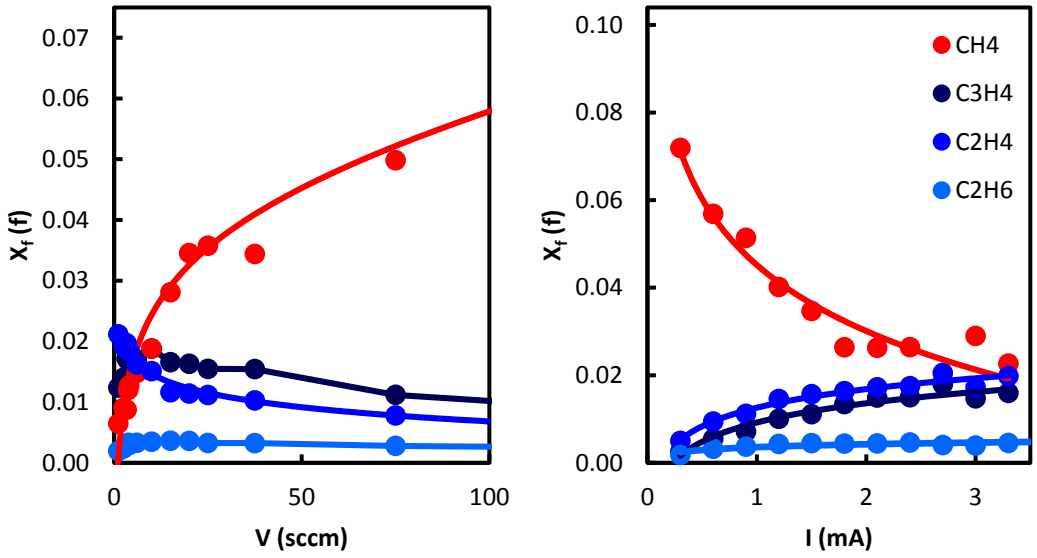

Figure 54: Three discharges in series both physically and electrically were used to treat a slow jet which is sent into the center of the diffusion limited discharge plume.

The smaller 1.58mm OD tubing provides the methane jet into the middle of the discharge for the below figures (seven sizes of IDs are possible for this1.58mm OD tubing PEEK and would provide an interesting reactor design relationship to product yield and selectivity). This is the most desirable and uniform contact pattern with the entire plasma and therefore provides the intrinsic kinetics of the plasma without mass transport limitations from bypass diffusion. This ultrafast flow velocity achieves correspondingly higher conversion and selectivity which micro technology in general is so capable of generating. The study emphasizes the need for improved gas to plasma contact pattern. Microarchitecture could be manufactured using traditional laser cutting equipment to form channels in commercially available and inexpensive fiberglass spacers 500µm before each discharge in a multidischarge device.

A clear minimum in consumed power is observed at 2mA which is the beginning of the complete formation of the cathode column which defines the plasma regime glow discharge. Plasmas should be operated in parallel physically to treat higher flows at this optimum power load and in series electrically to achieve the desired conversion.

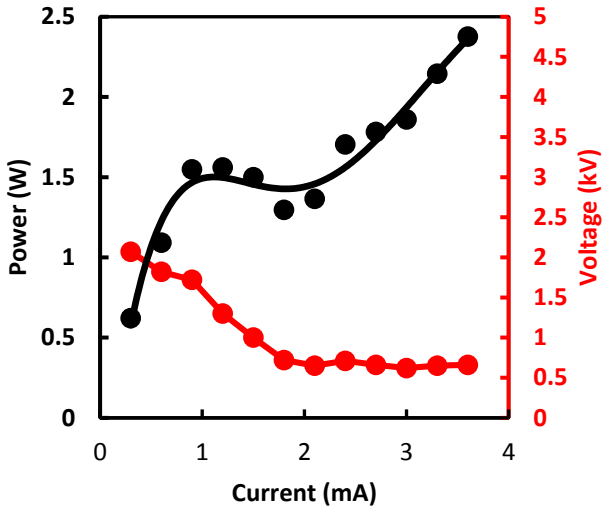

Figure 55: The spark to glow transition in methane and nitrogen shows reduced energy uptake at 2mA.

These observations allow the discharge energy which is actually transferred to chemical energy to be used to calculate a cumulative process efficiency.

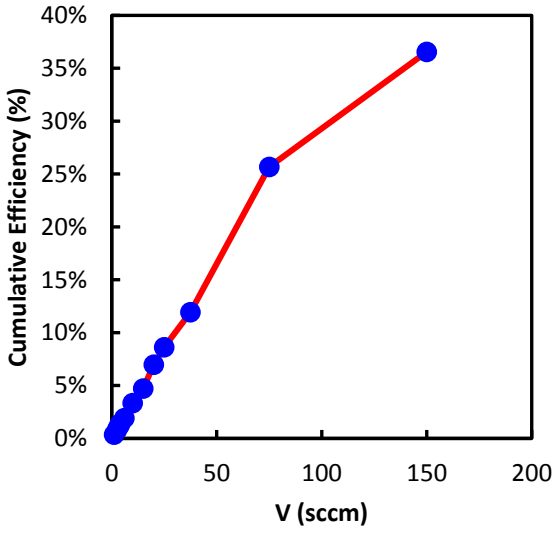

Figure 56: Cumulative efficiency is calculated based on product standard energy of formation minus the reactant standard energy of formation divided by the electrical energy.

At higher dilutions of 1:5 or 1:10 very little carbon is formed and this may be considered the threshold for long term performance. An inert such as the nitrogen is required to be recycled with uncaptured lower molecular weight hydrocarbons that are not easily collected. Steam may be used as a diluent to prevent coke formation or to remove formed coke within microplasma devices. The carbon formation closely follows the predictions made in DBD for methane and nitrogen flow ratios which tabulate ~1-5% for these conditions. Coke formation is very dependent on the discharge gap and electrode geometry. A brief recording of coke formation is seen as useful for future work. Identical single point and single rod reactors are built in parallel and coke formation is catalogued. The coke formation represents only a very small fraction of the feed (0.5-5%) for the 400-800µm plasma (dc glow) studied here. While it is a small percentage of the flow for these microchannel devices, it forms a thread that rapidly bridges the gap especially on sharp points or along glass if the point touches a glass surface. Coke formation experienced an extremely rapid drop at 30% methane that is likely due to the discharge having enough oxygen to consume the carbon from the surface. For this discharge gap of 750µm, the ratio was 30% methane for infinite life (ie. After four hours a carbon bridge or coking surface could not be identified).

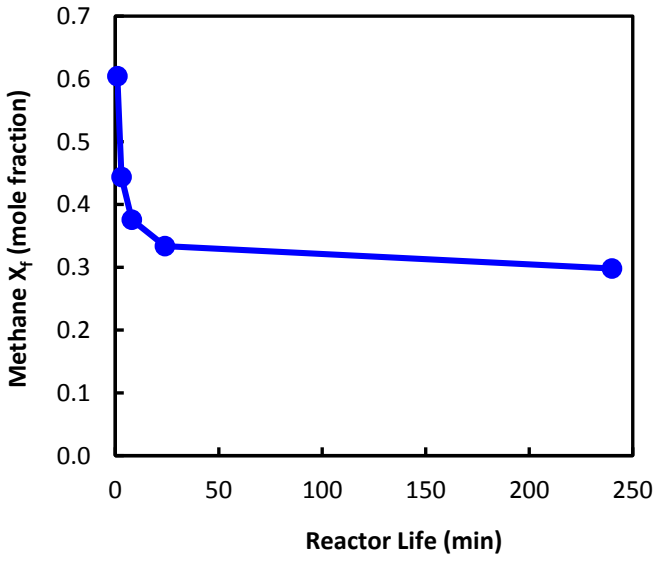

Figure 57: The coke formation required to short identical microgaps at each methane mole fraction is explored systematically.

The reactor geometry is altered to have a uniform slow velocity through the discharges to facilitate the addition of multiple plasmas to treat higher average flow rates.

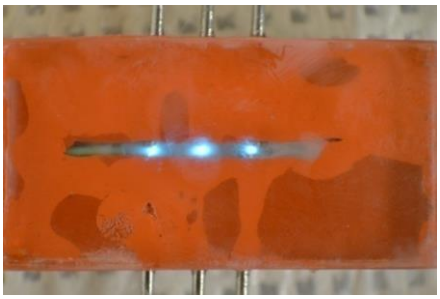

Figure 58: The reactor is fed with a 100µm inner diameter PEEK tube and higher average flow rates that are richer in methane to identify the optimum methane concentration for improved energy efficiency.

The flow rate is 33sccm for this study. The reactor is powered to 2.2mA and 3kV which was ideal for the three pin series reactors.

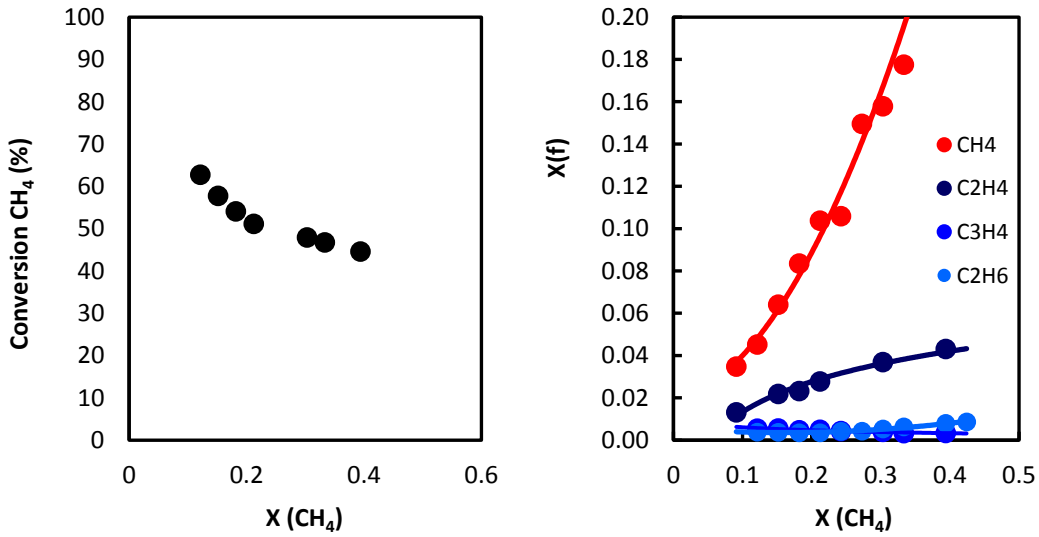

Figure 59: The increasing concentration of methane in the inlet shows C_2 hydrocarbon coupling to C_3 only in the presence of inert (at 0.1 X(CH_4)).

The previous data has been generated almost entirely within the glow regime. The electrode separation gap or current density can be adjusted and a power curve generated at the same powers but at lower currents due to the nonlinearity of the voltage versus current curve. The corona regime is equally interesting but found to be less efficient in converting methane by a factor of three. The value of exploring both diffuse regimes for hydrocarbon upgrading is in a comparison of selectivity toward different products which describes the average electron energy in the plasma. A corona discharge requires higher voltages (than glow discharge at the same electrode separation while both voltages tend to be very low for microplasma separations), has a positive differential resistance and has an extremely low formation threshold requirement for current density.

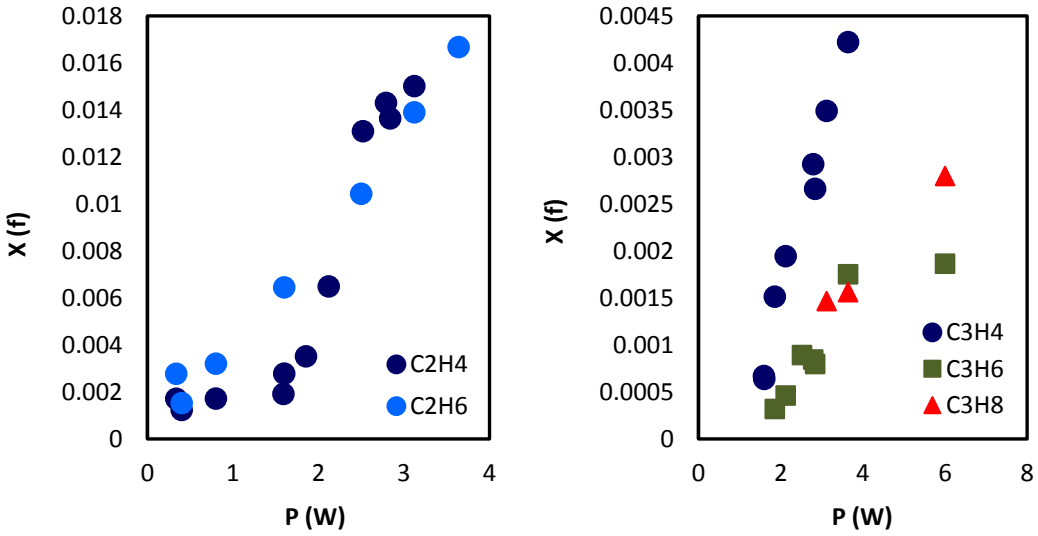

Figure 60: A low current, high voltage corona discharge produces larger yields of high molecular weight unsaturated hydrocarbons and cokes faster than the glow discharge regime at higher currents and lower voltages.

Increasingly concentrated ethane is preferentially produced over ethylene if the plasma is in corona regime. Ethylene is strongly converted to more unsaturated hydrocarbons such as acetylene and propyne. This contrasts sharply to the glow discharge regime in which the ethylene is five times higher in selectivity. The formed products (C_3H_4 and C_3H_6 and C_3H_8) which accounted for as much as 4% during other parts of the study,

here represent about 0.7% collectively. There are also chemical products possessing a longer retention time within the gas chromatograph column than water or C_3 which indicates large hydrocarbons (C_4 to C_6 or partially oxidized hydrocarbons).

3.6 – Results from fields of microplasma microreactors

Second scaled up reactor with plasma arrays spaced at 1.5mm intervals. The first image shows four middle rods activated. The second image shows the three last rods activated. With electrical series, the desired rods can be activated and conversion of methane and carbon dioxide examined to estimate bypass. The second set of data is done with only the first five rods activated due to thermal limits of the FR4 board to 20W without any cooling or heat sink. For a discharge operating in the hysteresis portion between glow and corona, the required operating voltage is 700V and typical currents are 1-5mA.

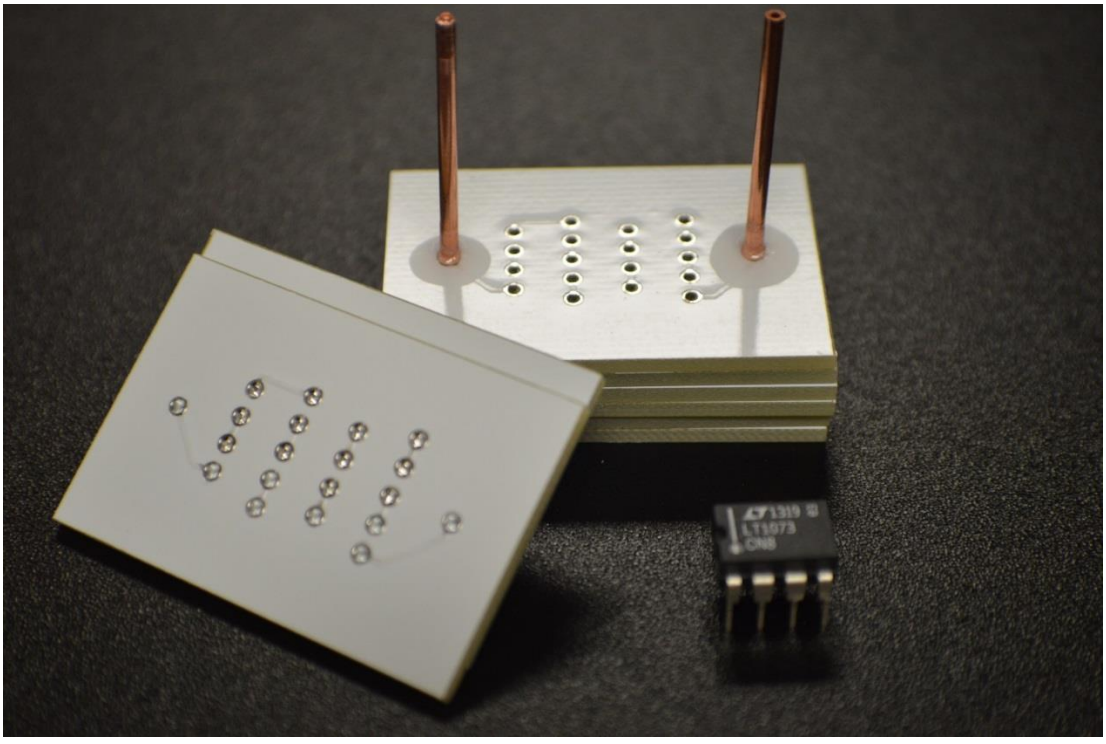

Figure 61: A manufactured PCB microreactor whose size is comparative to microelectronic packages.

For example, a linear array of four discharges utilizes 10W at the verge of the glow discharge regime. This array is used to process 10% methane in nitrogen. No internal microstructure is used in the device to direct flow into the plasma.

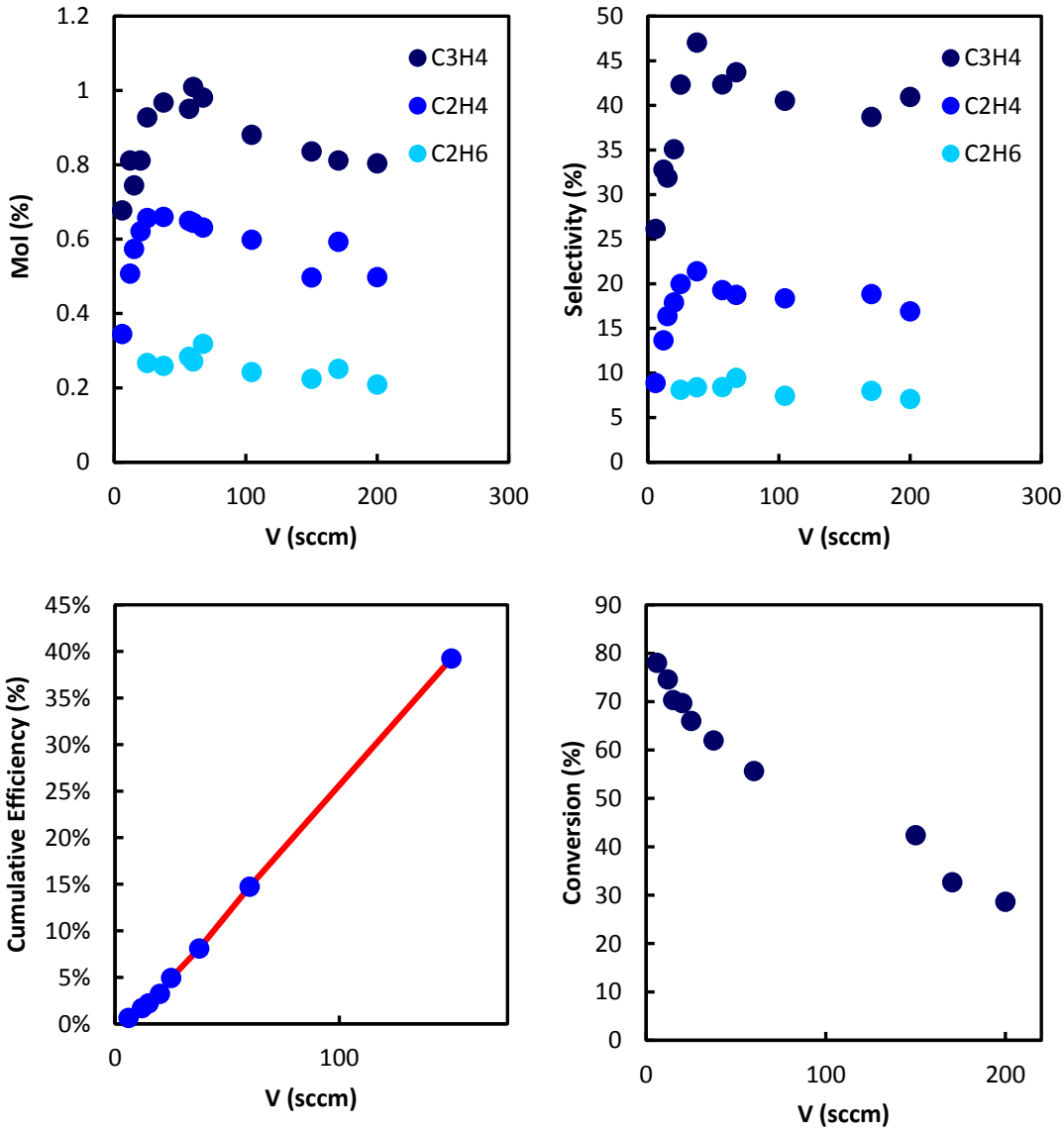

Figure 62: The 10W plasma array reactor converts up to 80% of a 100-200 sccm flow of methane in 90% nitrogen. The products are predominantly C_3 hydrocarbons which account for more than 50% of the carbon from the converted methane. The carbon balance holds to around 5%. The cumulative efficiency (kJ electrical / kJ chemical) spans from 1% to 45%.

3.7 – Conclusion

The ability is demonstrated by nonthermal plasma microreactors to convert 10 – 200 sccm mixtures of nitrogen and methane (10-30%, CH_4) with high yield to ethylene and other higher molecular weight hydrocarbon products whose relative ratios or further upgrading depends on plasma type and reactor design. The uniformity of the contact pattern of the flow with the plasma filament(s) is important and the strongest factor in determining the product distribution. For example, in a slow wide gas jet half of the fluid may pass through weakly ionized parts of plasma in the microchannels and produce C_2 hydrocarbons. The other half (the central faster part of the gas jet) will pass through the region of strongest electron density and produce high molecular weight products. The conversion of methane to higher hydrocarbons is feasible at high efficiencies. The process is scalable within a single device or by numbering up of devices. Pure renewable electrical energy can activate chemical processes with lower energies than thermal processes and have that energy stored in chemical potentials for later use. A reactor could be designed to recover heavy hydrocarbons from the inert stream for recycle with relative ease. Safety is increased since each reactor is modular to its own internal microvolume and poses no risk to the streams adjacent to it. Process control is improved over thermal processes because thermal process have very long start up and cool down time constants. Electrical response for a plasma array is instant which is advantageous when considering chemical industries integration with renewable energy or a smart grid.

References

[148]K Pornmai, N Arthiwet, N Rueangjitt, H Sekiguchi, S Chavadej, "Synthesis gas production by combined reforming of CO_2-containing natural gas with steam and partial oxidation in a multistage gliding arc discharge system" I&EC research. (**2014**) 53, 11891

[149]T Nozaki, A Agiral, S Yuzawa, J G E Gardeniers, K Okazaki, "A single step methane conversion into synthetic fuels using microplasma reactor" Chem. Eng. J. (**2011**) 166, 288

[150]M-W Li, Y-L Tian, G-H Xu, "Characteristics of carbon dioxide reforming of methane via alternating current (ac) corona plasma reactions" Energy & Fuels. (**2007**) 21, 2335

[151]M-W Li, G-H Xu, Y-L Tian, L Chen, H-F Fu, "Carbon dioxide reforming of methane using dc corona discharge plasma reaction" J. Phys. Chem. (**2004**) 108, 1687

[152]J Cormier, I Rusu, "Syngas production via methane steam reforming with oxygen: plasma reactors versus chemical reactors" J. Phys. Appl. (**2001**) 34, 2798

[153]B Wang, G Xu, "Conversion of methane to C_2 hydrocarbons via cold plasma reaction" JNGC. (**2003)** 12, 178

[154]S Starostin, P Premkumar, M Creatore, E Veldhuizen, H Vries, R Paffen, M Sanden, "On the formation mechanisms of the diffuse atmospheric pressure dielectric barrier discharge in CVD processes of thin silica-like films" Plasma Sources Sci. Technol. (**2009**) 18, 045021.

[155]A Agiral, T Nozaki, M Nakase, S Yuzawa, K Okazaki, J G E Gardeniers, "Gas-to-liquids process using multi-phase flow, non-thermal plasma microreactor." Chem. Eng. J. (**2011**) 167, 560

[156]P Thanompongchart, N Tippayawong, "Experimental investigation of biogas reforming in gliding arc plasma reactors." Intern. J. Chem. Eng. (**2014**) 609836

[157]M Dors, H Nowakowska, M Jasinski, J Mizeraczyk, "Chemical kinetics of methane pyrolysis in microwave plasma at atmospheric pressure." Plasma Chem. Plasma Proc. (**2014**) 34, 313

[158]E Ahmar, C Met, O Aubry, A Khacef, J Cormier, "Hydrogen enrichment of a methane-air mixture by atmospheric pressure plasma for vehicle applications." Chem. Eng. J. (**2006**) 116, 13

[159]K Teranishi, N Shimomura, S Suzuki, H Itoh, "Development of dielectric barrier discharge-type ozone generator constructed with piezoelectric transformers: effect of dielectric electrode materials on ozone generation." Plasma Sources Sci. Technol. (**2009**) 18, 045011

Chapter 4- Methane Coupling Finite Element Modelling of Reaction Data from a Multidischarge Microplasma Channel

Justin Pommerenck, Peter Kreider, Yu Maio, Yousef Alanazi, Goran Jovanovic, Alexandre F T Yokochi, Nick AuYeung

Industrial and Engineering Chemistry Research

ACS Publications
1155 Sixteenth Street N.W.
Washington, DC 20036, US

(to be submitted)

4.1 - Abstract

A preliminary model for the data from the experimental methane coupling reaction in a plasma microreactor is assembled using finite element modeling. The reaction engineering model determines changes in concentration due to flux and production rates. The production rates are confined to a reaction zone which the plasma visibly occupies. The distribution of electron energies and their space charge density is not considered in the model. The optimization module is successful in determining the kinetic parameters for a perfect fit to the experimental data using four pre-exponential Arrhenius kinetic parameters. A comparison of the models extensibility to predict the performance of the plasma microreactor products for different flow rates is performed. Good agreement in trends is found to result for a wide range of flow rates. The largest deviations from the model predictions are found at the extreme low and high flow rates. At low flow rates, too much methane is converted. At high flow rates too little methane is converted. This indicates that the electron energy and space charge density need to be approximated in the model. For instance, if the space charge density were predicted using a Warburg distribution from the center of the discharge, there would be higher space charge in the center of the plasma reactor. At higher flow rates, a larger portion of the flow is in the center of the reactor (assuming a laminar parabolic profile is maintained). This larger portion of the flow would then encounter a higher number of electrons in the center of the reactor and the reaction would proceed faster. Higher conversion from the altered flow pattern encountering more electrons would result in a lower methane concentration at the outlet. This modification of the existing model is to be performed during following studies. Despite these shortcomings of the model it proved to be a useful tool in designing high performance plasma microreactors for chemical synthesis.

Keywords:
Finite element model, COMSOL, reaction, model, methane, corona, microreactor, optimization

4.2 – Introduction

The chemical conversion of methane to C_2 and C_3 hydrocarbons, that is experimentally observed and reported previously, is evaluated based on finite element modelling in a finite element package in 2-D. The reactions of interest are facilitated by direct electrical activation of methane to its intermediates which results in hydrogen abstraction and subsequent hydrocarbon coupling. This electrical activation is accomplished in both the corona and glow regimes as described by optical diagnostics and electrical characterization. These atmospheric pressure regimes are accessed at microplasma electrode separation from one millimeter and smaller. Two alternative approaches are possible in modelling the experimental data. The first option is to use the governing differential equations for low energy plasma. This method can be used to track electrons and their energy distribution function based on several assumptions and classical theory. Each unobserved intermediate would also be tracked and depending on their activation energies resulting from the optimization module be labelled as likely or unlikely to be involved. The lesser computationally intensive modelling approach is to use an upper level reaction engineering approach and track only the experimentally observed species. An added complexity could be to spectroscopically measure the experimental spatial pattern for the electron density and calculate its energy distribution using classical models. This distribution of electron density could be confined to a geometry where it is physically observed to emit photons. The FEM model for the gas phase experimental data optimizes the minimized residual between the model average outlet concentration and the known experimentally measured concentration. This determines the observed kinetic rate pre-exponential and exponential terms. The determined kinetic parameters are then used to predict the experimental output of the reactor when the concentration at the inlet and its flow rate is changed through a detailed parameterization. The predictive robustness of the FEM model is evaluated by compared the deviation for different operating kinetics at the same power for that of this new data set.

4.3 – Geometry and mesh

The specific geometry to be modelled is a rectangular channel with two of the three possible discharge regions activated. The 2D simplification accurately handles the non-uniform reaction volume in x and y coordinates. The z coordinate is specified as a thickness of 400µm. The wall in the z directions of the reactor (out of and into the page) are optically polished glass except directly below and above the discharges where the electrodes are located. There is no jet at the inlet of the plasma reactor for this experiment in order to avoid adding unneeded complexities. The bypass for this data is expected to be high based on the physical space each discharge occupies.

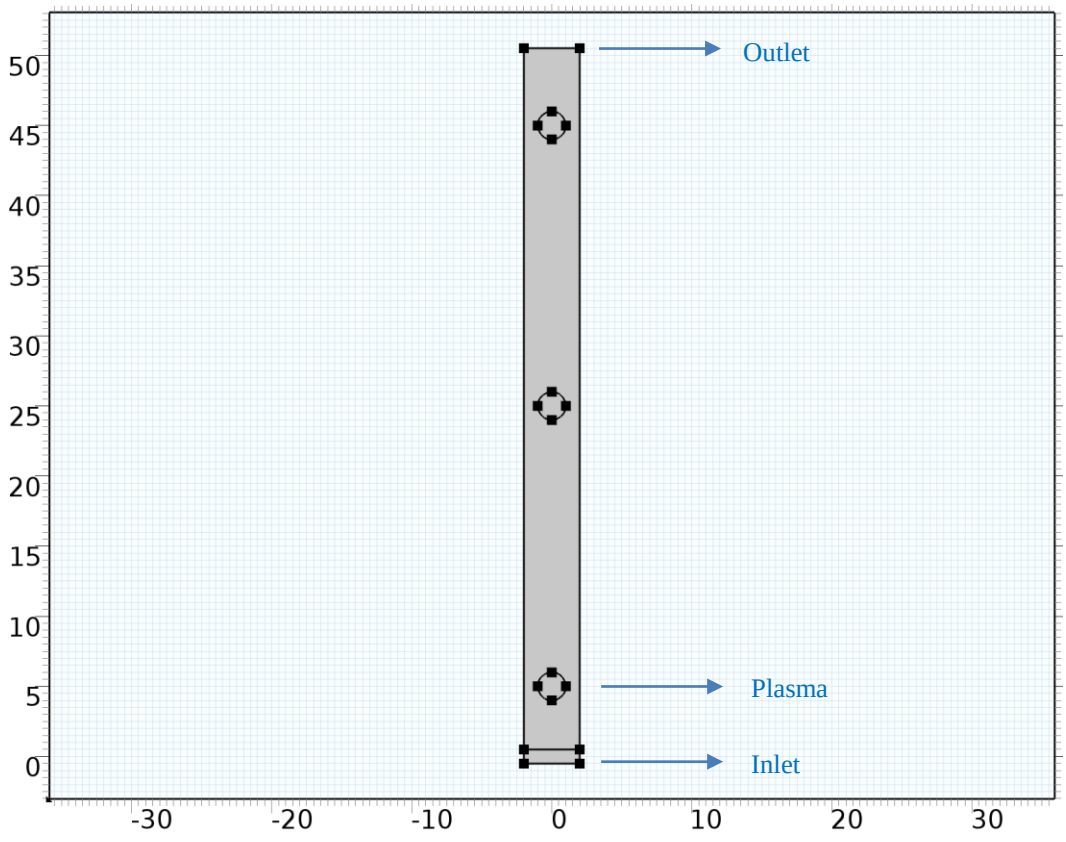

Figure 63: The flow enters the bottom line and flows through each of the possible discharge zones and out the specified top boundary.

The mesh for the microreactor geometry is as simple as possible since the high flow rates and rapid kinetics make the non-linear partial differential system of equations very stiff. The mesh is composed of 8275 triangular elements and 1136 quadrilateral elements. There are 684 edge elements and 18 vertex elements (since the two at the entrance are redundant and are for spatial probing only). The mesh quality is 0.33 on average and is made increasingly dense at the boundary of the plasma.

4.4 – Kinetic Development

The overall reaction rate laws are written to avoid assumptions in mechanistic reactions for which no specie data is taken. It is well known that the activation energy for direct methane activation is higher than the energy of activation for any oxygen bearing specie such as water vapor (which is present) which activates at 2.5eV and likely promotes hydrogen abstraction of the methane to CH_3^+.

$$\begin{aligned}
CH_4 + CH_4 &\xrightarrow{r_1} C_2H_6 + H_2 \\
C_2H_6 &\xrightarrow{r_2} C_2H_4 + H_2 \\
CH_4 + C_2H_4 &\xrightarrow{r_3} C_3H_4 + 2H_2 \\
C_3H_4 &\xrightarrow{r_4} C_{(s)}
\end{aligned}$$

The carbon balance is completed by coke formation from the heaviest measured hydrocarbon (other higher molecular species were produced but not measured due to column limitations). The rate expressions can be formulated based on the proposed reaction pathway.

$$\begin{aligned}
r_1 &= k_1 \cdot C_{CH_4} \cdot C_{CH_4} \\
r_2 &= k_2 \cdot C_{C_2H_4} \\
r_3 &= k_3 \cdot C_{CH_4} \cdot C_{C_2H_4} \\
r_4 &= k_4 \cdot C_{C_3H_4}
\end{aligned}$$

The Arrhenius parameters are composed of a pre-exponential and an exponential activation energy.

$$k_1 = A_{f1} \cdot e^{E_{f1}/RT_e}$$
$$k_2 = A_{f2} \cdot e^{E_{f2}/RT_e}$$
$$k_3 = A_{f3} \cdot e^{E_{f3}/RT_e}$$
$$k_4 = A_{f4} \cdot e^{E_{f4}/RT_e}$$

4.5 – Conservation laws

The governing conservation equations are described by the listed simplified partial differential equations which were developed for this FEM model. The transport equations relate to continuity (mass conservation) and incompressible transport at ambient pressure. The dispersion and convection of the gas may be augmented by the body force (F) if charged species are needed to interact with the electric field in the inner electrode gap.

$$\rho(u \cdot \nabla)u = \nabla\left[-pI + \mu(\nabla u + (\nabla u)^T) - \frac{2}{3}\mu(\nabla \cdot u)I\right] + F$$
$$\nabla \cdot (\rho u) = 0$$

This can be simply described in the context of the physical model which is a channel in dimensions (x,y) with a uniform shallow thickness (z). The divergence of the velocity field is easily determined by the velocity times it's coordinate.

$$\nabla u = ux + vy$$
$$\gamma = \sqrt{0.5 \cdot (4 \cdot ux^2 + 2(uy + vx)^2 + 4 \cdot vy^2) + \varepsilon}$$

The velocity at the wall is set to a boundary condition of no slip (zero gas velocity at the wall) since the gas does not flow at the rough surface. Laminar inflow is enforced since the entrance tube is over 1m in length which is an approximation since the tube shape changes from cylindrical to a channel in under 3cm of length. The Reynolds number changes during the flow parameterization data but is very close to laminar.

The mass conservation equations support a mixture averaged diffusivity matrix which is incorporated into the convection and diffusion flux expression for each specie.

$$\nabla \cdot j_i + \rho(u \cdot \nabla)\omega_i = R_i$$

$$N_i = j_i + \rho u \omega_i$$

$$j_i = -\left(\rho D_i^m \nabla \omega_i + \rho \omega_i D_i^m \frac{\nabla M_n}{M_n} + D_i^T \frac{\nabla T}{T}\right)$$

$$D_i^m = \frac{1 - \omega_i}{\sum_{k \neq i} \frac{x_k}{D_{ik}}}, \quad M_n = \left(\sum_i \frac{\omega_i}{M_i}\right)^{-1}$$

4.6 – Extracting the kinetics through optimization module fitting of power data

A cut line through the first plasma zone can be used to examine the spatial concentration within the model to determine the flow bypass and match it to experiment.

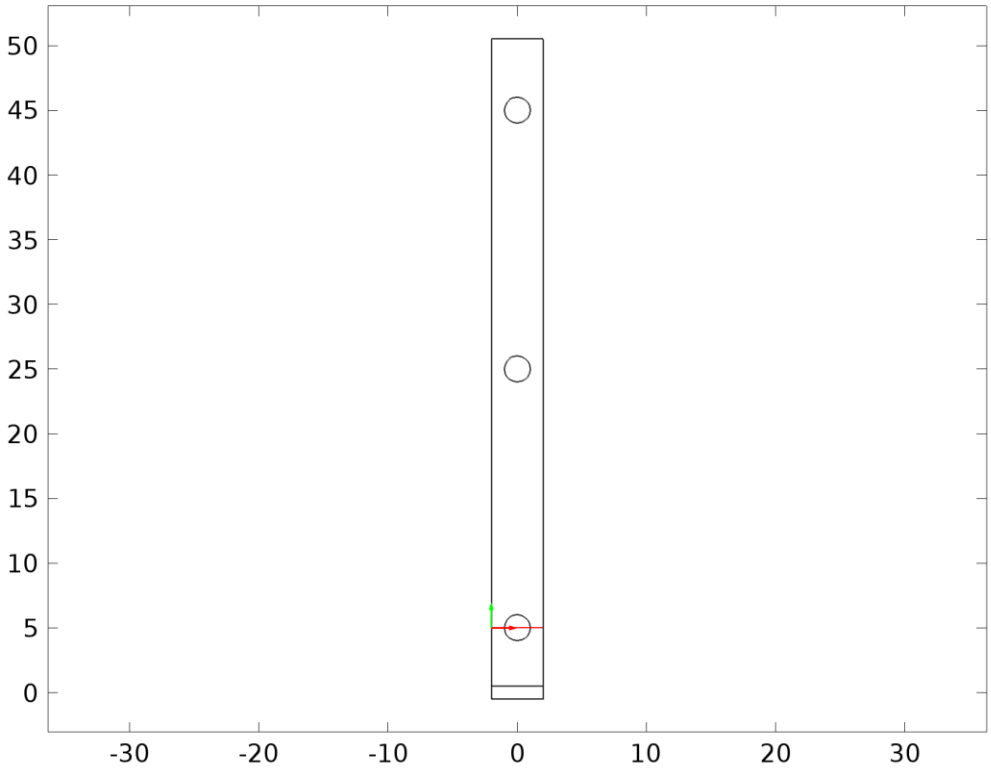

Figure 64: The first plasma zone cut line which is used to examine the transverse reaction profile.

The cut line along the transverse profile of the first discharge shows that ethane is dehydrogenated to ethylene within the first plasma. Ethane shows a change from convex to concave line shape at the densest part of the plasma as expected. This phenomena is natural since the denser filament will produce higher concentrations of ethane. This higher ethane concentration will then increase the production rate of ethylene through the rate law and result in its own increased consumption. Ethylene consumption is more complex since it must couple with methane to produce propylene.

Its rate law is therefore also dictated by methane concentration in the first plasma discharge.

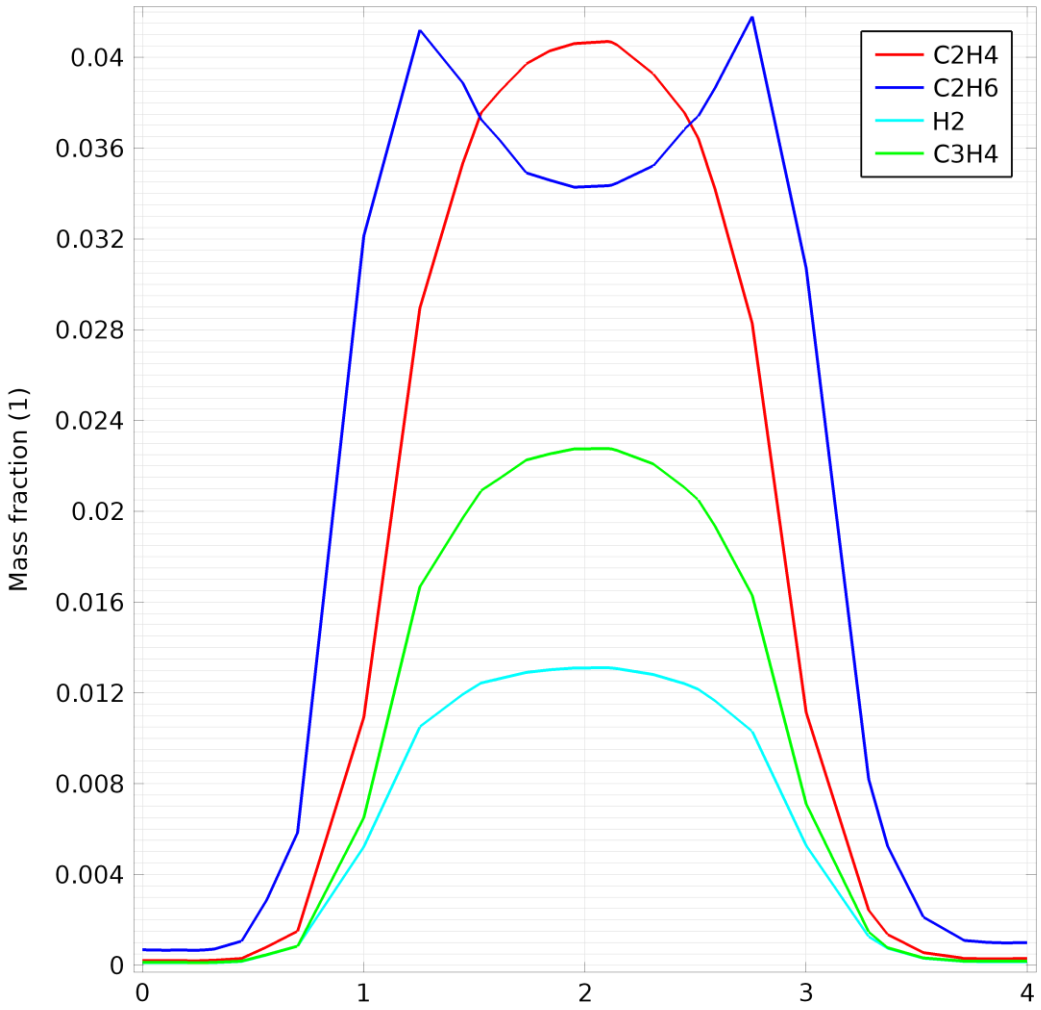

Figure 65: The transverse profile of the first plasma filament follows the expected behavior defined by the rate laws and their chemical concentration dependencies.

A longitudinal cut line shows the diffusion of products outside of the plasma zone. The impact of the flow due to electric field interaction with ions and bulk neutrals is neglected based on the diminutive relative magnitude compared to the intensity of the volumetric flow. The longitudinal cut line is taken down the length of the reactor and passes through both of the active plasma regions (the third region not being activated during the data collection of this particular study).

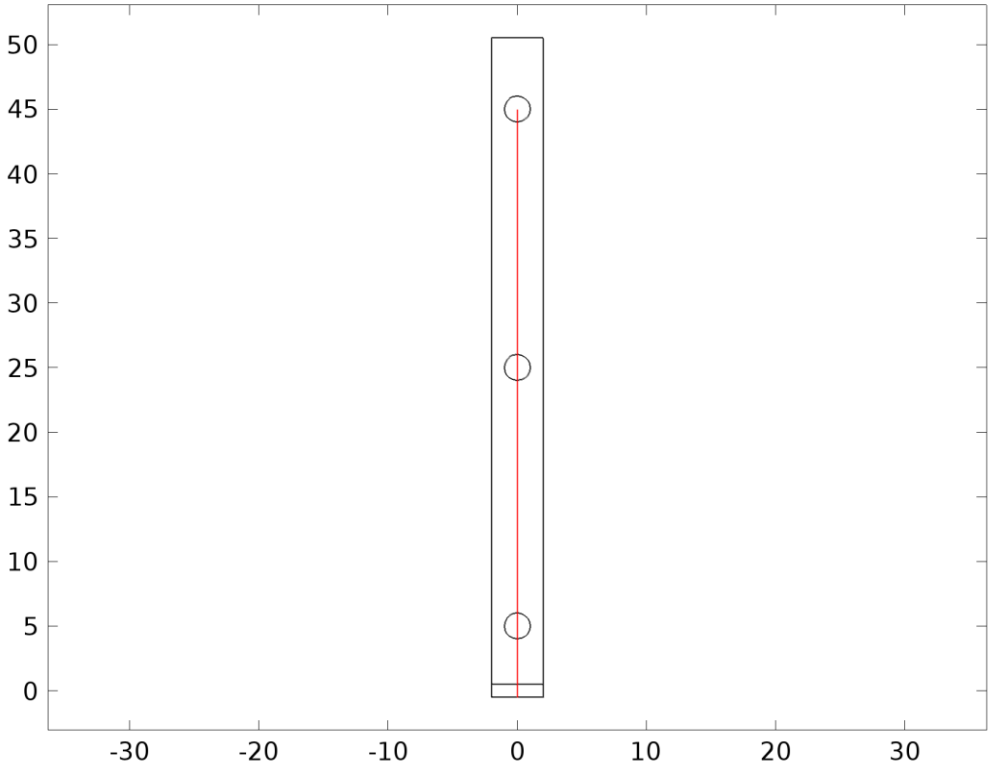

Figure 66: The longitudinal cut line which generates the 2D concentration profile of the reacting species.

The FEM output for a sample run shows a longitudinal mass fraction profile based on the cut line previously illustrated. The conversion of methane is rapid in the center of the filament at 5mm. Its concentration recovers as it mixes with the bypass methane after the plasma filament. This occurs after the plasma filaments centered at 5mm and 25mm. The outlet steady state concentrations for this power setting and flow selection can then be taken (at 50mm) and compared to experimental results.

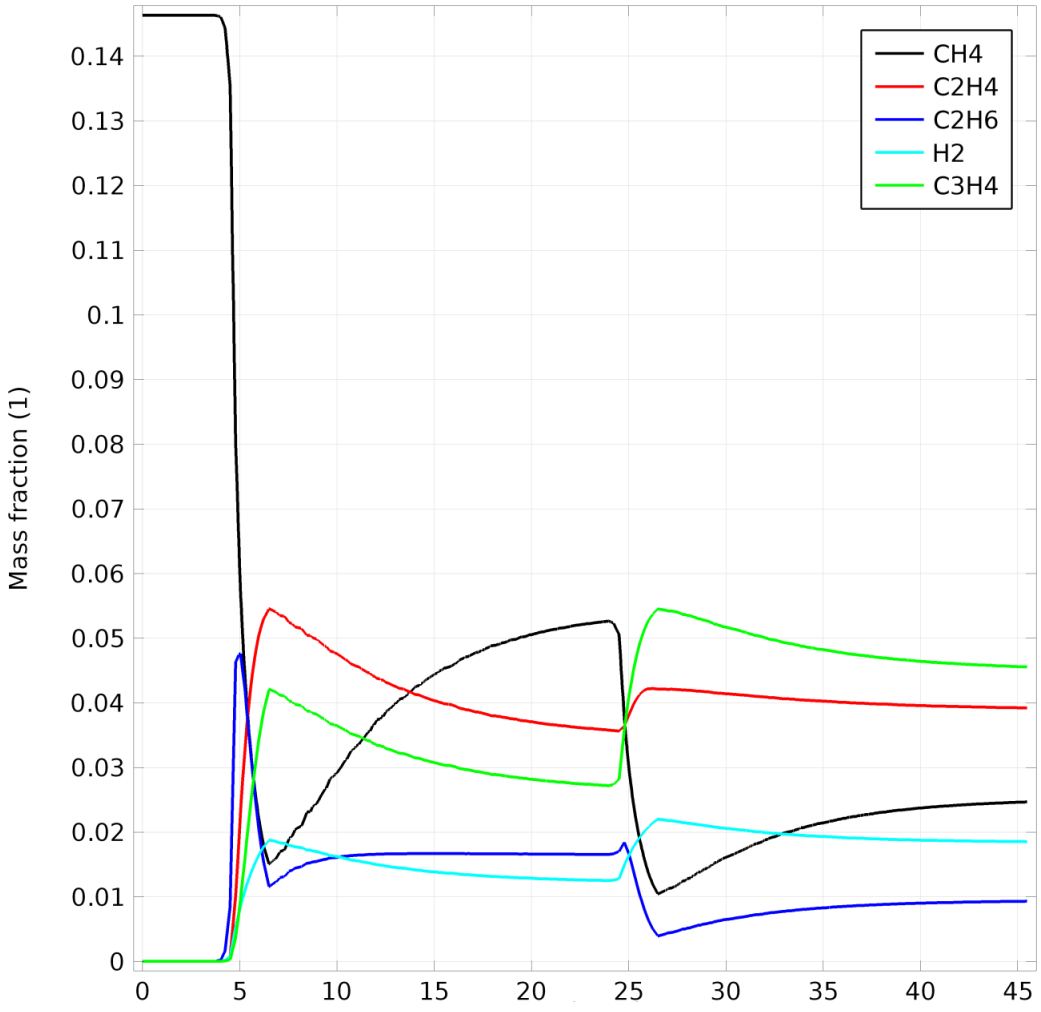

Figure 67: The longitudinal mass fraction shows the response of each species concentration as it passes into and remixes after each plasma filament.

The concentration surface profiles show the described flow bypass very clearly. The portion of fluid that enters the plasma filament is easily recognized to be less than half of the total flow. This is desired from a mathematical standpoint since the effect of interacting plumes would be difficult to model chemically. There are also physical limitations when studying a single plasma filament or filaments in series. They may not be placed close enough to interact with the spacer boundaries.

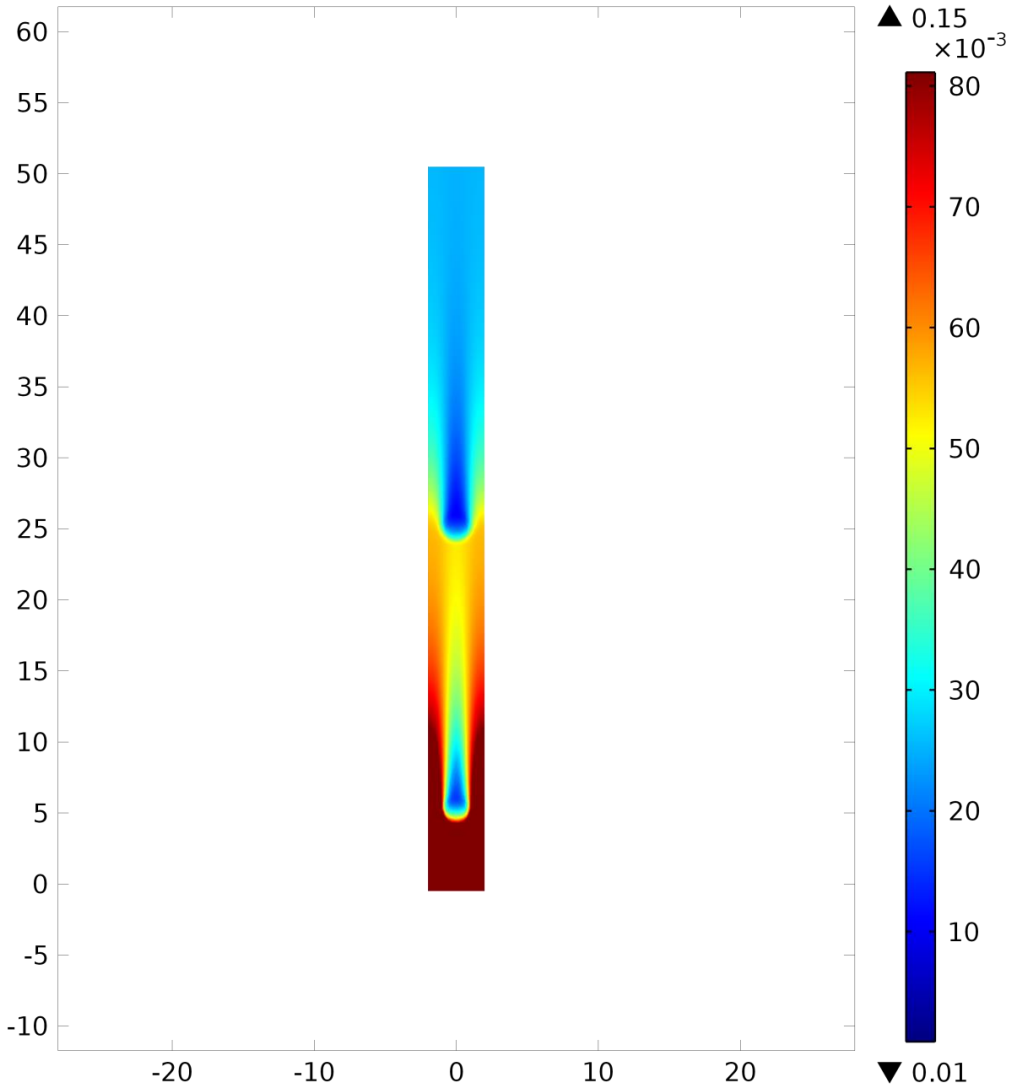

Figure 68: The surface profile for the reactor. Methane mass fraction is highest at the bottom inlet and lowest at the top exit.

The surface profile for the products is equally interesting and demonstrates the power of FEM models when designing reactors for certain products. For example, the products ethylene and ethane interact so that contacting ethane produces more ethylene. The arrangement of the plasma filament can be used to isolate intermediate products or to maximize the electrical efficiency of a process by converting ethane to ethylene using the most efficient plasma filament placement.

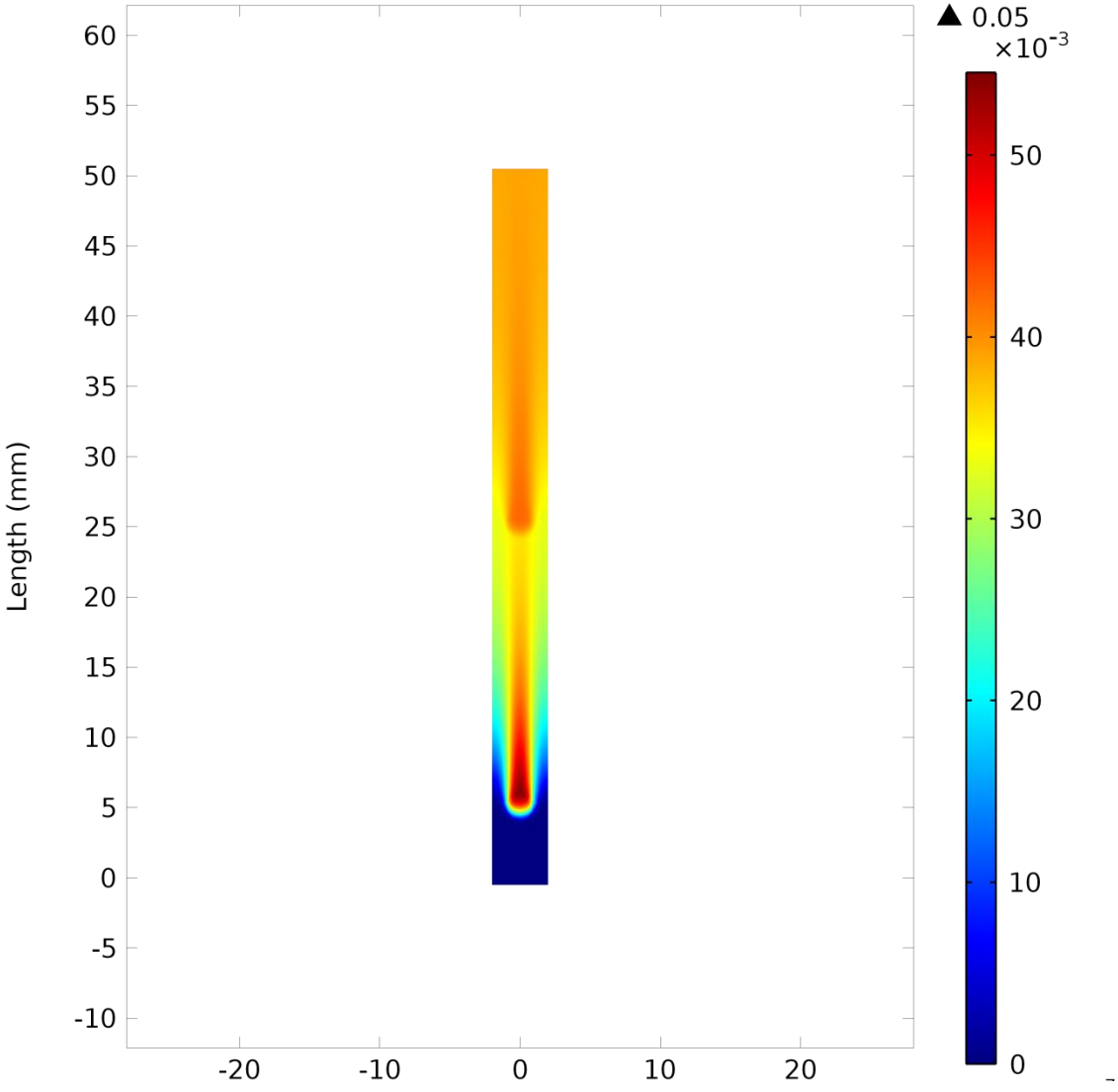

Figure 69: The ethylene mass fraction surface plot shows that the highest product yield is actually after only one plasma filament. If all the fluid were treated uniformly by placing many discharges in an offset and staggered formation much high electrical efficiencies than 40% could be achieved.

The ethane concentration surface plot shows similar information. Based on the mass fraction around the first plasma filament, a residence time reduction of ten or a hundred times would produce almost entirely ethane. It should be noted that a different energy distribution based on gap separation or on current density or plasma regime (location on the current versus voltage curve) could also easily yield the same effect at the higher residence time.

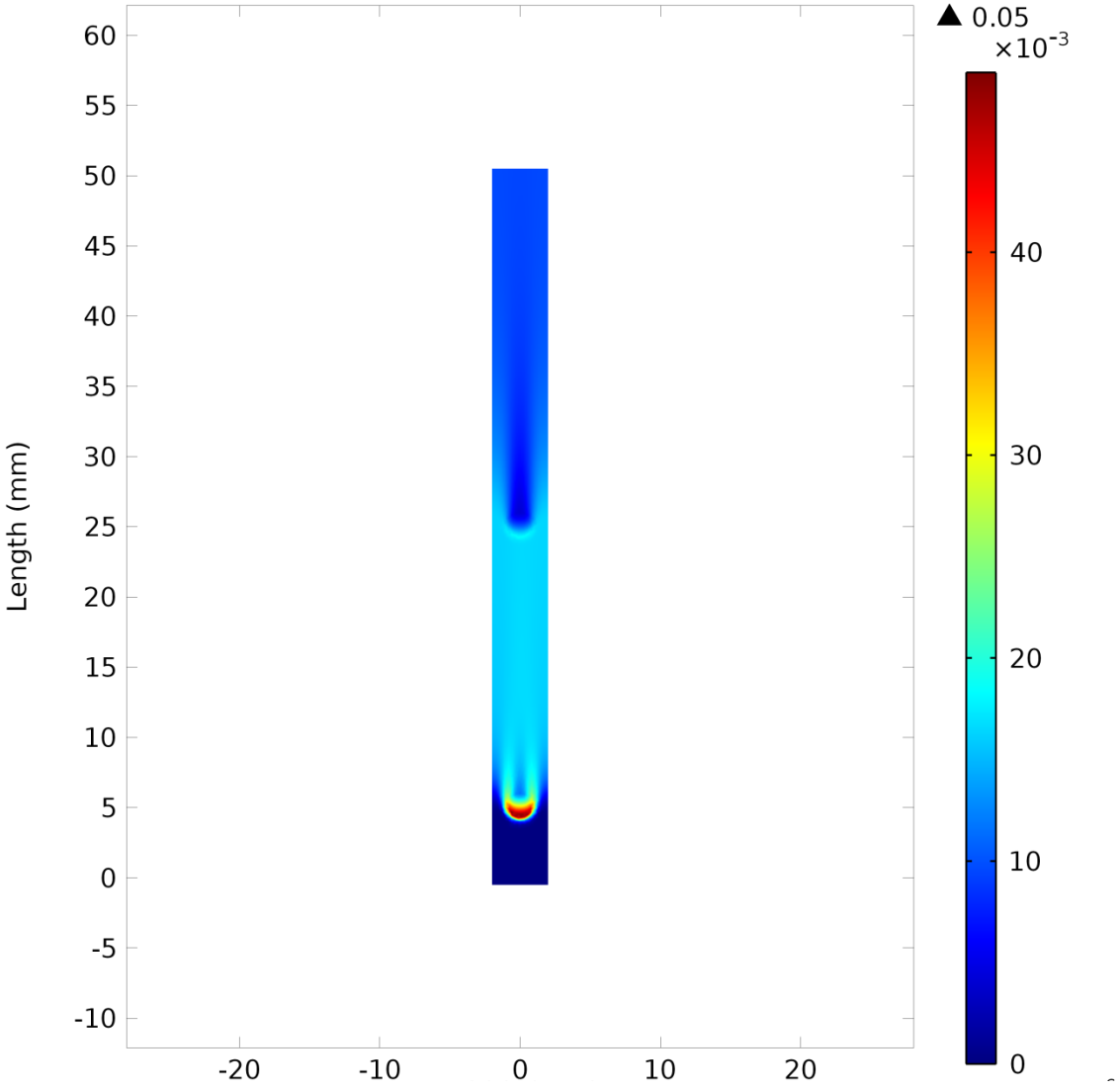

Figure 70: The surface mass fraction plot for ethane shows it is produced at the boundary of the first plasma filament and almost entirely consumed in favor of ethylene before reaching the exit.

The final cut line is placed at the end of the reactor and represents the point where the boundary average concentrations are taken from the FEM model in order to compare them with the experimental data.

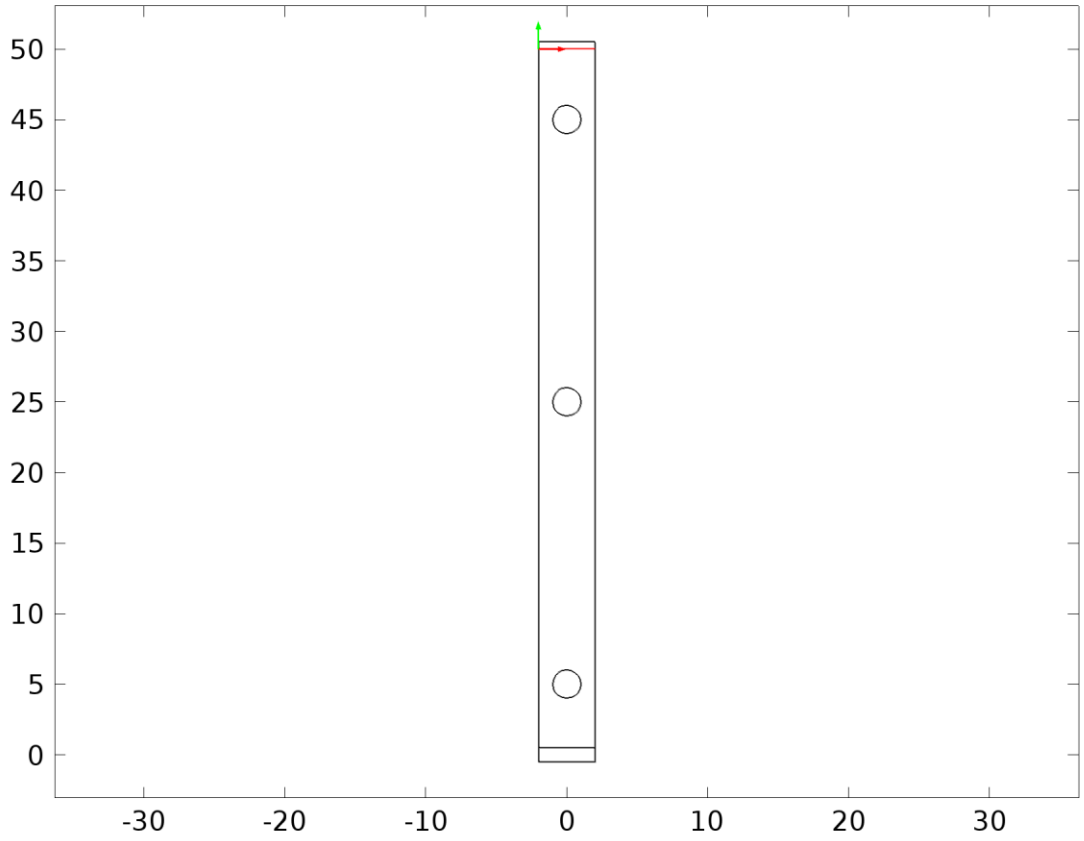

Figure 71: The average mass fraction for each species is averaged and exported to for comparison with experimental data using the boundary probe.

The pre-exponential kinetics are described previously as dependent on the number of electrons as determined by the current. These kinetics are adjusted by an optimization routine after an initial guess is provided. The optimization module in the FEM package is set to minimize the residual of the square of the difference between the model and experimental result at each of the power settings. These resulting kinetics are developed as a function of applied power. The electron temperature remains relatively constant (exponential electron temperature distribution) in the glow discharge regime since the

increase in voltage is slight over a large change in current. The pre-exponential kinetic term is in this way almost entirely determined by the current passing through the plasma filament. The relatively constant electric potential applied to the plasma filament determines the electron energy distribution and the constant exponential factor. The power data is plotted in terms of the controlling parameter (current density) and both the experimental data and the FEM output resulting from the optimization module. The FEM output fits the data perfectly (the red line is offered as a visual aid only – the red circles are the FEM output).

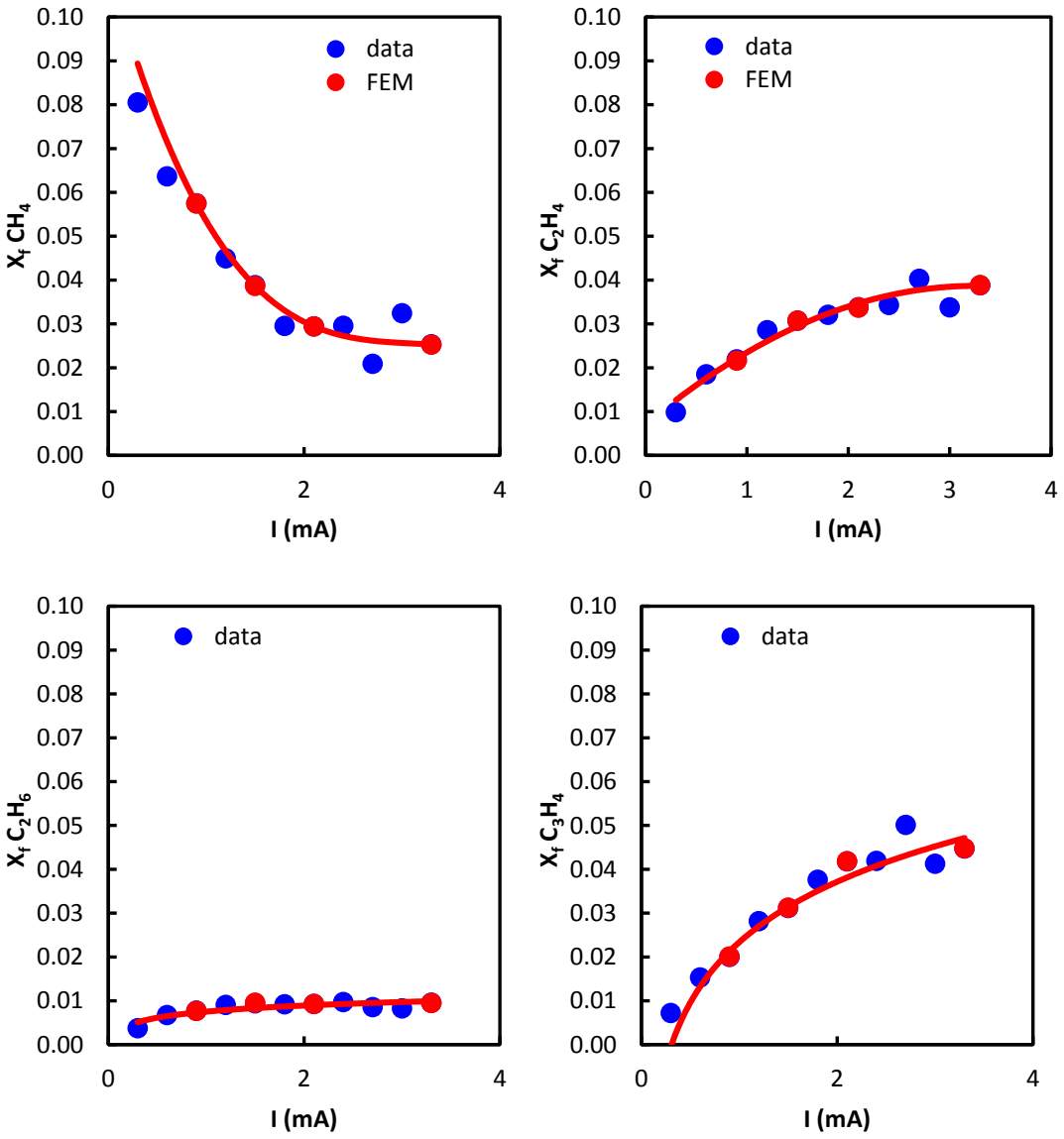

Figure 72: The conversion of methane to its coupled forms is accurately reproduced. The concentrations of C_2H_6, C_2H_4 and C_3H_4 are directly overlapping the experimental measurements.

The red line of the last plot is forecasted outside the bounds of the model in order to demonstrate that the model kinetics are valid only for the power for which the data is modeled against and extrapolation to conditions other than considered within this study must be done with experience and understanding.

4.7 – Evaluation of the reaction model for flow rate changes

The finished kinetic model, which is fitted to the previous power study, is evaluated for correctness or robustness by using the discovered current dependent kinetics at only one of the power levels and then applying the model to predict the resulting conversion and yields under different inlet concentrations of methane which are also delivered at varying flow rates. In this way, the model will have these rigorous demands to demonstrate its validity which otherwise would not be well known. Also, short comings, which are present in all models, reveal which simplifications are less valid.

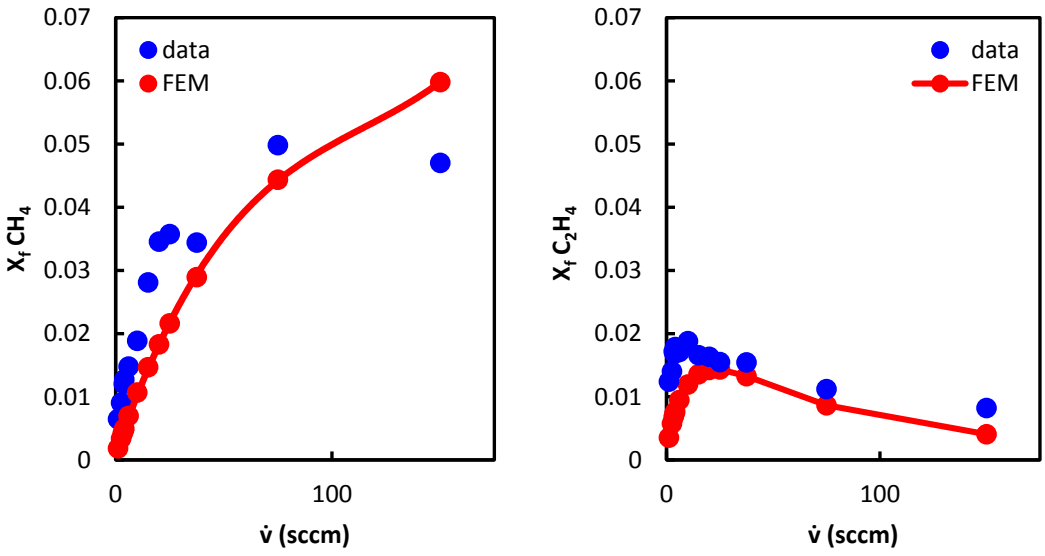

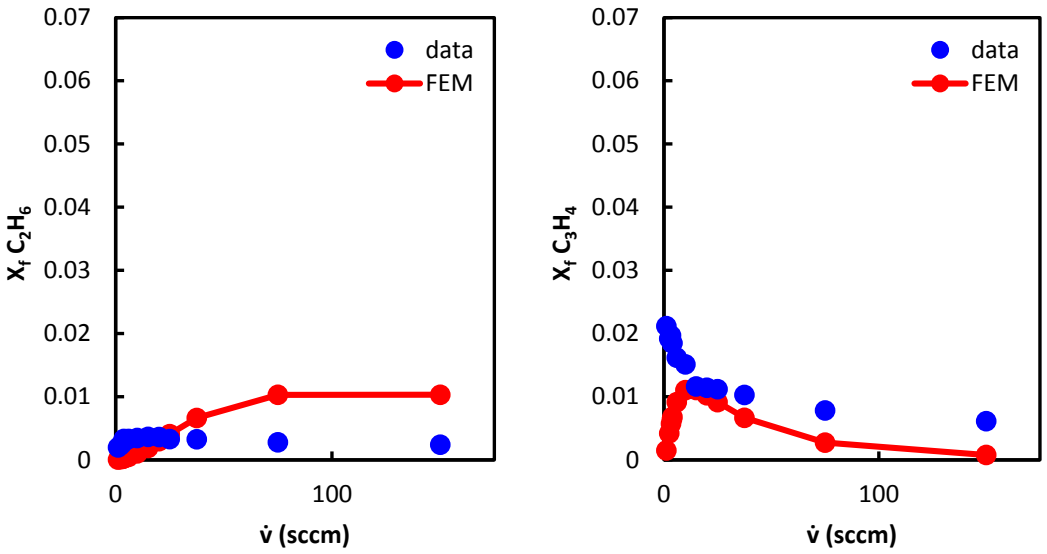

Figure 73: The previous kinetics extracted from the power study very closely predict the results for each of the species during the flow study.

The deviation which is observed in the mass fraction of ethane is likely based on an incorrect guess of the plasma reaction boundary which is probably an underestimate (it was taken as the visual bounds of the photoionized plasma channel which emitted light detected by human inspection). The model did accurately predict the results of that experiment except in one aspect. The low flow rates of the fourth plot deviate downward from the actual measured mass fraction. The experimental explanation is simple. A syringe pump is used to determine the flow from the reactor at extremely low flow rates while the mass flow controllers are opened upstream. The pressure regulator is set to 25psi which is a higher pressure than atmospheric. The syringe pump therefore increases the pressure in the reactor proportional to the lower draw rate. The C_3H_4 product kinetics respond rapidly to increased methane concentration which is proportional to inlet pressure (as previously observed in experimental conditions when varying methane ratio to nitrogen inert). Higher hydrocarbons were not measured during these runs due to column limitations but a more in depth study of $\sim > C_8$ hydrocarbons should be investigated at high flow rate and pressure.

4.8 – Conclusion

The process macroscopic kinetics are determined by the FEM optimization. The FEM model yields are compared to experimental yields during extraction of kinetic values and during predictive flow testing. The proposed model has four simple product rate laws, laminar flow in a microchannel, diffusion determined by mixture averaged properties, isothermal cooling of the product stream by the bulk during this room temperature plasma treatment.

The fundamental modeling knowledge that is gained here can be used to treat fields of plasma filaments which are staggered spatially in order to leave almost all of the flow directly treated by making less gas bypass and more flow path gas-plasma intersections. This can be accomplished by staggering plasma discharges and by using internal spacer microarchitecture to direct the flow into the center of the filaments for high conversion and selectivity at excellent electrical efficiencies.

The calibration for the products is accurate and based on injections from high purity standards. The value of the product yield is reliable since the product peak areas grow to the same size as products are reduced to a much smaller fraction of their original peak area on the HID. Coke formation is reduced by operating at 0.5 to 0.9 mass fraction nitrogen and could be eliminated by purging the reactor with steam at cleaning cycle intervals. High conversion of methane poor streams are achieved with electrical to chemical conversion efficiency upward of 40%. Reactor lifetime is prolonged by operating at microseparations that are optimally designed to soften the electron energy distribution. This is done by operating far enough from Paschen’s minimum for the processed gas mixture. Glow discharges in series can be modelled using finite element modelling. The kinetics are recorded for future use and are most useful in design iteration. An optimal reactor design could be produced which would optimize yield at the highest possible electrical efficiency using this package. Further study should focus on types of flow distributors, discharge array types, micropoint types and higher molecular weight hydrocarbons which facilitate product separation and recovery.

Chapter 5- Methane Dry Reforming in a Microplasma Device

Justin Pommerenck, Yu Maio, Peter Kreider, Yousef Alanazi, Goran Jovanovic, Alexandre F T Yokochi, Nick AuYeung

Industrial and Engineering Chemistry Research

ACS Publications
1155 Sixteenth Street N.W.
Washington, DC 20036, US

(to be submitted)

5.1 - Abstract

A plasma microreactor for the carbon dioxide dry reforming of methane successfully converted methane and carbon dioxide to synthesis gas at atmospheric pressure and ambient temperature. The maximum conversion is 70%. Flow rates ranged from 2-200sccm. The energy cost is as low as 200-400kJ/mol. More than 90% selectivity to synthesis gas is achieved during these experiments with C_2 and C_2 $C_{(s)}$ (1-2%) making up the remainder. Carbon solid formation is reduced to 1-2% from 8-12% by reducing the scale of the plasma from 1cm to 1mm and thereby increasing the flow velocity of the gas in the plasma itself to achieve ultrafast residence times necessary to maximize selectivity and conversion. The maximum conversion for low flow rates during flow rate parameterizations is used to characterize several plasma microreactor geometries in terms of gas bypass around the active electron region of the plasma. More than 30-40% of the gas is not directly treated in the plasma and could result in reducing the energy consumption per mole of synthesis gas by almost half. These experiments in single plasma microreactors and series of plasma microreactors are used to evaluate the dry reforming reaction for potential industrial application.

Keywords:
Dry reforming, methane, corona, microplasma, synthesis gas, dc plasma, carbon dioxide

5.2 – Introduction

Dry reforming of methane has been studied actively for its potential contribution to both a hydrogen economy and for synthesis gas production. The reaction is typically performed in the presence of thermally activated catalysts since the reaction must be operated at high temperature to proceed and low pressure for optimum yields. Non-thermal plasma is particularly effective as an activator for this reaction because the reactor can remain at low temperature and pressure and alleviates the formation of coke which is strongly coupled to a higher activation energy barrier than the activated reaction itself. The largest research focus has been directed toward dielectric barrier discharge and high current thermal dc torches.[160, 161, 162] This is due to the efficiency and yield gains which are perceived for ac over dc plasma in the improved contact area of the gas with the plasma accordingly proportional to the number of ac filaments formed during the average residence time of the gas. Several studies report good efficiencies (around 200kJ/mol at 70% efficiency). Often this is due to dilutions of the feed with noble gases such as helium or argon (up to half of the feed volumetrically). Very exciting controlled work in an alternating current non-thermal gliding discharge, which uses inertial flow effects and controlled power parameters to lengthen the plasma reaction volume, attains the highest dry reforming efficiency in literature at 50% conversion (89 kJ/mol at 91.4% efficiency).[163]

This study reports that a series array of continuous dc glow discharges in a microreactor can be shown to improve energy efficiency, conversion, yield, selectivity and reduce coking by uniformly treating the inlet feed gas using a microemitter array for the formation nonthermal microplasma. Inherent energy gains based on reduced electric potentials required to produce the same (lower energy) number of charge density in a plasma has long been understood. Plasma operation using microplasma gives more low energy initiators for select reactions that are desired. Since residence times required for fully performing the dry reforming reaction are on the order of microseconds, lack of conversion is typically bypass of the plasma filament itself in flow through reactors.

B. Zhu *et al* demonstrate (in Figure 1 of the referenced publication) that energy consumption (kJ/mol) increases and then decreases with gap separation.[164] This optimum implies that it is the space occupied by the plasma and the flow profile in the plasma device which work with or against each other in different reactor flow configurations.

It is a useful microreactor design utilizing arrays of microstructures which is capable of scaling the process from one discharge to multiple discharges at the same low power. Low powers are required to improve conversion and efficiency based on the uniform treatment of the flow at near microsecond residence times. This has the added advantage of reducing coking due to elimination of competing side reactions by having a uniform flow profile in the discharge.

R Snoeckx *et al* correctly reports that, "The effect of the frequency is more complicated: we observed that the product of frequency (f) and residence time (s), being a measure for the total number of microdischarge filaments which the gas molecules experience when passing through the reactor, was critical. For most cases, a higher number of filaments yields higher values for conversion and energy efficiency."[165] It is inherent in the design of plasma microreactors that allows for the uniform treatment of the gas flow in a plasma field. This is necessary both to reach high conversions and efficiencies.

With respect to the controlled low energy of the electron initiators in microcoronas or glows, it is possible to select certain chemical pathways that strategically results in higher efficiency based on improved yields. Korada Supat *et al* points out that the average electron energy in a centimeter corona discharge is less than 6eV and that dissociation but not ionization of methane is possible.[166] This control over product selectivity is not likely tunable when using high peak voltage ac plasma or pulsed dc plasmas that have pulse durations longer than nanoseconds (the time required to interact and accelerate an electron in the proximity of the corona glow). The trends are

very similar when relating process parameters between low energy and high peak energy plasma which makes those processes very intriguing.[167]

In this study, the direct chemical activation using continuous dc microplasma for carbon dioxide dry reforming of methane has been successfully performed. The product reactions yield synthesis gas with a selectivity of up to 90% with the remainder as C_2 hydrocarbons. The microplasma conversion of methane and carbon dioxide to synthesis gas is energetically competitive with thermal dry reforming (kJ/mol synthesis gas produced) at low conversion of methane (15%). In a scaled-up reactor (which unfortunately had high bypass (30 - 50%)), the process is more energy intensive than thermal dry reforming at high conversion (70%). Regardless, the highest reported efficiency for plasma conversion of stranded methane to liquid fuel precursors without the use of physical catalyst is achieved using dc microplasma in arrays on a microreactor platform.

5.3 – Methane dry reforming experimental setup and reactor geometry

Two 200 sccm Brooks™ mass flow controllers, which are operated by a single microcontroller, are fed methane and carbon dioxide by gas cylinders regulated to 25 psi. The mass flow controllers are calibrated volumetrically. A 20ml vial is filled with water and glass spheres. The inlet gas is sparged through the water to obtain a consistent water vapor content based on the flow velocity and ambient temperature. This mixture of methane, nitrogen and water vapor reaches a typical flow velocity of 0.5m/s in the inlet tubing which forms a jet into a perpendicular dc non-thermal plasma. The effluent is sampled using either an in-line 150μL sampling loop or 1μL Hamilton Syringe via the front port of a SRI model 6100 gas chromatograph using HID detection after a Hayesep D column. Mass spectrometry is used to identify products. The 150μL sampling loop is used for minor species while major species are measured using the 10μL Hamilton Syringe. A simple illustration for the setup is shown below.

Figure 74: The gas cylinder regulator and mass flow controller output flow to the microplasma device which is sampled by both a manual 150µL sample injection loop and 10µL syringe.

A single plasma discharge series using tungsten rods yields the fundamental conversion possible in single plasma filament. Bypass is a relevant issue since the plasma is not allowed to touch the walls and flow can pass through the reactor around the plasma.

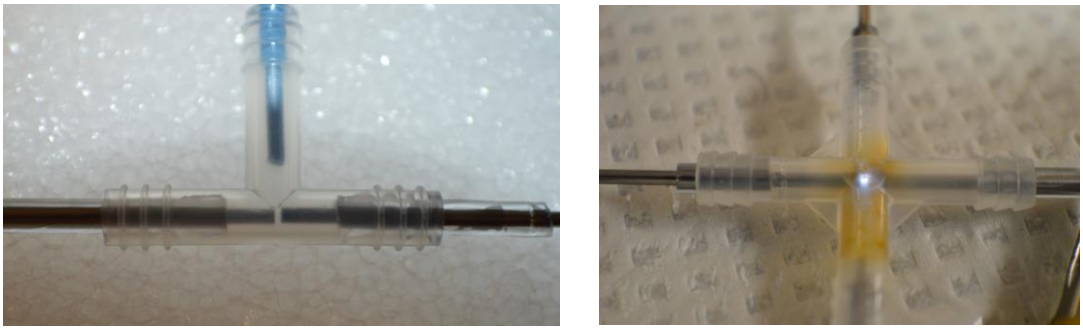

Figure 75: The T design (new) and Cross design (after 10hr operation) are used to produce dry reforming data.

The power supplied to a single discharge is 1 - 6W. Higher powers and conversion are reached by increasing the number of discharges in series. Higher residence times and conversion are reached by increasing the number of discharges in parallel.

5.4 – Results from series of single microplasma microreactors

An initial flow parameterization can be useful in determining the processing capability of a discharge. The cross design microplasma reactor is used to obtain an idea of the maximum conversion possible for each of the species relative to each other. While not mechanistically representative of the actual activation energy barrier for these reactions since third party species such as vibrationally activated water may interact in the reaction network process, it still offers an estimate of the effective energy required to make one molecule of desired product under these conditions.

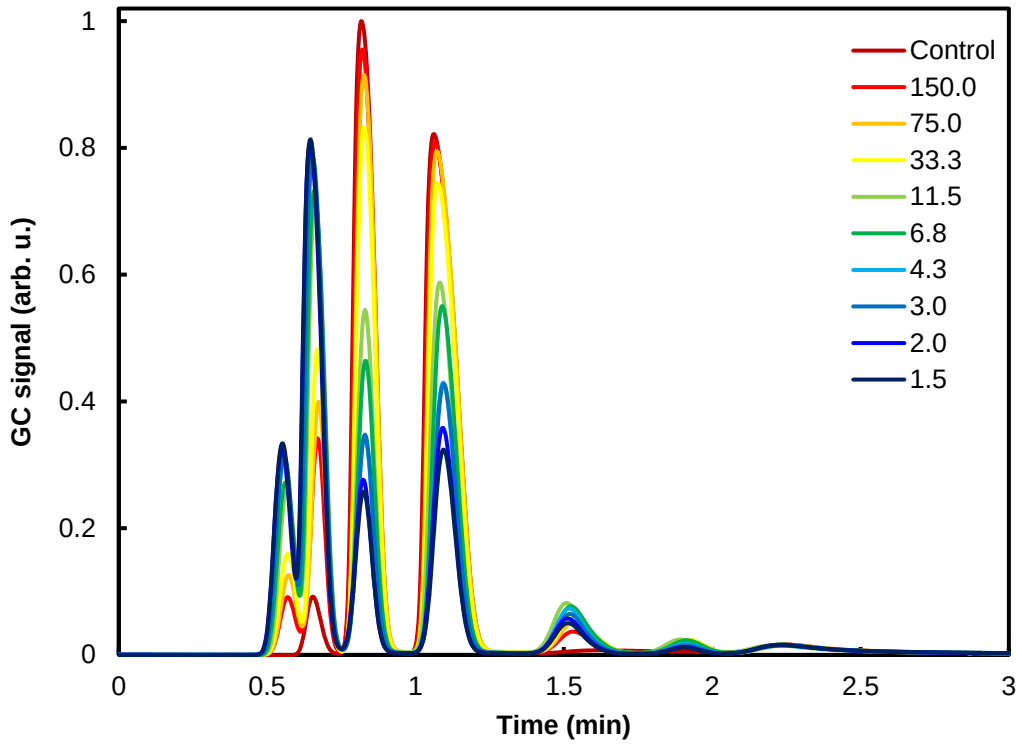

Figure 76: The raw data shows the elution of gas products over time for each of the flow rates (sccm).

The maximum conversion in methane is observed to be slightly higher than that of carbon dioxide. From this data, it has been identified that the effective activation energy for CO_2 is greater than that of CH_4. This

The previous raw data is then integrated and normalized (**Figure 76**) or calibrated using standard gas chromatography calibrations developed during this study (**Figure 77**).

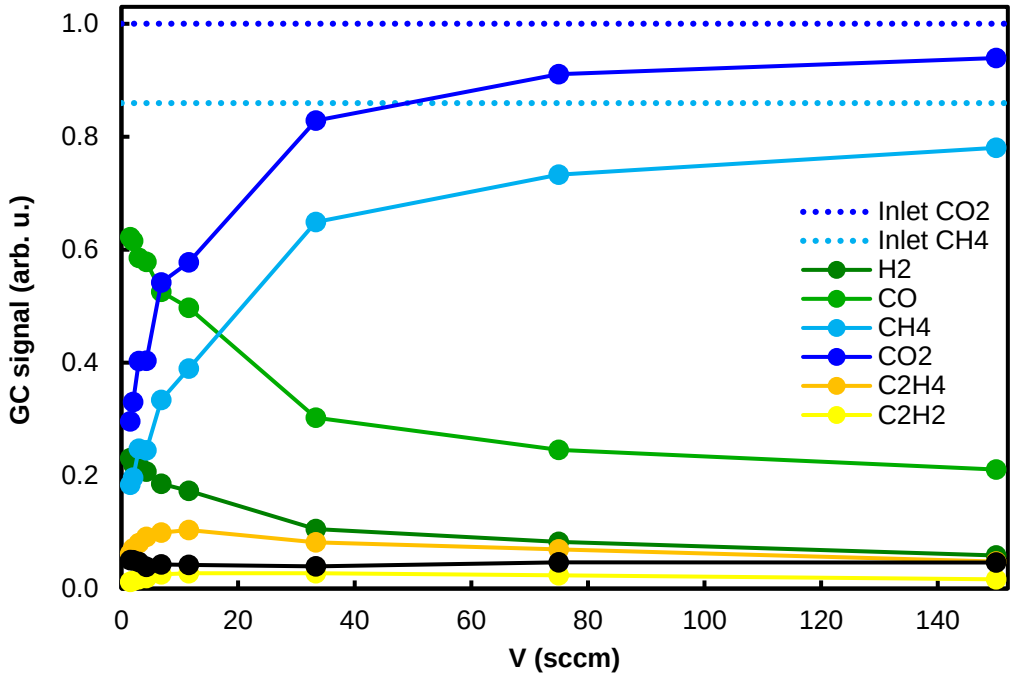

Figure 77: The products are identified as CO, H_2 and C_2 hydrocarbons.

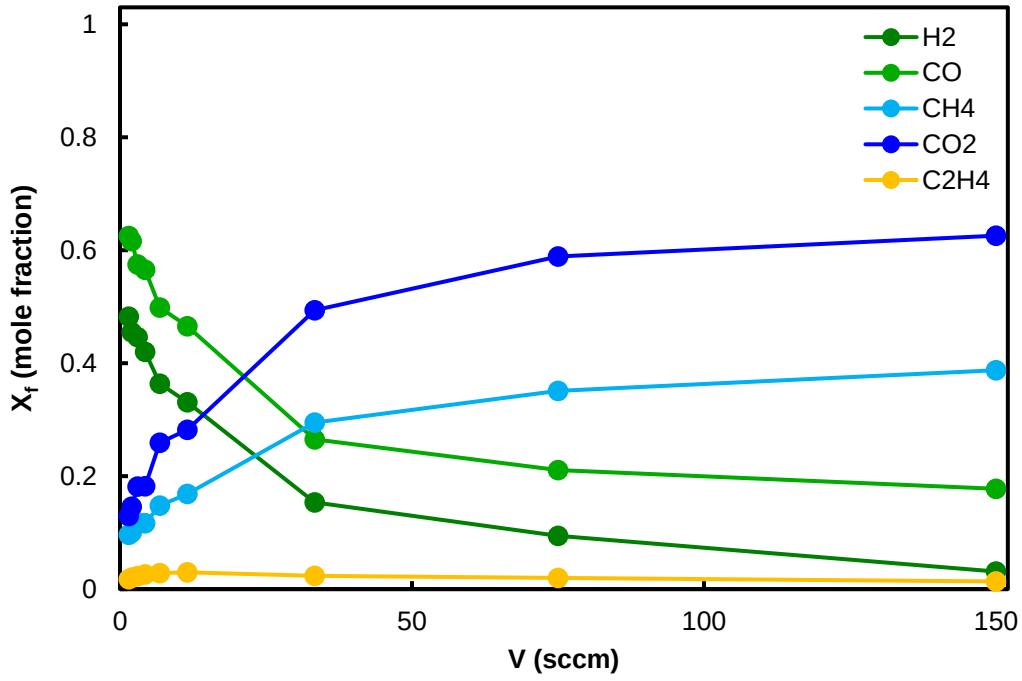

Figure 78: The product selectivity is very strong toward CO/H_2 (almost 95%) with a ratio of 1.3:1.

5.5 – Results from fields of microplasma in a microreactor

The second data set is the slightly scaled up reactor with an array of rods with 30 micron sharp points. These metal emitter electrodes are spaced at intervals which when activated could reduce bypass by intercepting flow that would normally move around a single horizontal line of electrode gaps. With a greater number of discharges, larger powers are required. However, with a greater number of discharges and a higher gas flow rate it is possible to increase both yield and the conversion due to bypass reduction. Both of these factors lead to higher process efficiency for microplasma dry reforming.

Figure 79: FR4 electrical board is used to house a channel that is hexagonal. The channel is defined from the inlet copper tube to the outlet copper tube on the opposite end. The rods have counterparts on the top and bottom face of the FR4 board and are soldered in such a way as to make an electrical series.

Second scaled up reactor with plasma arrays spaced at 1.5mm intervals. The first image shows four middle rods activated. The second image shows the three last rods activated. With electrical series, the desired rods can be activated and conversion of methane and carbon dioxide examined to estimate bypass. The second set of data is done with only the first five rods activated due to the unanticipated thermal limits of the FR4 board to 20W without using active cooling from a heat sink. For a CO_2 discharge operating in the hysteresis portion with what would be between glow and corona for a plasma air discharge, the required operating voltage is 700V and typical currents are 1-5mA. Carbon dioxide dry reforming of methane can be evaluated as an example performance indicator for the horizontal single array. The results are shown below. The raw integrated output from the gas chromatography unit (**Figure 79**) and the relevant

calibrated compounds that are involved in the carbon and hydrogen balance (**Figure 80**) are depicted as in the power parameterization described previously.

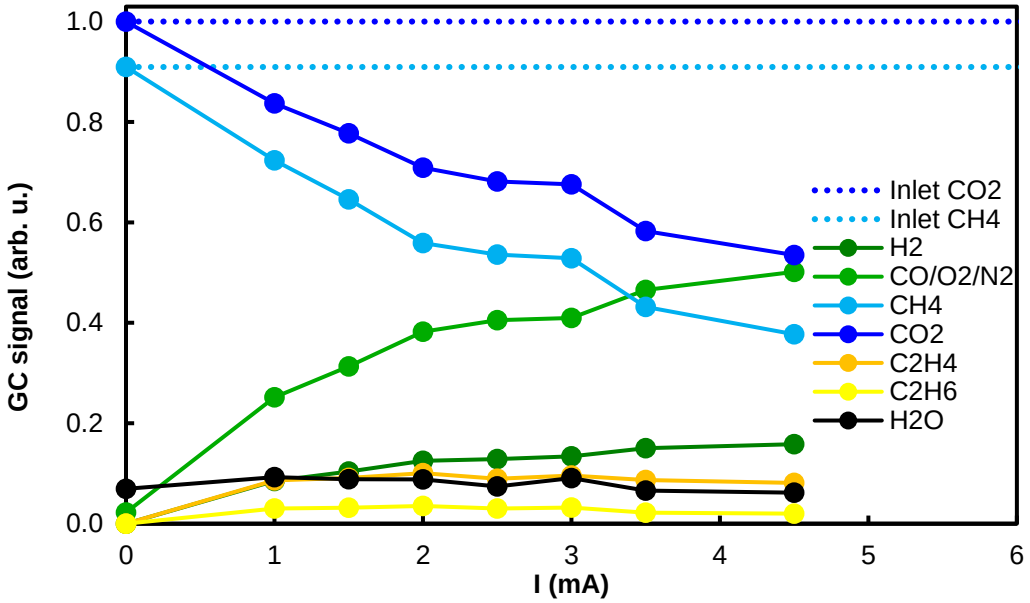

Figure 80: C_2 hydrocarbons are produced in minority while CO and H_2 show the strongest selectivity.

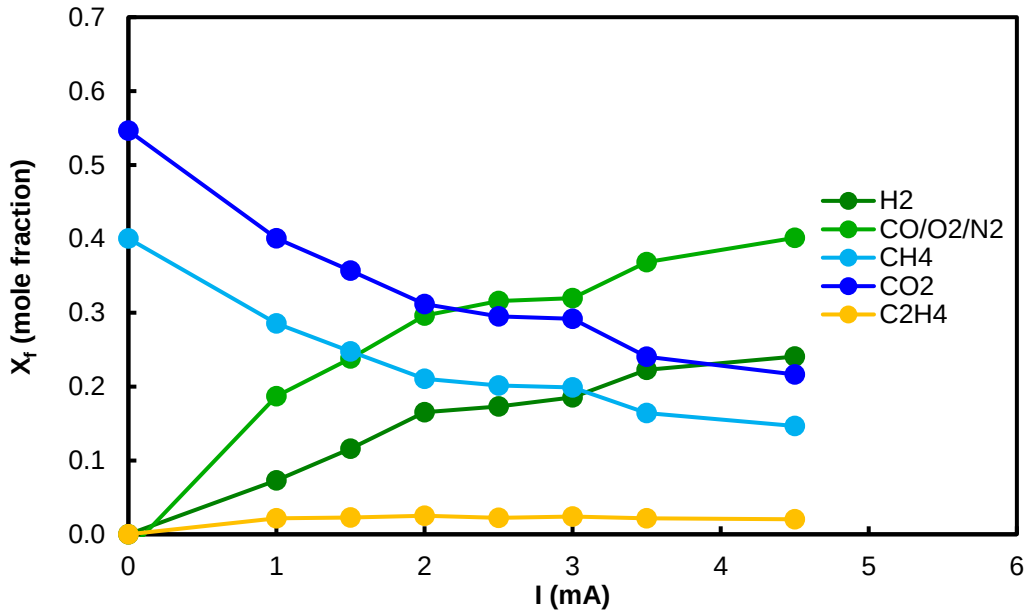

Figure 81: More than 60% conversion of CO_2 can be accomplished for more than 15sccm feed in the footprint of a quarter sized plasma carbon dioxide dry reforming microreactor.

The first and second reactor can be compared for energy cost as long as it is understood that the conversion at each flow rate or power dictates an additional energy cost that will be required in separations.

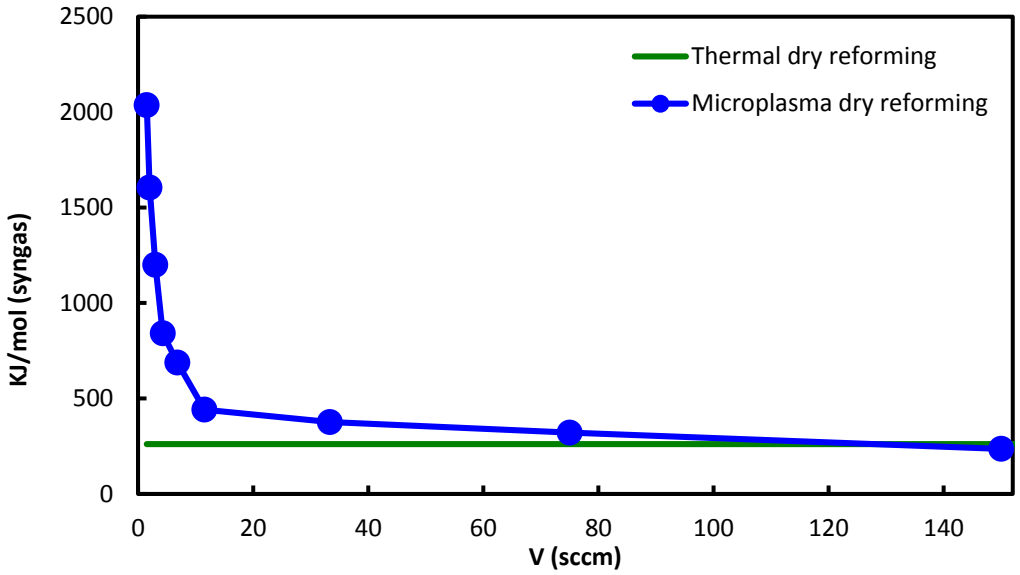

Figure 82: The flow rate shows that at 20 to 140sccm the microplasma dry reforming of methane with carbon dioxide is competitive with thermal dry reforming however the conversion of feed is 40% rather than 90%.

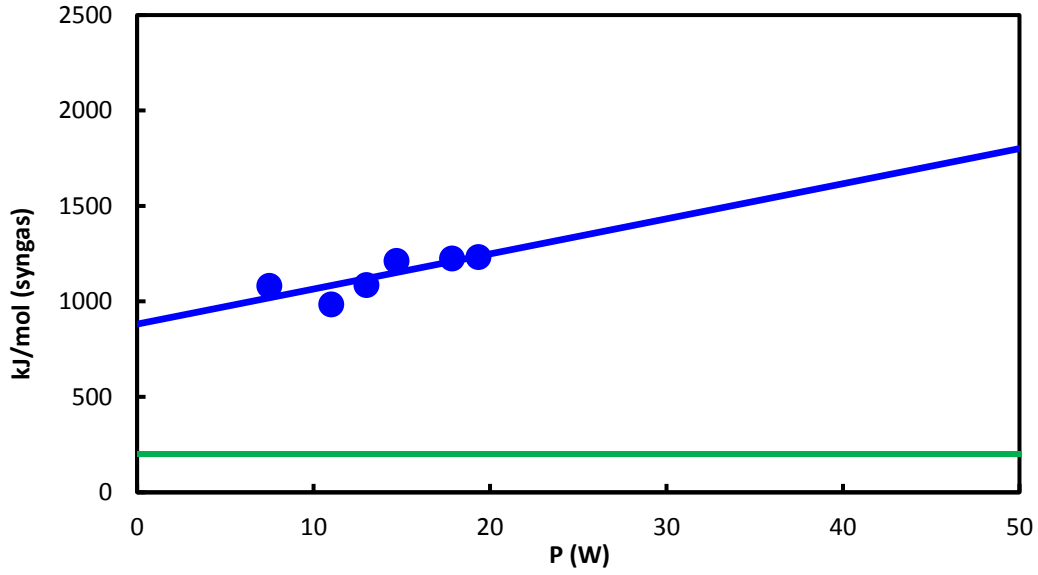

Figure 83: The array reactor has 50% bypass (which can be changed with reactor design and power delivery optimizations) as described before and would be about half the energy cost to run at the same conversion.

The bypass for a non-linear array of plasma spaced at intervals approximately equal to the size of each plasma filament is likely 50% (the plasma is spaced at 1.5mm intervals for the previous study). All of the rods (those staggered in a second row behind the first row) being active would likely result in higher efficiency with similar selectivity toward synthesis gas (90%) at higher conversions (90% instead of the achieved 70%) despite the increased power consumption if the flow rate is increased without increased bypass as preliminary data for scaled devices suggests.

5.6 – Conclusion

The feasibility of microplasma carbon dioxide dry reforming in a microreactor with a dc sustaining voltage under 1kV has been demonstrated. More than 70% conversion of carbon dioxide is achieved in an unoptimized reactor with only a single horizontal array of pins activated. The electrical efficiencies based on production of moles of synthesis gas is reported and compares favorably with the ideal thermodynamic efficiency of a thermal dry reforming process. The formation of carbon solid is reported at each of the methane mole fractions tested during the study. Reactor lifetime in pure is methane is 30s. Reactor lifetime is several days at 10-30% methane in carbon dioxide. Air purges can be used to clean the electrodes if it is not desirable to add an oxidant to the inlet stream. Glass should be avoided in the construction of microplasma dry reforming reactors. Especially, when glass would be in direct contact with the electrodes. The microplasma reactor is incredibly small for the feeds which it can process based on the usual reduction in residence time required for microtechnology. The devices are completely modular which means once the individual devices are optimized, no other optimization is necessary when scaling up. The number of the devices used to treat larger flows can simply be increased. This technology can be used to manufacture a useful product from point source carbon dioxide and methane emissions. The carbon dioxide dry reforming of methane to synthesis gas is a useful reaction when stimulated by nonthermal microplasma. Renewable energy can be used to reduce carbon dioxide at off-plant sites. Microtechnology is modular and at full scale might only by a cubic meter in size to treat the same flow rates that thermal dry reforming could treat while

it occupied a small building. Microplasma has energy savings that are built into its reduced length scale and should be the most efficient form of plasma that can be used to drive chemical reactions certainly more so than thermally driven processes. Room temperature catalysts with good absorption of electrically activated species could easily improve the process further. The microtechnology platform is naturally suited to enable this methane dry reforming application. The limitations to microplasma carbon dioxide dry reforming are the bypass when the technology is not fully scaled (not at full power or with enough pins to cover all the flow lines) which prevents reaching 99% conversion to synthesis gas. Engineering the design of multiple plasma filament formation in parallel takes careful design and experience.

References

[160] A Montoro-Damas, J Brey, M Rodriguez, A Gonzalez-Elipe, J Cotrino, "Plasma reforming of methane in a tunable ferroelectric packed-bed dielectric barrier discharge reactor" J. Power Sources (**2015**) 296, 268

[161] S Kameshima, K Tamura, Y Ishibashi, T Nozaki, "Pulsed dry methane reforming in plasma-enhanced catalytic reaction" Catalysis Today (**2015**) 256, 67

[162] Y Xu, Q Wei, H Long, X Zhang, S Shang, X Dai, Y Yin, "CO_2 reforming of CH_4 by synergies of binode thermal plasma and catalysts" Intern. J. Hydrogen Energy (**2013**) 38, 1384

[163] J Pacheco, G Soria, M Pacheco, R Valdivia, F Ramos, H Frias, M Duran, M Hidalgo, "Greenhouse gas treatment and H_2 production, by warm plasma reforming" Intern. J. Hydrogen Energy (**2015**) 1

[164] B Zhu, X-S Li, J-L Liu, X Zhu, A-M Zhu, "Kinetics study on carbon dioxide reforming of methane in kilohertz spark-discharge plasma" Chem. Eng. J. (**2015**) 264, 445

[165] R Snoeckx, Y Zeng, X Tu, A Bogaerts, "Plasma-based dry reforming: improving the conversion and energy efficiency in a dielectric barrier discharge" RSC Adv. (**2015**) 5, 29799

[166] K Supat, S Chavadej, L Lobban, R Mallinson, "Carbon dioxide reforming with methane in low temperature plasmas" Fuel Chem. Div. (**2002**) 47, 269

[167] V Shapoval, E Marotta, "Investigation on plasma-driven methane dry reforming in a self-triggered spark reactor" Plasma Process. Polym. (**2015**) 12, 808

Chapter 6- Rhodamine B Decoloration in Batch and Microchannel Devices

Justin Pommerenck, Alexandre F T Yokochi

Industrial and Engineering Chemistry Research

ACS Publications
1155 Sixteenth Street N.W.
Washington, DC 20036, US

(to be submitted)

6.1 - Abstract

Dc plasma has been applied in a corona discharge microchannel device. The plasma microchannel reactor is successful in completely decoloring part per million Rhodamine B dye in water. Rhodamine B is representative of numerous toxic organic contaminants in groundwater. Its complete removal to part per billion concentrations demonstrates the application of dc plasma microreactors for advanced oxidation of organic toxins in water. The energy consumption per mole of dye removed is recorded for a stirred tank plasma batch reactor and a plasma microchannel device. The effects of inlet flow rate, reactor volume, electrical ballasting, stir speed, applied power, pulse frequency and pulse duration are explored. The resulting batch reactor data is fit with an exponential psuedo-first order reaction rate. There are significant mass transfer limitations at the plasma interface where solvated electrons generate high energy reactive radicals that are short lived on the order of microseconds. While the mass transfer limitations exist in any plasma water system, they are reduced in the plasma microchannel device since the surface to volume ratio of the reactor interface is thousands of times higher than in the batch reactor. The parameters needed to achieve complete removal of the dye Rhodamine B from a water stream is recorded for the plasma microchannel device and its energy efficiency compared to that of the batch reactor using the same electrical discharge application technology.

Keywords:
Corona discharge, dc plasma, advanced oxidation, toxic organic contaminants, microchannel, plasma, Rhodamine B

6.2 – Introduction

Increasing urbanization of an expanding population intensifies the need for groundwater reuse. This introduces additional health concerns beyond chemical sanitation and storage of the reused water. There are chemical derivatives of medicinal drugs, fertilizer byproducts and even accumulation of haloacetic acids from city water sanitation treatment that need to be considered if groundwater is to remain healthy. For example, in Newfoundland a water quality report contained the following data.

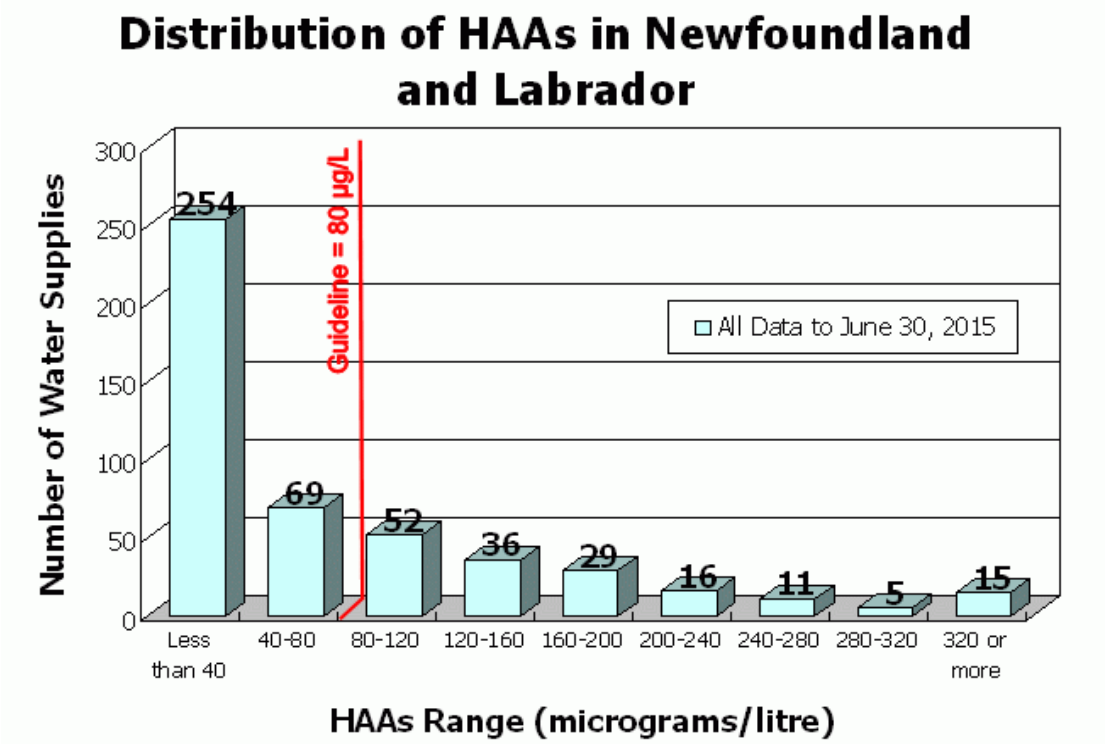

Figure 84: The concentration of haloacetic acids in Newfoundland and Labrador. More than a hundred sites are above the guideline of 80ppb out of the four hundred sites tested.

Only advanced oxidation techniques are capable of reducing these toxic organic contaminants to sub-ppm and sub-ppb levels. As groundwater reuse becomes intensified, it will be important to develop suitable solutions to mitigate water health problems before they occur. Many of these compounds are difficult for the environment to degrade and they persist indefinitely in some cases. Plasma advanced oxidation

processes is one of many types of advanced oxidation processes that can be used to address and remediate toxic organic contaminants in groundwater supplies.

6.3 – Advanced oxidation process alternatives

There are a variety of promising advanced oxidation processes that can be used to treat trace toxic organic contaminants. Photocatalytic, ozone, sonication, plasma techniques have all been applied to completely reduce ppm level toxic organic contaminants to ppb level and below. Photoelectrochemical and photocatalytic techniques have both identified benefits from using thin film catalyst on a microtechnology platform during application for dye removal.[168] Ozonolysis has been used for dye oxidation in micro and meso advanced-flow reactors as a visual metric prior to application for chemical synthesis using ozone on the same platform.[169] Sonication techniques are also viable for the removal of trace organic contaminants represented by dye.[170] Different types of plasma have also been applied to many reactor configurations. Examples include a surface dielectric barrier discharge above an open water dish.[171]

6.4 – Dye decoloration plasma chemical systems

A great deal of excellent research has been performed on plasma chemical advanced oxidation processes.[172, 173, 174] Dyes are most frequently used as a suitable representative for many toxic organic contaminants. Reactors are typically wire above liquid in a tube or point electrode above a column of water. High energy discharges inside a liquid microchannel device have been used to test the energetic efficiency for organic removal. [175] This study is the first application of pulsed low energy dc corona discharges above an open microchannel device for the destruction of Rhodamine B which demonstrates the feasibility of completely removing toxic organic contaminants in a microchannel device. Higher degradation efficiencies than for a stirred tank reactor using the same pulse system which further demonstrates that the highest energy OH radicals at the interface of the plasma can be used to reduce mass transport limits in a microchannel device.

6.5 – Power supply application technology

The trigger to the IGBT gate is much faster than the high voltage switch itself. The minimum pulse duration for the trigger is almost 20ns. The output from the function generator trigger is measured by a high speed oscilloscope.

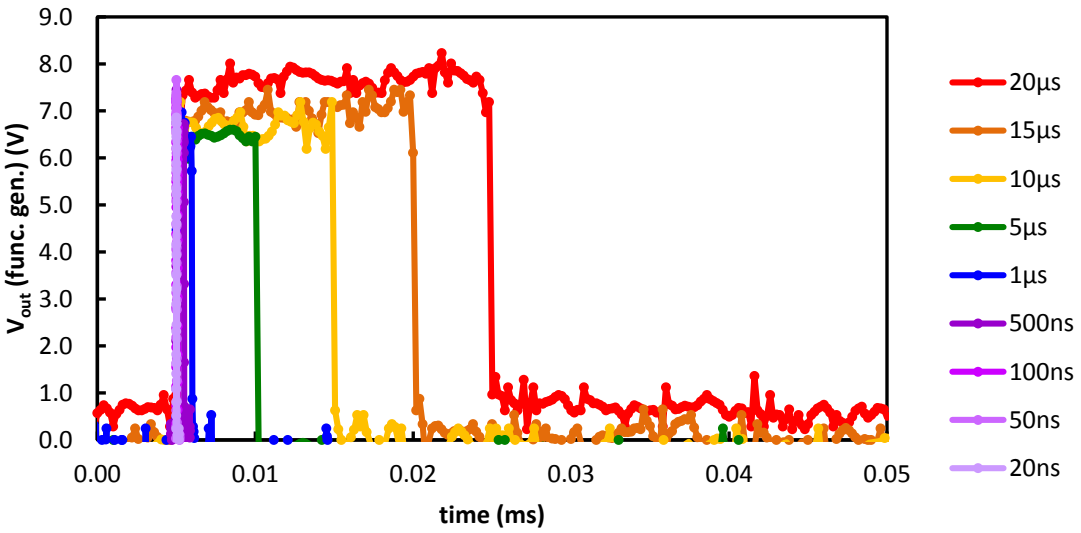

Figure 85: The function generator trigger sent to the high voltage switch that forms the pulse train controls the pulse duration for the plasma discharges to the water surface.

This shows the function generator output is capable of 20ns output maximum (the light purple). The IGBT is much slower than this due to the need for tolerating high voltages in the N^- layer (which makes it thicker) charge recombination is hence slower and the turn-off time is slow. This means that a dual IGBT slave relationship could switch off the charge side for increased speed or a stack of MOSFETs that are high speed (20ns) (stacked for higher voltage tolerance) would be capable of nanosecond solid state pulse application for the flow through and batch devices. This would be a better controlled output pulse generator than the widely used dual spark gap system applied during the study of the nanosecond microdrip reactor. The most useful electrical characterization is the actual output at 1kHz. This shows the pulse duration at the minimum switch speed for the IGBT is near 50µs. This is the measurement without a load attached.

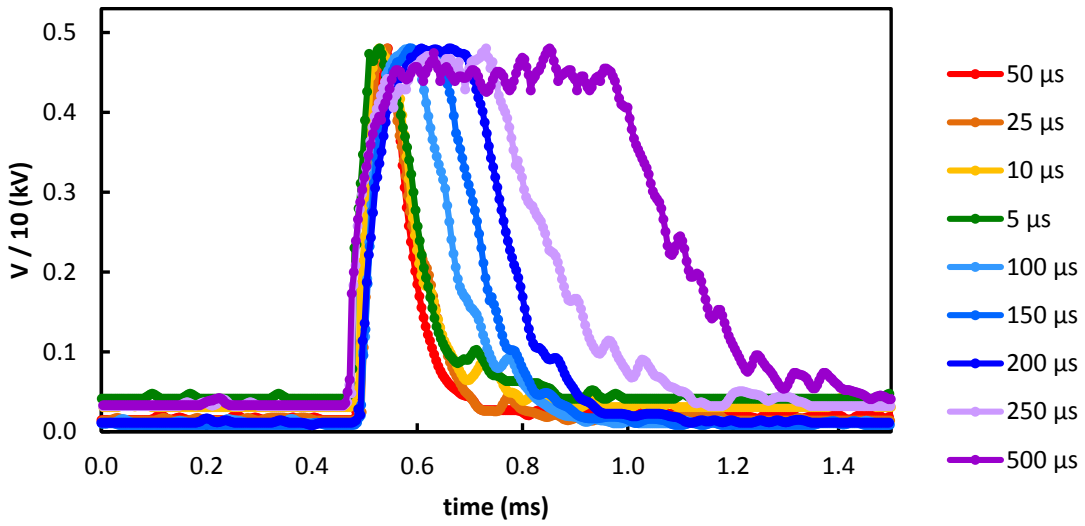

Figure 86: The generated pulse without a load shows a maximum peak applied voltage of 4.5kV.

The maximum pulse speed achievable by the pulsed IGBT solid state switch setup is 50 µs at (1kHz). Next, the impact of the applied pulse as it responds to the plasma load (which is capacitive) is recorded. The red, yellow and orange curves are different heights due to refilling the channel (the microsyringe pump is off) with water for the plasma (water height dictates the electrode gap and plasma voltage drop). It was checked that this did not interfere with the external pulse circuit by allowing it to change and examining the minimum pulse duration.

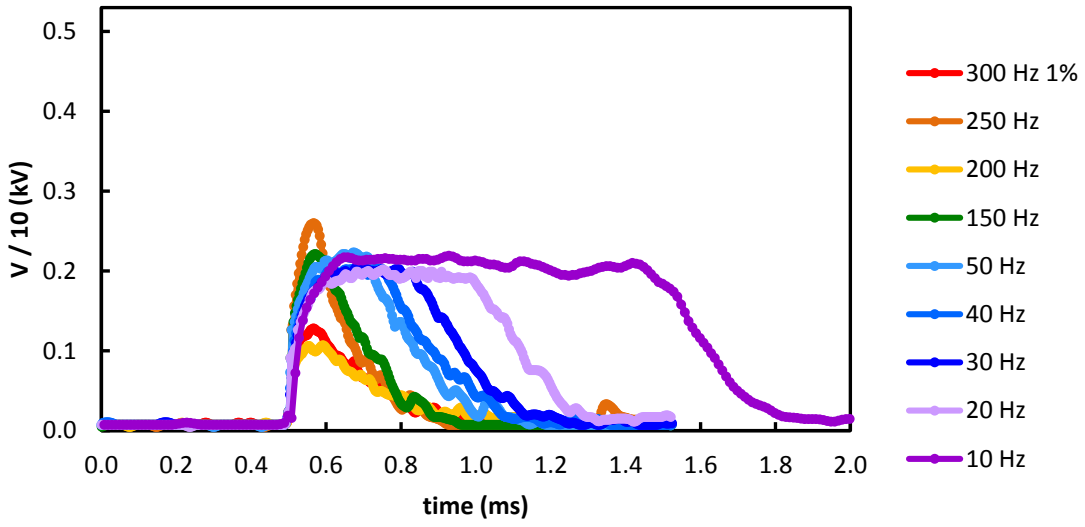

Figure 87: The applied voltage pulse to the reactor channel at lower frequencies for a 1% pulse duration.

This means the pulse generator is capable of 4kV pulses with a 400 µs duration when at sub-kHz frequencies. The experiments were operated with a 1% duty factor unless noted. At 5Hz, which would be the slowest waveform used in this study, a 5ms pulse duration is generated.

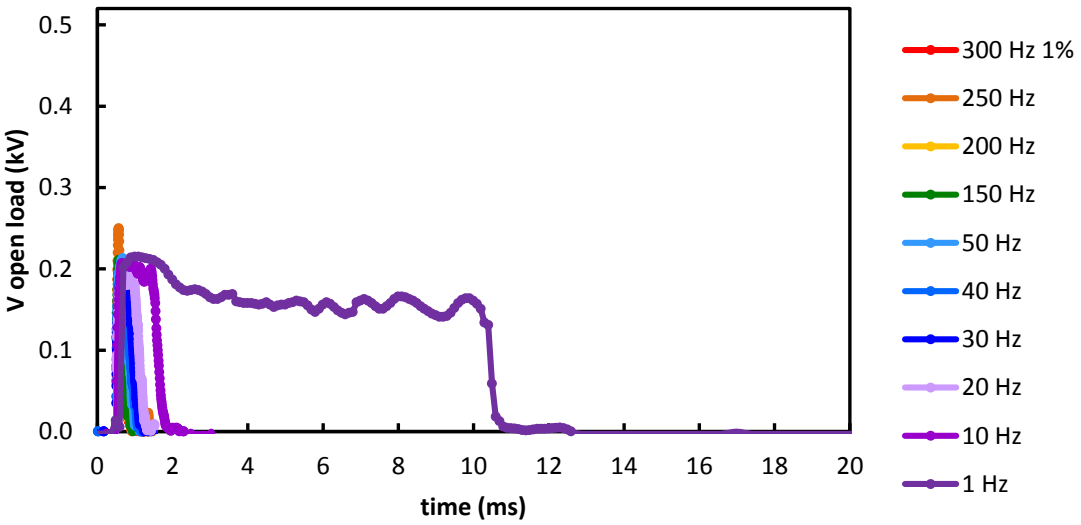

Figure 88: The plot can be extended to show the behavior of 10Hz to 1Hz pulses such as were used in the first efficiency plot and can be used to calculate the energy consumption during dye degradation for these very prolonged pulse discharges.

6.6 – Results from batch microplasma reactor

The batch liquid system consists of a quartz cuvette with spectroscopy couplings. A stainless steel wire applies positive electric potential to the water. The electrode is grounded and suspended above the surface of the liquid by less than 1mm. The liquid is raised in electric potential by a submerged metal disk. The batch reactor is fabricated to hold continuously stirred water to whose surface an electric potential is applied with a plasma filament as an electrode. This electric potential is applied using an ionized plasma filament driven by constant dc and pulsed dc electric fields from a microstructured emitter rod. The plasma is generated between an electrochemically etched probe or array of probes and the fluid. An example reactor schematic is depicted.

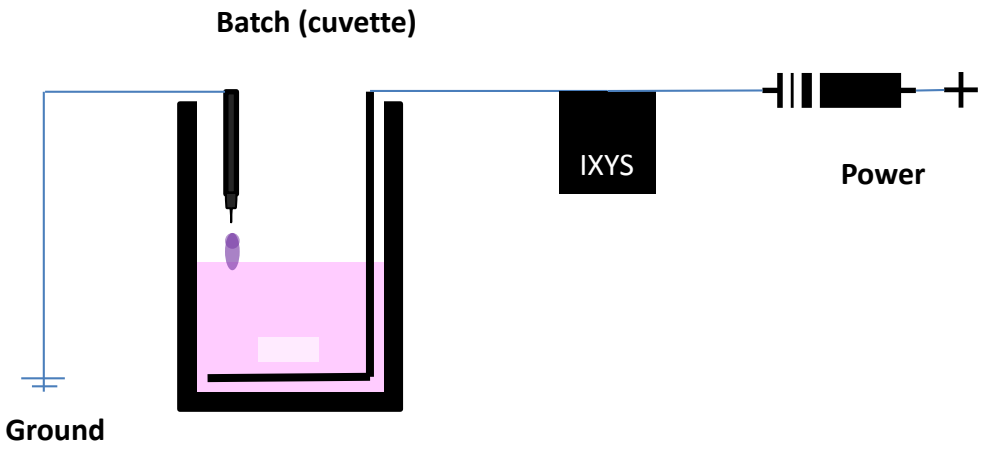

Figure 89: The batch plasma reactor system uses microplasma to decolor a toxic organic dye that represents toxic organic contaminants in general. A discharge from the tip of the needle forms to the surface of the dye mixture and the circuit is completed using a solid state switch.

Rhodamine B is used as a representative organic molecule for a variety of toxic organic contaminants that can be found in the environment. This dye is frequently used in a variety of advanced oxidation processes and will allow this electrochemical purification system to be evaluated in terms of efficiency that are strongly related to systems using other processes. The dye is decolorized while being continuously monitored under ultraviolet-visible light absorption spectroscopy.

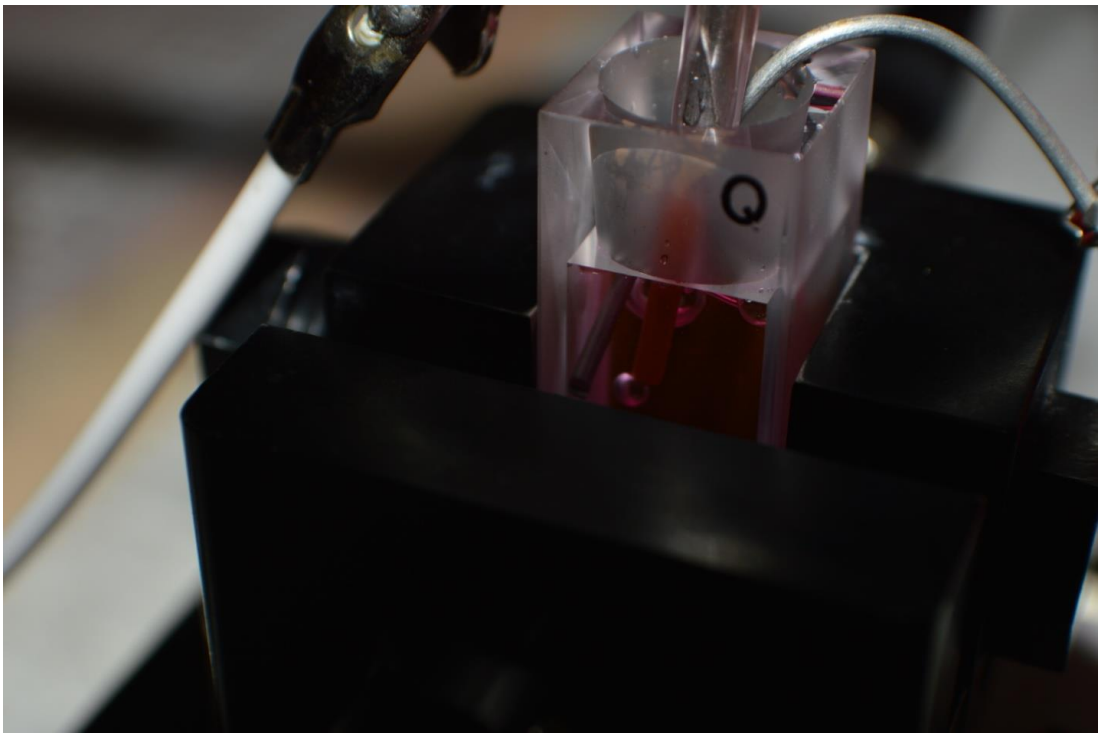

Figure 90: The quartz cuvette holds 4ml of water. The optical spectroscopy probes couple into the side of the steel receptacle. A stir bar is used to homogenize the dye.

A microplasma dc glow discharge or pulsed dc glow discharge with peak voltage at 3.5kV and average voltage around 500V is ignited with the liquid as the positive electrode. This system establishes a baseline dye degradation efficiency for the frequently studied plasma discharge batch system which will be compared to the plasma microchannel device to identify improvements in radical transport through the films of reacting liquid which are being exposed to the discharge. In situ absorbance measurements give real time results without samples being extracted from the batch reaction vessel. The temperature is maintained at room temperature by natural heat transfer.

It is observed that the efficiency barely changes as power is linearly deposited into the fluid for the batch system. The frequency of pulses can therefore be adjusted to increase fluid treatment rate to the desired concentration reduction chemical contaminant.

The results of the batch reactor are necessary to confirm that activating a large volume of fluid using a small volume activation is inefficient compared to microplasma flow through devices. The comparison is made by calculating a G factor for both systems. For the batch system, the reported $G_{50\%}$ does change slightly with other parameters such as pulse frequency but with only a small long term statistically significant change in a single order of magnitude for degradation efficiency of the dye (energy savings of four times with a two order of magnitude decrease in number of discharges per second – this is likely due to changes in the plasma filament). The treatment time for several discharge frequencies is reported where efficiency is based on the delivered power to the digital IGBT and reactor. The pulse frequency is the equal to that of the pulse train delivered to the IGBT gate where a positive 7.5V allows current across chip and through discharge into the reactor at the interface.

$$G_{50\%} = 1.3E-11\,\text{mol/J}: \quad 6.9E-12\,\text{mol/J}: \quad 3.0E-12\,\text{mol/J}$$

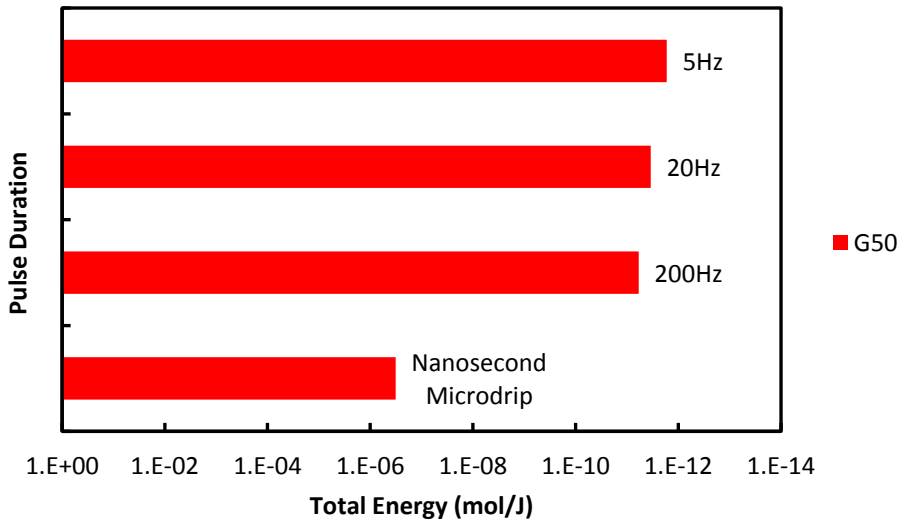

Figure 91: Batch reactor and drip tests for pulse frequency. The plot tabulates the 50% removal efficiency by comparing the moles removed to the total power required to generate the partial discharge.

For contrast, the energy efficiency of a nanosecond microdrip reactor is displayed with the batch reactor data taken at each of these frequencies. The complete covering of the droplet with the electrical discharge which has a confined pulse duration to several hundred nanoseconds shows more than twice the dye can be degraded for the same energy demand. This system has a lower throughput which puts it at a disadvantage to the batch system (Hence, the microchannel flow through reactor design being selected as the following liquid study of interest. This system has higher throughput and still retains the higher average concentration of dye exposed sequentially and completely at each plasma filament. This results in higher efficiencies). The G factor for the batch and microdrip agree well with literature results for tabulated treatment efficiencies while those studies which were performed with different power supplies and different volumes and flows but similar systems. The exact efficiency values are important to corroborate if the results of the following flow through system are to be extensible to other research systems. An example image of the discharge collected from the microdrip reactor over several passes through the device is shown to establish the appearance of the dye during the ultraviolet-visible spectroscopy. The starting concentration of the dye is 4ppm.

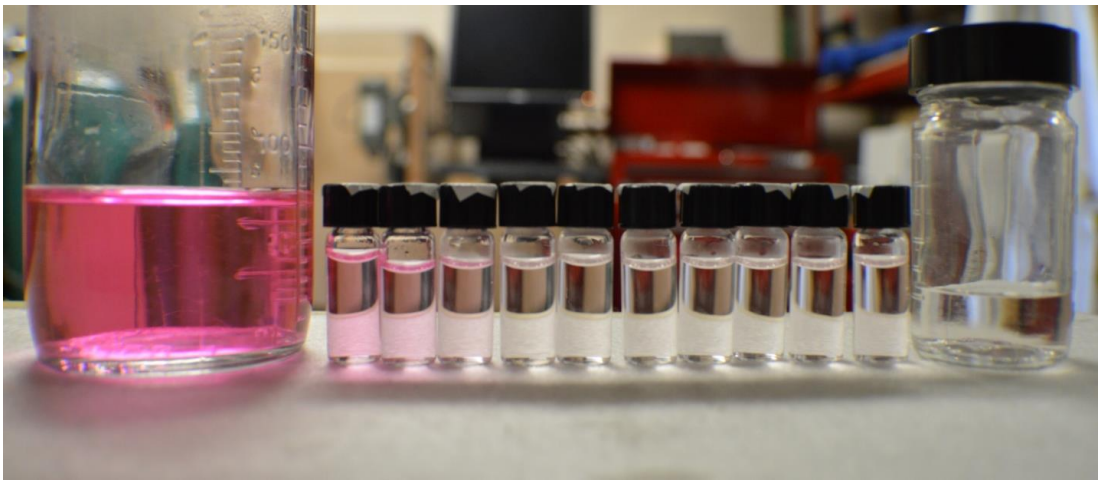

Figure 92: The water on the left is the dye solution. The water on the right is the remainder of a 60ml of dye solution recycled through the microdrip reactor during discharge.

An example plot from the batch reactor data shows that the $G_{50\%}$ is attained at roughly 130 minutes at this treatment volume and power. The volume is 4ml and the power is 0.35W applied at 5Hz.

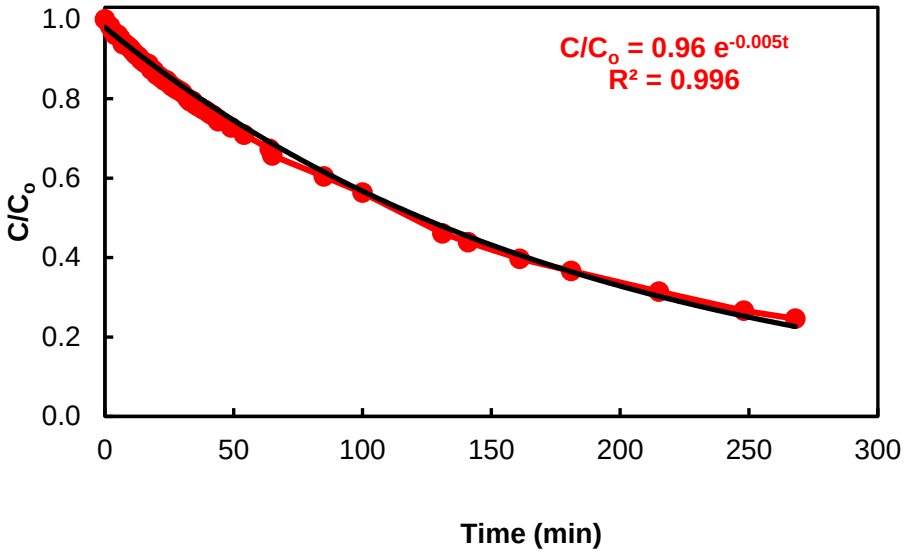

Figure 93: A typical degradation curve for the batch system fits an exponential decay. This is likely not due to homogenous batch reactor kinetics but mass transfer from the point of reaction through the interface at the boundary of the pulsed partial discharge.

The data from the batch reactor follows exponential first order form. This is due to mass transport limitations rather than purely kinetic limitations based on information using dye fluorescent spectroscopy to identify the spatial mass transport of dye in a flow through experimental system. This is the reason that the kinetics from any specific research literature are not applicable between publications with each group proposing "effective" kinetic parameters valid only for their own system or systems which are very similar.

A parameterization of pulse duration (at 5Hz) which means that the total pulse duration is of the type of a slow millisecond pulse in which the pulse duration is not short enough to interact with the development of the individual plasma formation shows that net effect of increased pulse duration is current flowing through the cell. The efficiency is relatively unchanged.

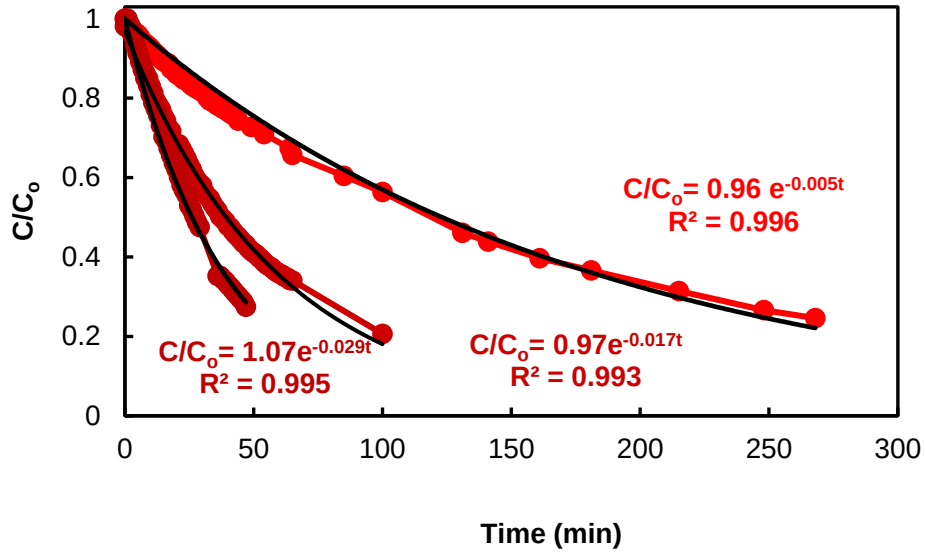

Figure 94: The variable duration of the pulse train at low frequency (5Hz) shows a predictable changes in the degradation kinetics based on applied pulse duration (1%, 5% and 10%).

The pulse duration is varied from 1% to 10%. The higher pulse duration diminishes the dye concentration more rapidly (at megahertz frequencies where the pulse can affect a plasma's electron acceleration timescale this will come at the expense of reduced efficiency). The effect of increased pulse duration is the measured current (0.1mA, 0.3mA and 0.5mA) that is delivered at 3.5kV and 5Hz. At these slow hertz pulse rates no substantial trend in efficiency is detected.

It is of interest in these batch systems to understand if the power application technology or the external ballast impact these particular results. The external ballast is varied under the same applied power, frequency and reactor type to isolate any effect on the degradation efficiency. Changing the resistance from 100kΩ to 200kΩ to 300kΩ to 500kΩ to 700kΩ only affects the power delivery from the IGBT to the load and left the degradation efficiency relatively unaffected. A plasma has its own capacitive behavior and an electrical optimization would not be difficult. It is sufficient to note that the efficiency remained constant based on the deposited power at the reactor.

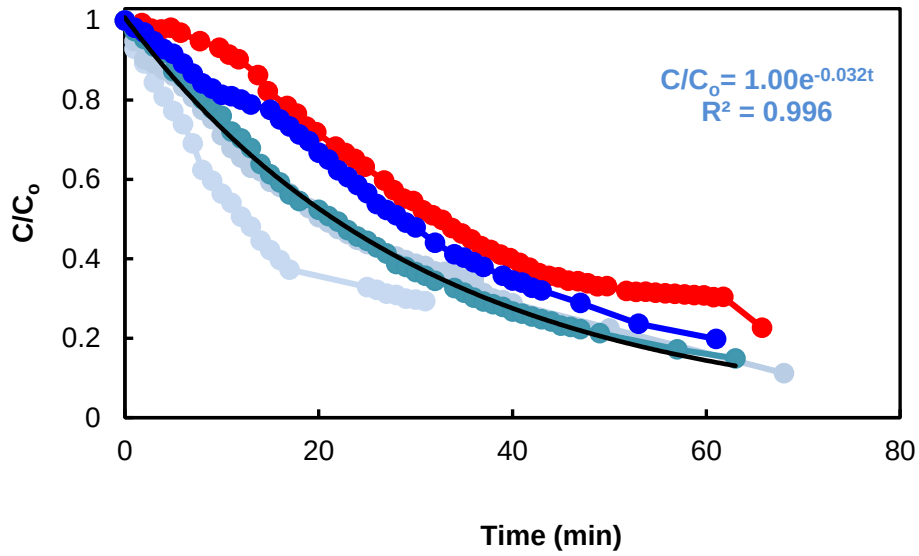

Figure 95: The ballast resistance can improve degradation rate but not efficiency since it only changes the deposited power from each pulse. Larger ballasts take longer to deposit enough power to degrade the dye (red) while smaller ballasts allow higher currents during each pulse (blue).

The stir speed within the vessel homogenizes the dye concentration within the vessel. The stir speed is changed from 0 to 1.8W to 2.5W. This is done to make certain that the dye changed identically through the whole reactor as interfacially reactive species are generated at the interface of the plasma liquid boundary. Without any stir rate, a strong color boundary is seen moving gradually downward from the interfacial point. Once the stir rate was increased to 1.8W, the data from both the 1.8W and 2.5W stir rates overlapped. This demonstrates that the dye is sufficiently well mixed. It does not mean that transport limitations do not exist. For example, several of the most reactive radical species persist in aqueous conditions for less than 10μs (for example OH^-) before lowering their energy state through non-useful reactions. This means their mixing time is on a completely different mixing length scale than the dye or other longer lived electroactive species. It is these highest energy reactive species which can be better utilized in microsystems (as demonstrated by the four order of magnitude increase in plasma spray systems over batch systems). The stir velocity presented here is more than adequate to achieve well-mixed dye within batch reactor system. Stir powers 0W, 1.8W and 2.5W (overlapping the 1.8W) are plotted to demonstrate that the mixing is complete in terms of dye concentration. The batch reactor concentration will

be continually lowered. The lowered concentration will be passed through the small volume adjacent to the surface boundary with the plasma and react slower and slower as dictated by the rate law. This is the inherent disadvantage for batch systems with respect to flow through systems where in the highest concentration fluid is sent in and then out of a reactive element consecutively to the fluid packet preceding it. This ensures that the regions of high concentration of dye are not mixed with regions of low dye concentration. That contact pattern enhances the process conversion efficiency.
The plot depicts the stir speed…(0), (1800mW), (2500mW) at 50% duty factor with an applied voltage peak at 3.5kV repeated at 5Hz. Poor mixing at 0W increases the variation implicated by the correlation coefficient of that trial.

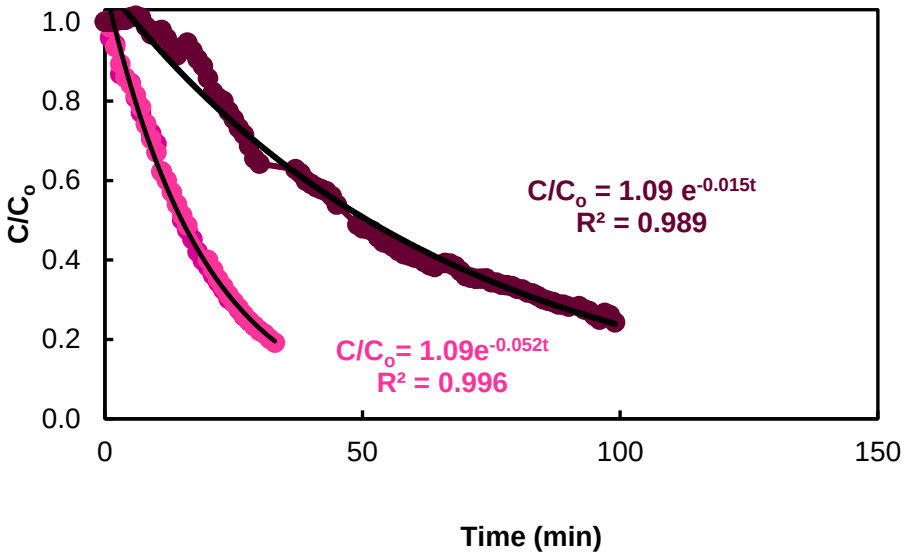

Figure 96: The dye is well mixed even if the most reactive radical species remain confined near the interface between the plasma and liquid boundary as defined by the lifetime of those species. The three curves (two overlap exactly) demonstrate the decoloration time for the same applied power under no stir power, 1.8W stir power and 2.5W stir power.

Frequency can also be changed for a constant pulse duty such as the 10% which is applied during the 5Hz study. Of interest, is the exponent which at 3MHz and 10% duty factor shows the exact same degradation rate as the 5Hz and 1 - 5% duty factor. The efficiency is improved by an order of magnitude (based on oscilloscope measurements). This demonstrates that turning the discharge on and off does make a

higher overpotential and correspondingly higher concentration of high energy species. The only efficiency that can be achieved in these batch systems is to control the development of the plasma filament itself (which will not occur from small changes such as from 5Hz to 200Hz) or improve mass transport of short lived high energy radicals. This can be done by controlling plasma regime, nanoscale pulse durations (which was constant between these two studies) and improving the fluid interfacial contact. The best way to optimize the plasma filaments energy efficiency is to limit the discharge duration which is done by applying as short a pulse as possible at a moderate frequency to prevent discharges from interacting with each other. Again, when the frequency is adjusted at the same duty factor there is no improvement in efficiency until it begins to be on a time scale that limits the development of an individual plasma pulse. Otherwise, only the degradation rate is affected. The slower degradation rate on the following plot shows a degradation rate equivalent to that of 5Hz and 1 – 5% duty factor (oscilloscope averaged current of 0.1 to 0.3mA). The frequency is changed from 5Hz to 3MHz at 3.5kV with the current drawn for each trial recorded as an average oscilloscope reading (0.5mA, 0.02mA) at 10%. The fluid is mixed at a stir power of 1800mW.

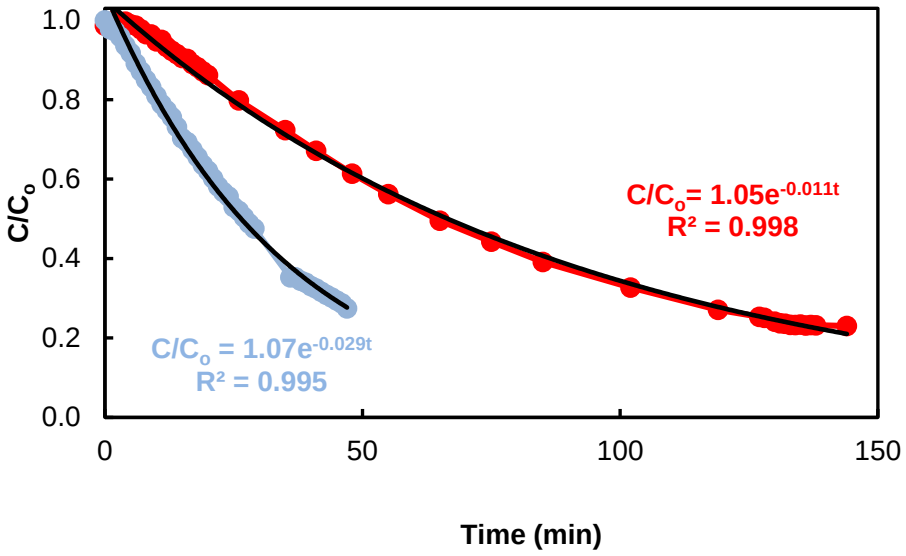

Figure 97: The frequency is changed from 5Hz to 3MHz at 3.5kV and it does impact efficiency once its pulse duration approaches the time scale that determines the development of the plasma filament. The efficiency is improved almost one order of magnitude by reducing the pulse duration at high frequency.

The optimum pulse duration for balanced generation of electrically active high energy and high concentration is investigated at the end of the flow through study using oscilloscope measurements of the applied signal. The batch reactor energy efficiencies appears highest for moderate kHz frequencies with microsecond pulse durations. The microplasma gap separation yields energy savings due to the reduced voltage necessary for that air separation. The influence this has on the rise and fall times of the pulse can easily be offset by pulse technology and circuit design compensating for the altered plasma capacitance and inductance.

A final measurement of discharge efficiency is used to demonstrate that a batch system remains equally efficient regardless of its size (as long as it is well mixed in terms of dye). This is necessary to prove that the reactor type (flow through microplasma reactor) is inherently more efficient even at the same degradation rate based only on improved contact order mass transfer limitations. The 4ml cuvette batch reactor is filled to 2ml, 3ml and 4ml and the same applied pulse and separation gap maintained between trials. The resulting degradation rate is proportional to the volume and the final efficiency for each experiment is unchanged.

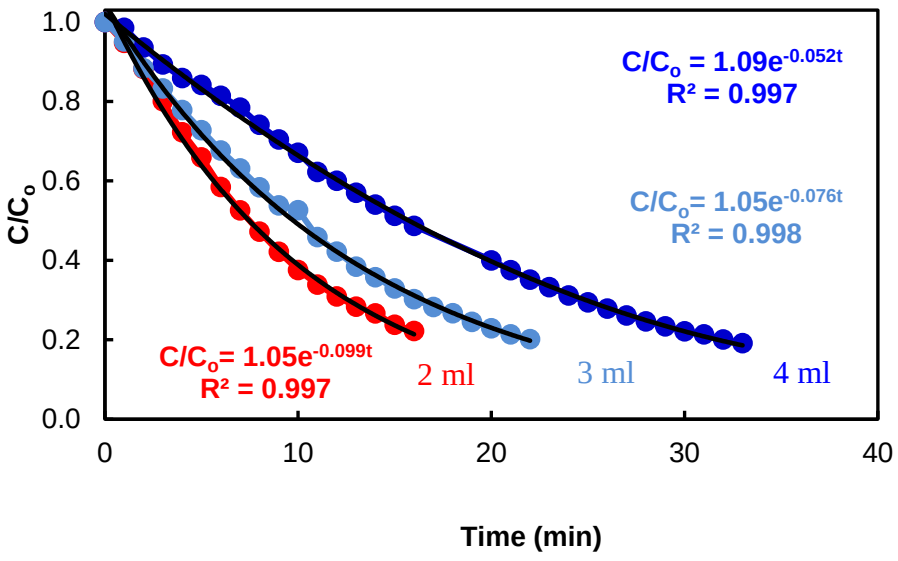

Figure 98: The degradation rate is proportional to the vessel volume (2ml, 3ml and 4ml). Power input is equally efficient regardless of the starting fluid volume in the batch reactor.

6.7 – Results from a microplasma microchannel reactor

The flow through microchannel device treats flow rates from 8.3ml/hr to 120ml/hr at peak voltages of 3.5 kV, average voltages of 500V and currents measured at under 8mA. Liquid enters the cell through a stainless steel tube and travels from left to right. The electrodes emit plasma in the dc corona, spark discharge or glow regimes. Both the corona and glow discharge regimes can be pulsed by the external circuit to 50μs minimum pulse durations. The spark (left discharge) and corona (right discharge) are visible in the photograph below. The two different discharges are present at the same current due to the interchangeable relationship of current density with separation gap (ie. electric field). The separation gap is maintained at under 1mm.

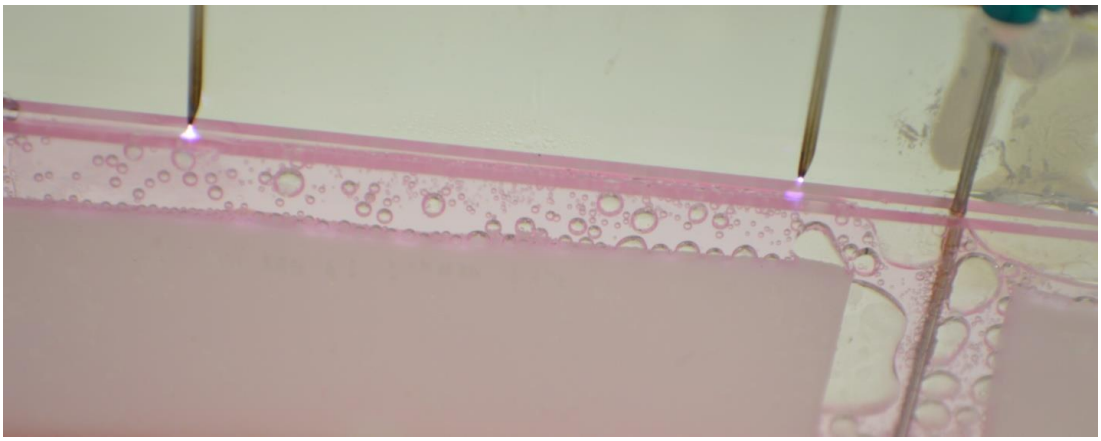

Figure 99: The flow through microchannel is 250μm wide as defined by the teflon spacer which is separating two glass microscope slides. Multiple plasma discharges are above the channel.

The flow-through microplasma system passes fluid rapidly through the interface area between plasma and water. This prohibits fluid regions that are initially high in dye concentration from mixing with the downstream lower concentrations as is done in plasma batch reactors. Kinetic expressions include dye concentration in the degradation rate law. Since the concentration of dye is part of the kinetics, its increase in value does improve the expected degradation rate. This will improve efficiency based on greater utilization of the highest energy radicals that only exist at the plasma-water boundary.

These highest energy radicals have very short lifetimes before they chemically create lesser reactive oxidants that are longer lived.

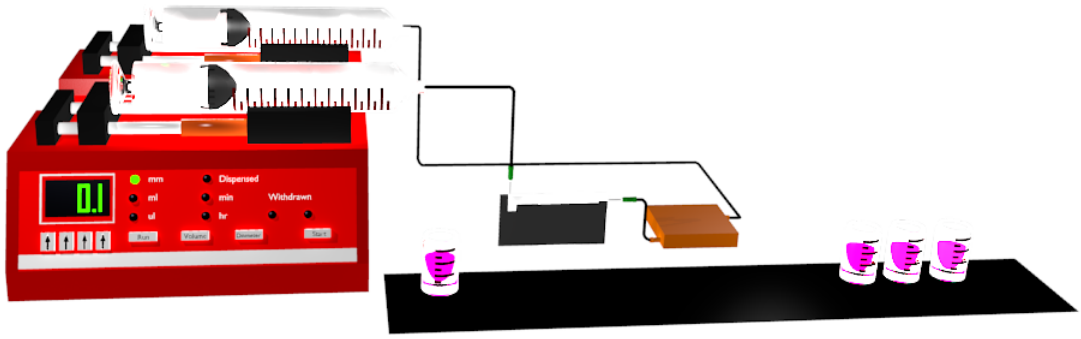

Figure 100: One microsyringe pump delivers dye to the microplasma reactor. The second microsyringe pump withdraws liquid out of the uv-vis spectrophotometer flow through cell. Continuous data is generated as the power or flow rates are altered and steady state performance is recorded.

The first set of data that is generated to understand how much energy can be saved by using a flow through microreactor microplasma device. The flow rates are set to mimic the typical treatment rates in large scale batch reactors. The applied power at 3.5kV is reported. Data trials which are shown twice in the legend represent separate repeats of the experiment with repositioned electrodes. The results are consistent. The data forms a perfect fit with either natural logarithmic or exponential trends. Both of these mathematical forms being similar under the region of values to which they are applied. The trend in power would be expected as an exponential based on electron energy distribution formulations which could be suggested.

A microreactor is capable of completely removing dye at improved flow rates and efficiencies compared to batch reactors. Superior heat and mass transport make the process controllable and scalable. The G factor for 50% removal will are recorded.

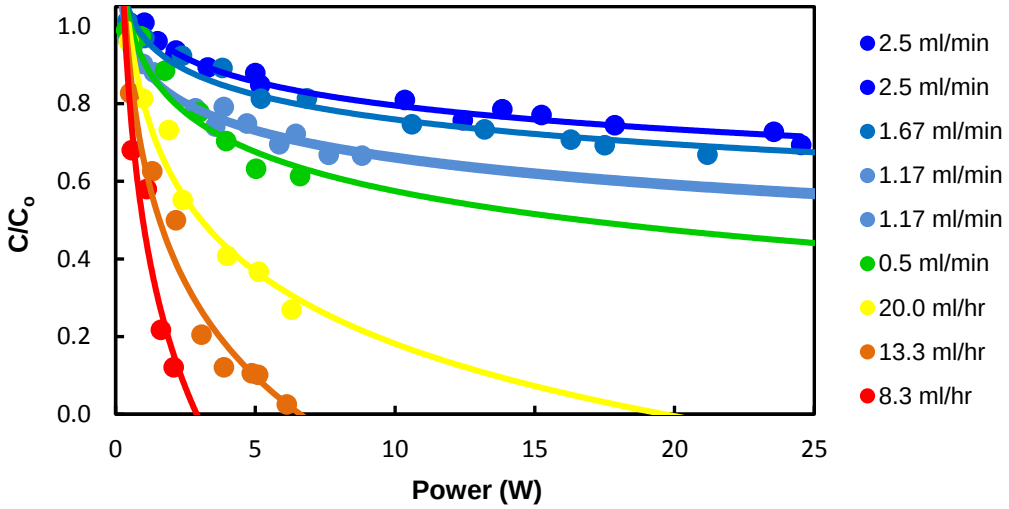

Figure 101: The power parameterization at a variety of different flow rates gives an idea of flow through reactor efficiency. The fastest flow rate is 2.5ml/min and the slowest flow rate used is 8.3ml/hr.

It is useful to observe that a natural logarithm fits the data above very well at high flow rates. The same data can be plotted versus an exponential trend which fits the lower flow rates better. It is surmised that two effects exist. Dye degradation due to electrochemistry often show the natural logarithmic behavior. Batch reactor data almost always shows exponential behavior. The limiting factor for these kinetics is likely mass transport at the interface. This mass transport resistance should transition from limiting to non-limiting when the flow rate increases. This data is positive evidence that mass transport does alter the pseudo-first-order kinetics of the degradation process. This has been previously described using proportionalities to the plasma surface area.

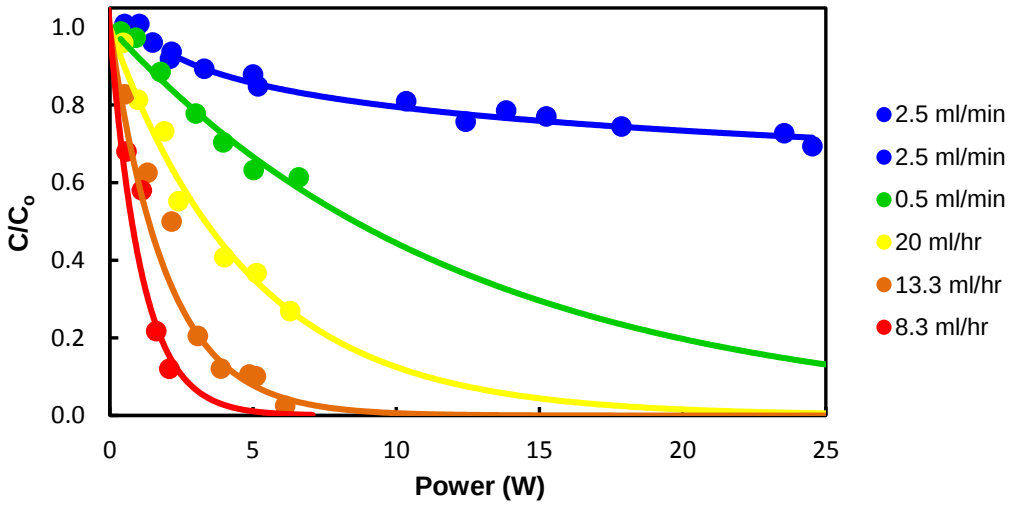

Figure 102: The data transitioning to exponential kinetics for the microchannel flow through device.

An optimal load line can be generated from the data by taking the interpolated degradation values along intersecting power consumption lines. The degradation for several power consumption rates is shown to possess a similar relationship to flow rate. The net implication is that a processing flow rate can be selected such as 0.25ml/min and the energy cost for the desired removal percent optimized.

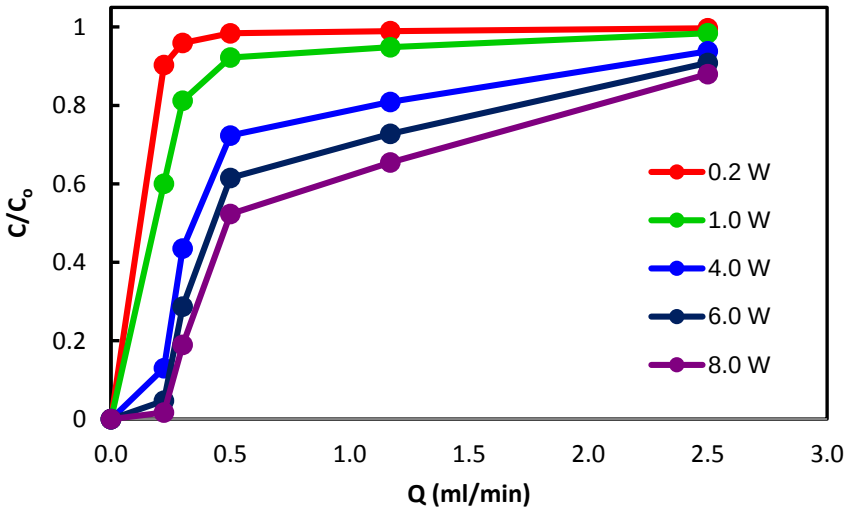

Figure 103: A typical batch reactor requires 100min to purify 100ml of water at much higher power consumption than 8W. This reactor treats 0.25ml/min from ppm to ppb concentrations with 8W.

The electrical frequency set at the function generator switching the IGBT open also depends on the plasma load. The transition point between plasma regimes impacts the energy efficiency. The crossover point from corona discharge to spark and to glow discharge occurs at the average currents such as that which is observed under 100kHz at this duty factor.

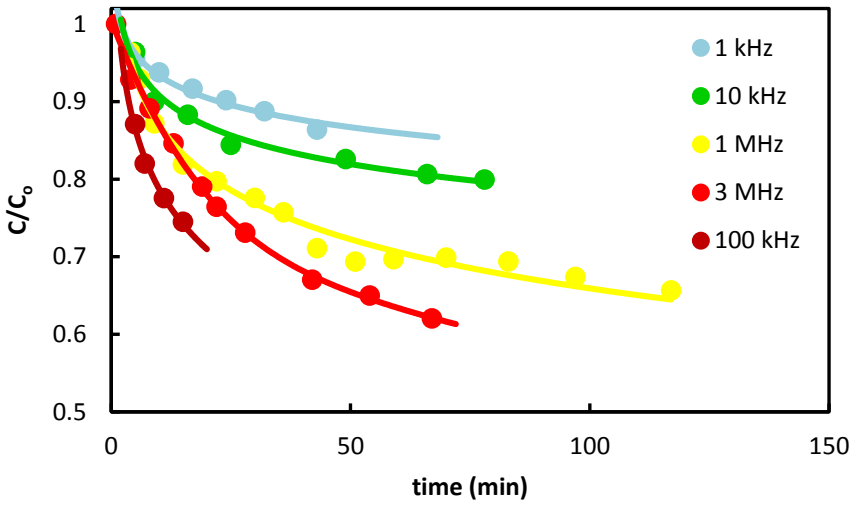

Figure 104: The lower frequency measurements show no change in the degradation efficiency. Here the degradation rate can be seen to change at high frequencies until the system limit for opening the pulse network switch is reached.

The electrical measurements also show how the current is used by the process. The reversal in degradation efficiency shows that the plasma discharge has stopped switching at this pulse duration. The reversal of the degradation rate is fully explainable by the applied waveform data. The transition from regime to plasma regime impacts the pulse network. Thus, the trend which contains the most information is kilohertz frequency pulses from 1-100 kHz. This pulse frequency allows the network to dictate the applied pulse and minimize wasted energy due to mass transport limitations by applying limited power pulses. Faster pulse frequencies interacted with the electrical generation system. Pulse duty must be very rapid to generate savings in electrical efficiency. These improvements in energy efficiency require sub-microsecond pulse durations.

A concise summary of the magnitude of energy savings possible when changing from batch to flow through microchannel devices is reported. Assuming no down-time for the batch system being refilled, the throughput flow rates are nearly identical. The energy efficiency is highly discharge dependent. The discharge is a function of the pulse forming network. The most efficient discharge is very short in pulse duration and has a very high interfacial area which is maximized using low energy discharges that can have multiple origins. Increasing the area and flow velocity and number of microdischarges all positively impact the energy efficiency of the system. The microdrip system is operated at 0.1ml/min and with a peak voltage of 10kV and was the only study to achieve nanosecond pulse duration. The current was limited to the corona regime which is at milli-amperage current levels for microgap separations. At microgap separations, water filaments were observed to form from which the propagating discharge. It may be the increase in surface area due to this filamentation of the dripping fluid which is responsible for the increased efficiency. It is possible to achieve higher electrical efficiency in a microchannel flow through plasma reactor which is open to the air.

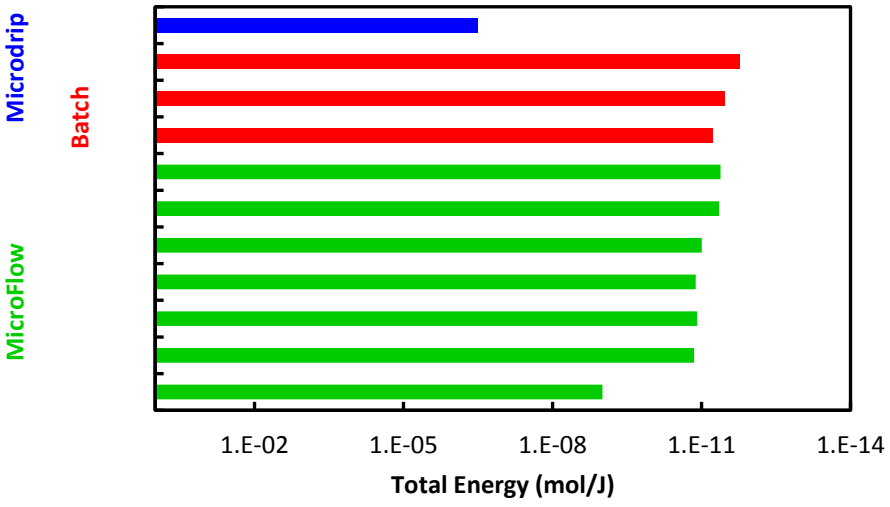

Figure 105: The energy efficiency results from the microdrip, batch and microflow devices tested during this study show increasing electrical performance for microflow devices using fast microsecond pulses with short pulse durations.

The device is scalable in series or parallel. The throughput is higher than can be tolerated in batch systems. The flow through system lasts longer than the duration of 100+ hours. There is no noticeable electrode erosion from the low power discharges. The scale up from 1ml/min to 100ml/min can be accomplished by increasing the number of channels and creating an array of electrodes via EDM which would be in parallel electrically or by increasing the number of electrodes in series and using a higher voltage power source. The advantage of pulsed dc operation is the simplicity of the pulse forming network. The throughput of the microdrip reactor could also be increased by using stainless steel disposable injection arrays from micropoint technology. The liquid could drip from each of the tips towards a thin film of flowing liquid in the channel beneath. This device would easily treat 10ml/min.

6.8 – Conclusion

Corona discharge at a liquid interface of a conductive condensed phase is successful in completely decoloring Rhodamine B dye at high efficiencies in single pass through a microchannel device. The pseudo-first order kinetics are reported. The pre-exponential and activation energy terms are cataloged for different pulse frequencies, pulse durations, flow rates, feed concentration and input power. These parameters are used to calculate the efficiency factor $G_{50\%}$ which is the energy needed to remove 50% of the initial dye concentration. This energy is compared to the energy required for the same initial dye concentration in a batch system. The understanding of the performance limitations and benefits of flow through microsystems has allowed higher electrical efficiencies to be achieved. Strong performance increases are encountered when using nano and micropoint electrodes at short pulse durations. Microplasma gap separations allowed orders of magnitude in power to be conserved during pre-breakdown phase. This study represents a complete dataset generated by a single electrical delivery system for both batch and flow through microchannel devices. A table of efficiencies has been generated from several of the experiments that are recorded in order to establish the parameters that benefit advanced oxidation of organics in water streams. Both the stirred cuvette reactor and flow-through microchannel device are used as a

reaction vessel in which Rhodamine B is completely decolored with different efficiencies. The stirred cuvette reactor is studied by parameterizing starting volume, applied power, pulse duration, pulse frequency, electrical ballasting, and stir speed. The flow-through microchannel device had a much higher surface to volume ratio which is typical for microreactors. This higher surface area utilized a greater number of OH radicals at the plasma interface before their brief chemical lifetime (~10μs) generated lesser reactive oxidative species in the bulk. The processing power and flow rates necessary to completely decolor Rhodamine B (C_o is 5ppm) have been determined. The concentration has been monitered in-line with the flow-through microchannel reactor using coupled Avantes spectroscopic probes. A detailed electrical pulse generation study has been performed to make this study relevant and comparable to other research using different pulse generators. Processing curves relating power to flow rate and degradation rate are generated for future study of more numerous arrays of microchannels capable of processing larger flows (> 100 ml/min). The energy cost in moles degraded per joule of input energy is recorded for the experimental systems.

References

[168]C Montero-Ocampo, A Gago, G Abadias, B Gombert, N Alonso-Vante, "In situ photoelectrochemical/ photocatalytic study of a dye discoloration in a microreactor system using TiO_2 thin films." Environ. Sci. Pollut. Res. (**2012**) 19, 3751

[169]M J Nieves-Remacha, Klavs Jensen, "Mass transfer characteristics of ozonolysis in microreactors and advanced-flow reactors." J. Flow Chem. (2015) 5, 160

[170]K Thangavadivel, M Konagaya, K Okitsu, M Ashokkumar, "Ultrasound-assisted degradation of methyl orange in a microreactor." J. Environ. Chem. Eng. (**2014**) 2, 1841

[171]P Olszewski, J F Li, D X Liu, J L Walsh, "Optimizing the electrical excitation of an atmospheric pressure plasma advanced oxidation process." J. Hazard. Mater. (**2014**) 279, 60

[172]M Simek, M Clupek, V Babicky, P Lukes, P Sunka, "Emission spectra of a pulse needle-to-plane corona-like discharge in conductive aqueous solutions." Plasma Source Sci. Technol. (**2012**) 21, 055031

[173]J Franclemont, S M Thagard, "Pulsed Electrical Discharge in Water: Can Non-volatile compounds diffuse into the Plasma Channel." Plasma Chem. Plasma Proc. (**2014**) 34, 705

[174]B R Locke, S M Thagard, "Analysis and Review of Chemical Reactions and Transport Processes in Pulsed Electrical Discharge Plasma Formed Directly in Liquid Water." Plasma Chem. Plasma Proc. (**2012**) 32, 875

[175]M M Sein, Z Bin Nasir, U Telgheder and T C Schmidt, “Studies on a non-thermal pulsed corona plasma between two parallel-plate electrodes in water.” J. Phys. D: Appl. Phys. (**2012**) 45, 225203

Chapter 7- Conclusion and Future Research

7.1 – Conclusion

The study of the activation of chemical reactions using room temperature corona and glow discharge plasmas has been accomplished. The similarity between high pressure microplasmas and low pressure plasma is explored in terms of electrical characterization. This information is used to create the first stable field of microcoronas which are confined in a microchannel device for chemical synthesis. Micropoint electrodes are activated in atmospheric pressure air and other gas streams. Optical emission of the plasma in nitrogen and methane is recorded.

This use of electrical energy to drive chemical reactions has been applied to enable high conversion of methane to ethylene in an ultrafast nitrogen flow. Single microplasma devices, series of microplasmas and arrays of microplasmas have been tested using methane in the hydrocarbon coupling reaction. The hydrocarbon upgrading of methane towards C_8 hydrocarbons in 50%-90% nitrogen feed is extensively examined and forms the basis for a finite element gas phase reaction engineering model. Methane conversion reaches as high as 80% with 80% selectivity to C_2 hydrocarbons which is predominately ethylene. The efficiency of the conversion of electrical energy directly to chemical potential is as high as 45% even under conditions of gas bypass.

Finite element modelling is successful in extracting useful kinetic parameters from fitting of power data. These parameters form the basis for a predictive model that allows the conversion and electrical efficiency to be known for a wide variety of reasonable flow and feed compositions. This model can lead to improved reactor design by structuring the placement of discrete plasma filaments in residence time controlling arrays based on their relative positions. FEM software has successfully predicted trial runs from experimental datasets. Several different gas phase reactions have been investigated in terms of conversion and electrical efficiency.

The dry reforming of methane with carbon dioxide to produce synthesis gas is examined on a microreactor platform. Single microplasma devices, series of microplasmas and arrays of microplasmas have been tested in the dry reforming reaction of methane with carbon dioxide. Carbon dioxide conversions as high as 70% were achieved with 90% selectivity to synthesis gas. Coke formation has been catalogued based on feed composition and is reduced from 10-12% in 1cm discharges to 1-2% in microdischarges with ultrafast flow rates. A notable discovery is that, unlike thermal processes, nonthermal microplasma can process feeds rich in methane (30%) without any accumulation of carbon solid due to carbon radical suppression from flow induced cooling.

Low energy dc corona discharge has been used to decolorize dye in a stirred cuvette reactor and in flow-through microchannel devices. The electrical pulse system has been simplified and thoroughly documented. The peak voltage of the low power plasma is set at 3.5kV and the electrical efficiency across several different types of reactor platforms has been accomplished within a single study. The average power of the discharge ranges from 1-10W. Absorption spectroscopy of the fluid in a flow through uv-vis cell is used to monitor concentration changes over time. Factors that improve the electrical efficiency or fluid throughput are recorded for each system change or parameter sweep. Nano and microsharp electrodes have been tested. Nano and microsecond pulse durations have been studied. Fluid volume in the batch configuration and flow velocity in the microchannel configuration have been compared to find fluid turn-over treatment times. This is the first known microchannel device in which dye can be completely decolored at high efficiencies compared to point electrode tank systems. This is accomplished by the understanding the lwo energy dc corona microplasma generated from microsharp electrodes and electrode microarrays, nanosecond pulse generators, microchannel devices and nonthermal microplasma regimes.

7.2 – Future Research

This research lays the foundation for more detailed studies focusing on ultrashort gas residence times in fields of dc microplasma generated at micropoint electrodes. There are six fundamental recommendations for continued research in chemical synthesis in corona microreactors.

Future optimization of the flow path using microarchitectured channels should be pursued in order to reduce bypass limits which exist in the present systems. The dimensions of inlet holes that are valuable for this type of chemical conversion has been detailed in this study. The 100μm tube diameter at the inlet creates meter per second flow velocities in the microchannel devices.

Ultrafast flows through venture tubes could induce gas cooling. This is a useful tool for plasma microreactor systems that might allow them to obtain extremely high selectivity at a specific stage in the hydrocarbon coupling reaction. For example, a venturi tube can induce cooling after the flow path crosses five plasma discharges and methane has been completely converted to butene to stop the reaction from progressing.

The gas flows in this study have always been saturated with water vapor which may inhibit large hydrocarbon formation through oxidation reactions and quenching. A detailed parameterization of water vapor content might result in a better understanding of how this quenching can be used to optimize selectivity or control product type.

Active reactor cooling using water cooled heatsinks on fiberglass microreactors would result in the ability to compare the electrical energy efficiency in terms of another (besides chemical energy) of its primary sinks (waste heat). Other energy sinks include the flow work done on charged gas in the electric field and optical light emission.

A unique feed implementation could improve the overall productivity and resulting product type. For example, side addition of methane (added methane along the length

of the microreactor) would provide reactant that is fully saturated to the sequentially dehydrogenated coupled hydrocarbon products to prevent overdehydrogenation to less valuable chemical commodities while still promoting chain growth to high molecular weight liquid fuels confined to the vapor phase at moderate temperature.

Temperature and pressure should be parameterized within the microreactor to examine its effect on chain growth and carbon formation.

7.3 – Broader Impacts

Beyond the research kinetics and experimental data generated in this study, there is a framework for new chemical industries based on dc corona microreactor devices that would broaden the US national energy portfolio. Many US methane resources are not currently economically feasible to exploit. Methane venting from coal beds in rural pockets, methane hydrates and biogas fuels all offer potential energy sources. These remote sources, some of which are potential renewable fuels, are lost to the atmosphere. This technology promotes energy capture by chemical synthesis to produce recoverable liquid chemicals from untapped, existing methane sources.

Also, it is possible to utilize carbon dioxide in combination with methane during carbon dioxide dry reforming of methane. This dc corona microreactor system has been demonstrated to produce synthesis gas from the carbon dioxide dry reforming of methane. Synthesis gas is a valuable precursor to liquid fuels. If renewable energy could be directly incorporated into reconverting carbon dioxide and methane into fuels, a more effective fuel based transportation system could be maintained indefinitely.

As mentioned before, increasing urbanization of an expanding population intensifies the need for groundwater reuse. This introduces additional health concerns beyond chemical sanitation and storage of the reused water. There are chemical derivatives of medicinal drugs, fertilizer byproducts and even accumulation of haloacetic acids from

city water sanitation treatment that need to be considered if groundwater is to remain healthy. The dc corona microchannel reactor has proven capable of completely decoloring Rhodamine B water streams at a concentration of 5ppm to below the quantification limit of the spectroscopy system.

Low energy dc microcorona reactors have the potential to positively impact the combination of renewable energy and chemical synthesis and clean groundwater streams of trace toxic organic contaminants. These are key society challenges facing a growing US and world population.

7.4 – Appendix

Gas chromatography is performed by sampling three background gas chromatography traces for each of the following: air without plasma, air with plasma, the gas mixture with plasma and then with whatever changes are made to plasma parameters. The sample loop is reloaded after the first two peaks in the GC trace are completely described. During replicates, the time to steady state prior to sampling is varied in order to make certain that sampling does not impact the process. After the experimental period is completed, the methane is turned off and gas chromatography traces taken until the methane peak is completely gone. If all byproduct peaks are also eliminated in the air plasma, they were a direct result from plasma reactions driven with methane. If not the reactor walls must be removed further from the electrodes to prevent reactive sputtering of the spacer and exposed polymers. In the final study, these polymers were replaced with flame proof fiberglass spacers. A helium ionization detector with 30sccm helium flow is used throughout the study. The column tube is a Haysep D (3.17mm outer diameter that is 2m in length). An example raw output from the helium ionization detector is shown in Figure 106.

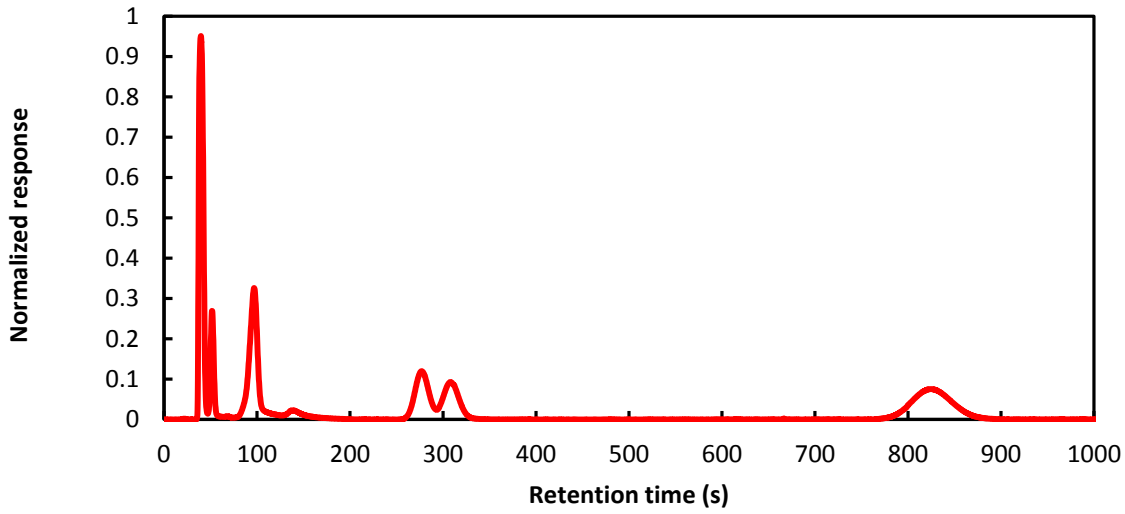

Figure 106: The raw chromatogram of carbon monoxide, methane, ethylene, acetylene, propene, propane and butane.

An example calibration curve for the response of these compound with changing injection volume is shown in Figure 107.

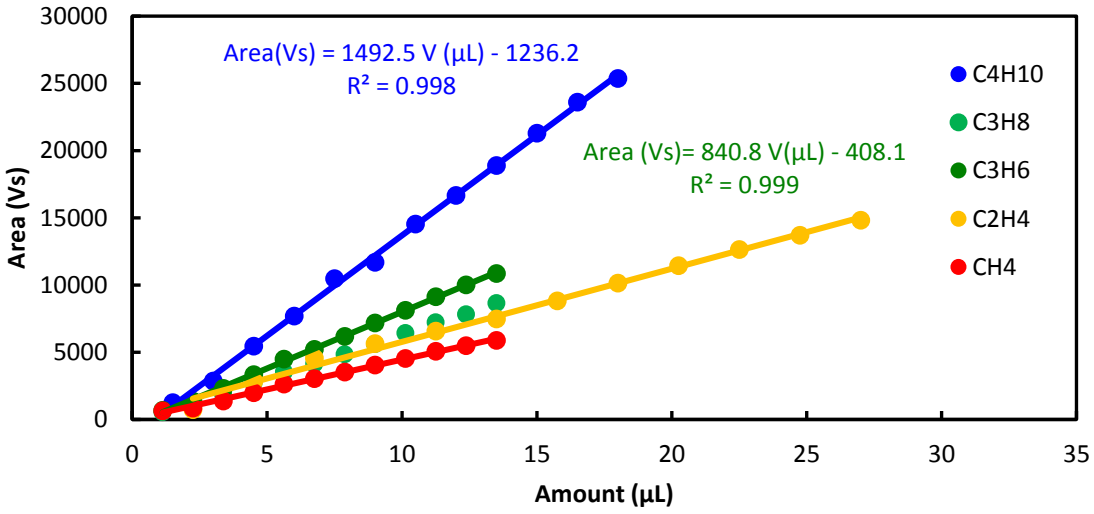

Figure 107: The calibrated injection volume shows a linear detector response over the required injection amount for each compound.

The data from the gas chromatograph is recorded as a response area verses residence time. This area is integrated. The injection column that is used during experimentation is 150µL. A response of for ethylene of 11,400 Volts·s corresponds to an injected amount of 20.25µL. This would correlate to a 20/150 molar ratio or 13.5mol% (considering that volume is related to molar amount linearly by the ideal gas law). The 13.5mol% can then be converted to a mass rate or mass percent since the total mass input and specie molecular weight is known. This mass balance includes input, output and accumulation and is used to compare FEM calculations to the experimentally extracted data sets.

Uv-vis of liquid samples is studied in two liquid reactors. A quartz cuvette with fiber optic attachments is used for the stirred tank reactor study. The quartz cuvette is transparent on each side and strongly transmits ultraviolet light. It holds 4ml. Its raw

absorbance profile and the resulting calibration curve for absorbance versus concentration under a combined deuterium tungsten lamp is shown below.

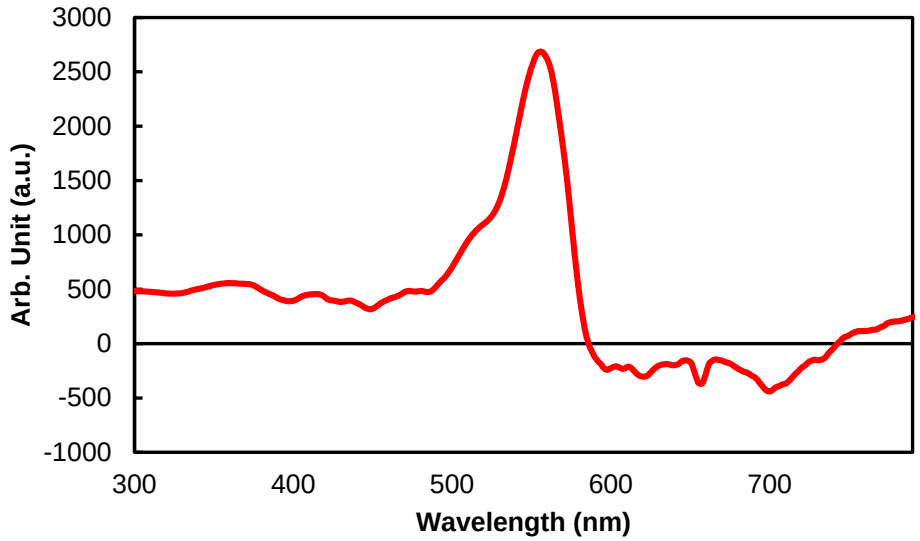

Figure 108: One of the data samples used to create the calibration curve near 1 ppm is shown as an example of the raw colorimetric absorption study.

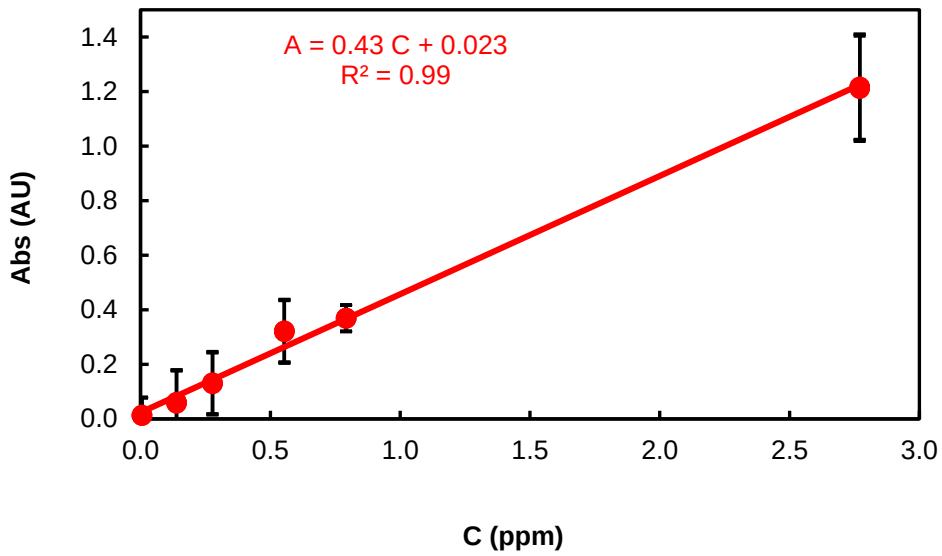

Figure 109: The photon count at the frequency of 530 nm is used to calculate the absorbance from blanks to produce the classical Beer's law relationship which is linear between concentration and absorbance under dilute conditions.

The second uv-vis cell is for the flow through study. A brass fitting is fashioned on a microCNC machine with an optimized path length for the rhodamine compound. Avantes optical fibers with windows were inserted into 1.58mm ferrules in-line with the flow path of the cell. The flow-through cell calibration curve for normalized concentration versus absorbance units is shown in Figure 110. The maximum concentration for the study is 4ppm based on signal saturation at higher concentrations.

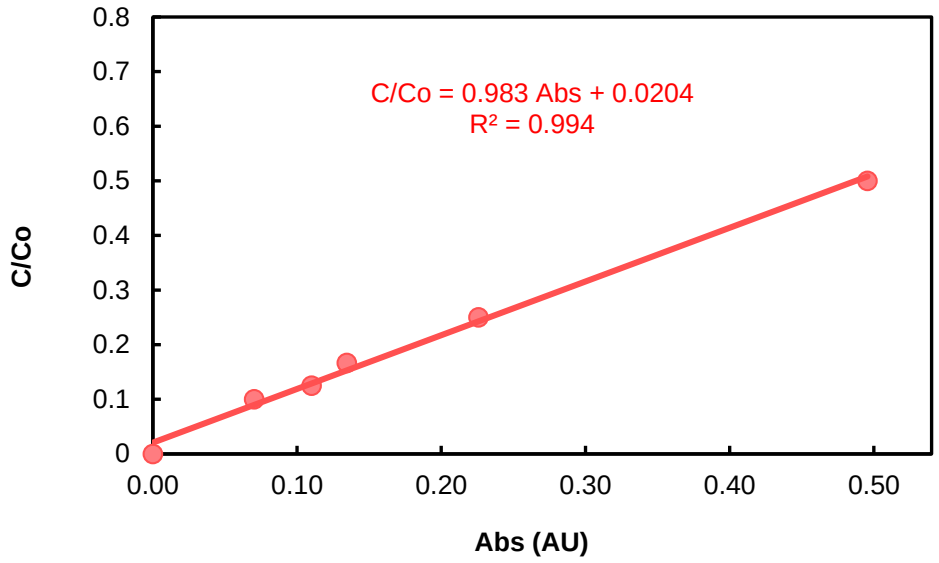

Figure 110: A second calibration was required for a custom fabricated flow cell which had a different pathlength than the cuvette coupled Avantes cell. The custom flow cell is milled on a microCNC brass and fabricated with a 1.58mm ID using stainless windowed Avantes optical fiber inserts.

The tungsten and deuterium lamp for the detector also is replaced at the 1000hr mark of this study. The data for the liquid uv-vis system is recorded as an absorbance and converted to concentration by calibration curve. The calculation of G-factor or energy consumption is also simple convention. The following definition for fifty percent removal energy efficiency will be used throughout this thesis.

$$E_{50}\left(\frac{mol}{J}\right) = \frac{\left(C_f - C_o\right)\cdot \dot{Q}}{MW\cdot\left(P\cdot 50\%\right)}$$